Fall 2021

Development of high-performance hydrogels

Buddhabhushan Salunkhe

Department: Chemistry

DEVELOPMENT OF HIGH-PERFORMANCE HYDROGELS

by

BUDDHABHUSHAN PUNDLIK SALUNKHE

A DISSERTATION

Presented to the Graduate Faculty of the

MISSOURI UNIVERSITY OF SCIENCE AND TECHNOLOGY

In Partial Fulfillment of the Requirements for the Degree

DOCTOR OF PHILOSOPHY

in

CHEMISTRY

2021

Approved by:

Dr. Thomas Schuman, Advisor
Dr. Baojun Bai, Co-advisor
Dr. Klaus Woelk
Dr. Manashi Nath
Dr. Paul Nam

TO

MY PARENTS

PUBLICATION DISSERTATION OPTION

This dissertation consists of the following four manuscripts that have been published, accepted or submitted for publication, formatted in the style used by the Missouri University of Science and Technology:

Paper I, found on pages 26–71, has been published in *Chemical Engineering Journal*.

Paper II, found on pages 72–101, has been submitted to *SPE Journal*.

Paper III, found on pages 102–113, has been published in *Data in brief*.

Paper IV, found on pages 114–157, has been accepted in *Macromol.*

ABSTRACT

Here, we present a systematic approach to design robust hydrogel compositions. The goal was to achieve excellent properties to open up new opportunities in especially two challenging applications not previously well-served by hydrogels.

The first part of this research will discuss the systematic screening of polymers for their hydrothermal stability under brine, acidic, neutral, and basic pH conditions followed by novel designs of hydrogel compositions. Certain hydrogel compositions withstand temperatures of up to 150 °C for more than 24 months in high salinity brines. This novel hydrogel composition fills a technology gap between the existing polyacrylamide-based preformed particle gels (PPGs) technology, which readily degrades above 110 °C temperature. We demonstrate the hydrogel ability to reduce effective permeability of open fractures through a core flood test.

The second part of the research will discuss the application of these hydrogels as superadsorbent materials for removal of organic dyes from industrial wastewater. The hydrogel composition discussed showed superabsorbance properties with swelling ratios of up to 27,500% which contributed towards an excellent methylene blue dye adsorption capacity of 1270 mg/g with more than 98% dye removal efficiency, and good recyclability. Additionally, the dye-polymer adsorption process demonstrates pseudo-first order kinetics and follows a Freundlich adsorption isotherm model that applies for multilayer, heterogeneous adsorption processes.

Owing to the novel features provided by the compositions, the hydrogels show significant potential for use in many other high-performance, advanced applications.

ACKNOWLEDGMENTS

First and foremost, I would like to express my heartfelt gratitude to my advisor, Dr. Thomas Schuman, who gave countless hours to make this dissertation reality. His caring nature has made him more than just an advisor. His positive attitude towards research, wonderful insights, critical thinking, and endless enthusiasm is something I am going to carry with me for a lifetime. Pursuing the Ph.D. under his guidance was one of the best decisions I happened to make, and I have realized it at various stages throughout the journey of my doctorate. I would also like to thank my co-advisor, Dr. Baojun Bai, for his constant guidance, critical attitude, dedication, and diligence which have encouraged me to improve my research skills and to become a better researcher.

I would like to extend my gratitude to my committee members, Dr. Klaus Woelk, Dr. Manashi Nath and Dr. Paul Nam, for their valuable suggestions and assistance with my graduate research work. I want to thank our sponsors, ConocoPhillips Co; Occidental Petroleum Corporation (OXY), Daqing Wantong Chemical Co. and PetroChina for their support and funding for this project. I would like to thank the Department of Chemistry, Missouri S&T, for providing resources and support.

My mom, dad, aunt, and uncle have been a great source of support who always brought positive energy and always believed in me, which has helped me to reach to this stage in my life. A special thank you to my sisters, brother, cousin, nephew, nieces, and all family members for their never-ending love, trust and continuous support.

Special thanks to Dr. Harris, Carmen, Srikanth, Harish, Santhosh, Siddhesh and all my friends for their constant help, love and emotional support throughout this journey.

TABLE OF CONTENTS

Page

LIST OF ILLUSTRATIONS

SECTION Page

PAPER IV

LIST OF TABLES

LIST OF ABBREVIATIONS

Abbreviation	Description
EOR	enhanced oil recovery
OOIP	original oil in place
M	mobility ratio
K	permeability
PPGs	preformed particle gels
HPAM	hydrolyzed polyacrylamide
PEI	polyethylene imine
HMTA	hexamethylenetetramine
AMPS	2-acrylamido-2-methylpropane sulfonic acid
NVP	N-vinyl pyrrolidone
PBDT	poly (2,2’-disulfonyl-4,4’-benzidine terephthalamide)
LCST	lower critical solution temperature
UCST	upper critical solution temperature
F_1	mole fraction of monomer 1 in copolymer
PEDOT: PSS	poly(3,4-ethylenedioxythiophene) polystyrene sulfonate
CO_2	Carbon dioxide
HT-PPG	Ultra-high temperature resistance preformed particle gels
G’	Storage modulus
KCl	Potassium chloride
NaCl	Sodium chloride

PSSS	Poly (sodium-p-styrenesulfonate)
PDMA	Poly (N'N'-dimethylacrylamide)
PAM	Polyacrylamide
VA-044	2,2'-Azobis[2-(2-imidazolin-2-yl) propane] dihydrochloride
NaSS	Sodium styrene sulfonate
DMA	N, N'-dimethylacrylamide
DVB	Divinylbenzene
DI	Deionized water
FTIR	Fourier transform infrared spectroscopy
CPMAS ^{13}C NMR	Solid State Cross Polarization Magic Angle Spinning ^{13}C Nuclear Magnetic Resonance
TOSS	Total suppression of spinning sidebands
FID	Free induction decay
TMS	Tetramethylsilane
TGA	Thermogravimetric analysis
SEM	Scanning electron microscopy
VSC	Void space conduits
SR	Swelling ratio
EQSR	Equillibrium swelling ratio
F_{rr}	Residula resistance factor
MB	Methylene blue
GelMA	Gelatin methacryloyl
^{1}H NMR	Proton nuclear magnetic resonance spectroscopy
D_2O	Deuterium oxide

1. INTRODUCTION

1.1. ENHANCED OIL RECOVERY

Oil and gas are crucial commodities in USA and global energy portfolios as a major provider for growing energy and chemical industries demand. To fulfill this growing demand, a new methodology and techniques need to explore to recover oil from these existing oilfields economically. Oil recovery process can be categorized in three stages depending on the life of a reservoir: primary, secondary, and tertiary or enhanced oil recovery (EOR). Primary production stage consists of displacement or production of oil from the reservoir using the reservoir own natural drive which corresponds to around 15% of the original oil in place (OOIP) in the reservoir [1].

In the secondary recovery stage, processes like waterflooding or gas injection implemented to recover oil from the reservoir which corresponds to additional 15 – 20 % of the OOIP [1, 2]. In waterflooding process, water is injected into the reservoir to displace residual oil form geological pore structure. The water from injection wells physically sweeps the displaced oil to adjacent production wells (Figure 1.1).

A tertiary stage recovery is also known as EOR that relies on injection of materials like miscible gases, chemicals or thermal energy, which changes the physical properties of the oil resource to change the oil displacement and recovery efficiency. A tertiary stage contributes towards recovery of additional 25 – 30% of the OOIP [1, 3]. The oil recovery stages can be used in any order depending on the oil reservoir and type of oil present. Thermal recovery, gas recovery, chemical flooding and microbial flooding are the major types of EOR technique commonly used in oil recovery [2].

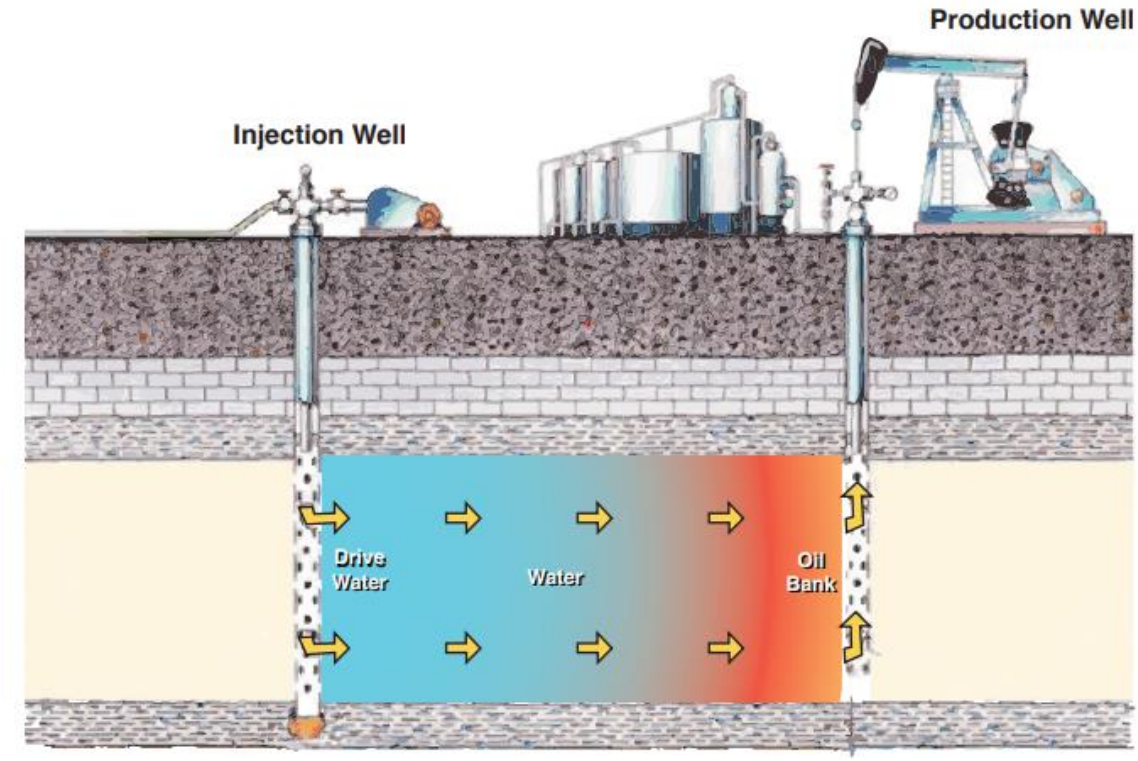

Figure 1.1. Water flooding process for oil recovery [4]

Oil is present in porous rock layers in an oilfield reservoir, which can have variable permeability regions. Some fields possess a high degree of pore size heterogeneity. These reservoir heterogeneities can consist of very fine porosity regions amongst open fractures, wormholes, or large pore flow conduits that become void space conduits. Large pore conduits are high flow conductivity areas resulting in large proportion of water passing through them but an overall poor volumetric sweep efficiency for the oilfield. Once the large pore flow conduits are liberated of their oil content, they become void space conduit regions that can directly connect injection wells to a producer well. Void space conduits thus result in an excessive water production problem leaving behind large amounts of oil as unswept oil but a poor ability to remove

the remaining oil resource and inefficient production. Underground erosion can also lead to void space conduit formation.

A flow conformance problem can be explained based on reservoir geology, which is not uniform throughout the reservoir formation. The rock layers as shown in Figure 1.2, in case of ideal conformance, have equal permeabilities of K_1, K_2, K_3 and K_4 which results into mobility ratio (M) less than unity. Under such conditions, injected water flows through all the rock layers equally, results into better volumetric sweep efficiency and higher oil production. On the other hand, reservoirs with conformance problem, will have geology where these rock layers will have variable permeabilities somewhat like $K_3 > K_2 > K_1 > K_4$ as a result major proportion of water will flow through high permeability rock layer (K_3) leaving behind majority of oil as unswept oil in other rock surfaces. This type of heterogeneities are main reasons for excess water production.

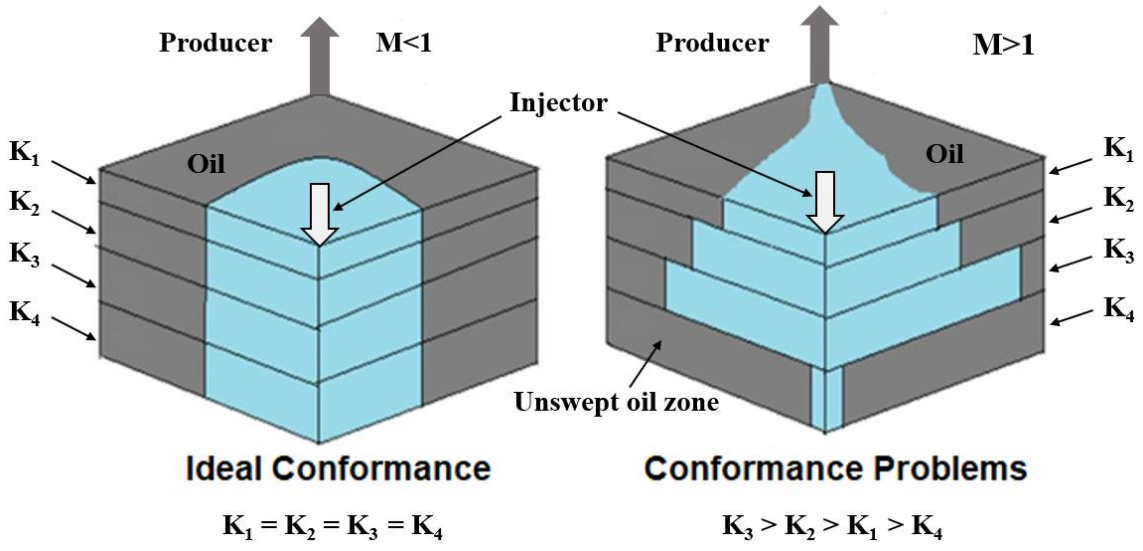

Figure 1.2. Distinction between ideal conformance and conformance problems, where K_1, K_2, K_3 and K_4 are permeabilities of rock layers and M is mobility ratio

1.2. EXCESS WATER PRODUCTION AND ITS SOURCES

Excessive water production is a major concern for most of the mature oilfields around the world. After multiple water flooding projects, as reservoir becomes mature, its potential for increased water production increases [5]. Water production comes with added costs of handling produced water, lifting, pumping, disposal or treatment of the water, making the oil recovery less economic. As a double-edged sword, excess water production drastically reduces oil well productivity, causes corrosion & scale, increases environmental concerns and impacts [6], and can elicit sometimes severe economic challenges [7], which can result in closure of production wells [8, 9].

The water production problem can be caused by various sources, during oil and gas production. Table 1.1 summarizes different causes and categories of water production in increasing order of treatment difficulty.

Table 1.1. Excess water production problems causes and categories [10-12].

	Order of difficulty	
Category A: "Conventional" treatments are eormally an effective choice	1	Casing leaks
	2	Flow behind pipe
	3	Unfractured wells (injectors or producers) with efective barriers to crossfow

Table 1.1. Excess water production problems causes and categories [10-12]. (Cont.)

Category B: Tretaments with Gelants normally an effective choice	4	2-D coning through a hydraulic fracture from an aquifer
	5	Natural fracture system leading to an aquifer
Category C: Treatments with Preformed Gels are an effective choice	6	Faults or fractures crossing a deviated or horizontal well
	7	Single fracture causing channeling between wells
	8	Natural fracture system allowing channeling between wells
Difficult problems for which gel treatments should not be used	9	Three-dimensional coning
	10	Cusping
	11	Channeling through strata (no fractures), with crossfow
	12	Single zone (no fractures) with a high mobile water saturation

Depending on the type of problem and characterisitic cause, different strategies need to be followed to resolve water production problem. The treatment strategies are selected based on understanding of the water production problem. Different strategies exist depending on the failure location, for example, right at the wellbore, or for a type of failure such as fracture or fracture-like features present in the reservoir, or the source of

water production such as crossflow between reservoir domains as shown as layers in Figure 1.2, etc. [13].

1.3. GEL TREATMENTS FOR CONFORMANCE CONTROL

Among different approaches to tackle excess water production concern, polymer gel treatment are proven, cost-effective technologies with considerable success in improving sweep efficiency [14]. The goal of conformance control strategy is to improve macroscopic sweep efficiency which can be attained through plugging high permeability "water thief" zones. Thief zones are plugged and water flow redirected with a polymer or other material, to redistribute the injection of water to flow through less porous, unswept, oil-rich regions, thereby improving oil recovery. For instance, these gels can be placed into fractures of a reservoir surrounding an injection well, where gel acts as both blocking and diverting agent and thus increasing oil production and reduce competing water production. The gel treatments can be used alone or in combination with other techniques. The plugging of high permeability zones can be done by two methods, *viz*; in-situ crosslinking gels and preformed particle gels (PPGs). The choice of technique to be used or combination of techniques used depend on type of reservoir and its production history.

1.3.1. In-situ Gels. In-situ gel treatments are very popular and most commonly used gel treatment for conformance control. The first field application of polymer gel system containing partially hydrolyzed polyacrylamide (HPAM) and aluminum citrate was reported by Phillips Co. in 1974 [15]. In case of in-situ gel treatment, polymers and crosslinkers are simultaneously injected to the formation where in-situ 3-D network of a

crosslinked gel is formed under reservoir conditions and seal off these water thief zones [16]. There are numerous reports for development and use of in-situ gel systems have been reported after circa 1970. Most commonly used polymer systems are based on polyacrylamide, starch, xanthan, guar, cellulose polymers and their chemical modifications [17]. Different types of crosslinkers viz; metallic crosslinker including aluminum, chromium [18], zirconium [19] and organic crosslinkers including phenol-formaldehyde [20], hexamethylenetetramine (HMTA) [21], polyethyleneimine (PEI) [22-24] are used in developing these in-situ gel systems.

Despite this characteristic, in-situ crosslinking gels can exhibit inherent drawbacks in plugging these thief zones, i.e., possess a lack of application control over the gelation time, thermal stability, gelling uncertainty due to shear degradation, chromatographic fractionation, and/or dilution [8, 25]. Several groups have presented different modifications of in-situ gels to improve their thermal stability using associative metallic crosslinkers like Cr^{3+}, organic crosslinkers like phenol–formaldehyde gels [26, 27] and PEI based systems [28-30], hydroquinone HMTA systems [21], etc. As yet, most of these systems cannot withstand higher reservoir temperatures greater than 140 °C and high salinity, concentrations greater than for instance 225,000 mg/L for more than 1 month [31, 32].

On the other hand, to overcome the drawbacks of in-situ gel treatments [8, 25, 33-35] toward solving conformance control problems, industry experts and researchers came up with a novel approach of PPGs to provide in-depth flow diversion for reservoirs with high temperature, high salinity, severe channeling conditions. The first PPG technology

was developed by PetroChina in 1996 with millimiter-size particles capable of high swelling capacities.

1.3.2. Preformed Particle Gels (PPGs). PPGs are three-dimensional, dried, cross-linked, polymeric granules that, on contact with/dispersion in formation water, have ability to swell from several to several hundred times their dry particle size [8]. The swollen gel particles produced are elastic and deformable in nature, which can be injected into reservoirs to control water fluid flow in fractures. Despite their advantages, PPGs can be sensitive to physiochemical conditions of reservoirs like pH, multivalent ions, salinity, temperature, etc. which affect swelling capacities, and other intrinsic properties that can be controlled through the composition of gels [36, 37].

PPG technology was novel in terms of addressing problems posed by in-situ gel treatments, including sealing as damage to low permeability zones [5]. As an all-in-one package, PPGs avoid segregation via chromatographic problems, associated with traditional in-situ gels and also more thermally stable in high salinity water. PPGs treatments are of interest because they have decades-worth of successful field application and are inexpensive, relatively easy to synthesize and handle in the field. PPGs are used to redirect water flow from high permeability zones or fractures with residual hydrocarbon saturation towards unswept hydrocarbon rich zones [38-42].

Since 1997, a series of PPG products have been developed like particles with hydrophilic groups, with carboxylic acid or polyacrylamide functionalities, with swelling capacities of several hundred [14, 42]. The most commonly used PPGs are polymer-clay composite gels with swelling capacities up to 100 times in formation water and thermally stable up to 120 °C temperatures [5]. Another kind of PPG developed with limited

swelling capacities demonstrated excellent flexibility, elasticity, and thermal stability up to 120 °C for in-depth diversion [43]. PPGs with low surface tension was reported by Cui, et al. [44] to reduce residual oil saturation and found to enhance stability towards high temperatures and salinity. Haliburton company developed a PPG with controlled swelling capacities for conformance control [45]. Thousands of oilfields have been treated using different types of PPG products all over the world, especially in Chinese oilfields.

Despite their advantages, PPGs have not provided a complete solution to conformance control problems associated with reservoir heterogeneity at high salinity and high temperature conditions. Conventional PPGs are based on polyacrylamide homopolymer networks, which degrade at higher temperatures and high salinity conditions [46, 47]. Upon exposure to harsh conditions of high salinity, formation hardness, and temperature, they undergo syneresis as a result of hydrolysis of the amide groups causing rapid structural degradation of its primary structure [48]. It has been observed that PPGs can suffer mechanical degradation under shear conditions. Toward improving thermal stability and other harsh conditions, several approaches, *viz.*, introduction of inorganic fillers [49], copolymerization with 2-acrylamido-2-methylpropane sulfonic acid (AMPS) or N-vinyl pyrrolidone (NVP) monomers [31] have been reported. These PPGs have proven more stable at relatively harsh reservoir conditions of temperature and salinity for periods of several months. However, to our knowledge there are no PPGs with long-term thermal stability at temperatures up to 150°C have been reported.

Therefore, it is important to follow systematic approach for development of ultra-high temperature resistant product with long term thermal stability. Polymer backbone and its hydrothermal stability towards degradation under reservoir conditions is the key factor in developing such ultra-high temperature resistant PPG product.

1.4. STABILITY OF POLYMERS FOR EXTREME SERVICE CONDITIONS

Polymers are widely used for innumerable applications specific to their properties and performance based on a principle of maintaining their properties over the expected timeline for any specific application [50]. Most polymers are an organic backbone structurally and hence, likely to undergo chemical changes through attack from their surrounding environment, *viz*; sunlight, water, air, temperature, etc; which bring changes in the properties of these polymers over the period of their service time. Most of these changes are associated with the change in effective molecular weight of polymers, through degradation, additional crosslinking or other mechanisms responsible for changing their properties and in turn their effectiveness. Depending on the mechanism causing changes in polymer properties, changes can occur on a molecular level, by changing the functional groups in the backbone of the polymer [50] affecting their long-time durability. Therefore, it becomes utmost important to understand the behavior of polymers under extreme service conditions before product development.

1.5. POLYACRYLAMIDE STABILITY AND DEGRADATION

For oil recovery applications, the most commonly used and widely studied polymer backbone is polyacrylamide based on its ready availability, cost-effectiveness,

and facile synthesis protocols [51]. However, their applications under high temperatures of more than 100 °C and high salinity conditions, limit their application as they readily degrade under such conditions [52]. Polyacrylamide degradation is widely studied topic, where various mechanisms of degradation viz; mechanical degradation, chemical degradation, biodegradation, etc. have been reported.

Mechanical degradation of polyacrylamide can occur due to high shear under flow through pores and fractures during oil recovery [53]. Mechanical degradation can cause breaking of polymer chains and thus decreasing the viscosity of these polymers [54]. High salinity and temperature conditions can enhance the rate of mechanical degradation further. Chemical degradation through action of hydroxyl radicals can cause chain scission of polyacrylamide backbone. Hydroxyls ions can be generated through different routes. e.g., interaction between oxygen and transition metals, ozone and UV treatments (photolytic degradation) [46]. Free radicals attack polymer backbone via hydrogen abstraction at secondary, tertiary carbons, primary amines which generates polymer radicals [46]. These polymer radicals further react with dissolved oxygen to form polymer peroxy radicals, which are responsible for chain scission and to form polymer fragments [46, 55, 56].

Oxidative degradation of polyacrylamide results into main chain scission through a series of elementary reactions. Polyacrylamide has a primary amide side chain group which hydrolyzes to form corresponding acid moieties. The hydrolysis occurs through various mechanism depending on pH and temperature conditions. Under neutral conditions in presence of water, through nucleophilic addition mechanism, corresponding acid functional compounds are formed through release of ammonia [57]. Transition

barriers for such mechanism under neutral condition is very high with the order of 50 kcal/mol and more (Figure 1.3), making it difficult [58]. Although presence of metal ions and high temperature can increase degradation rate significantly making polyacrylamide susceptible to degradation [59].

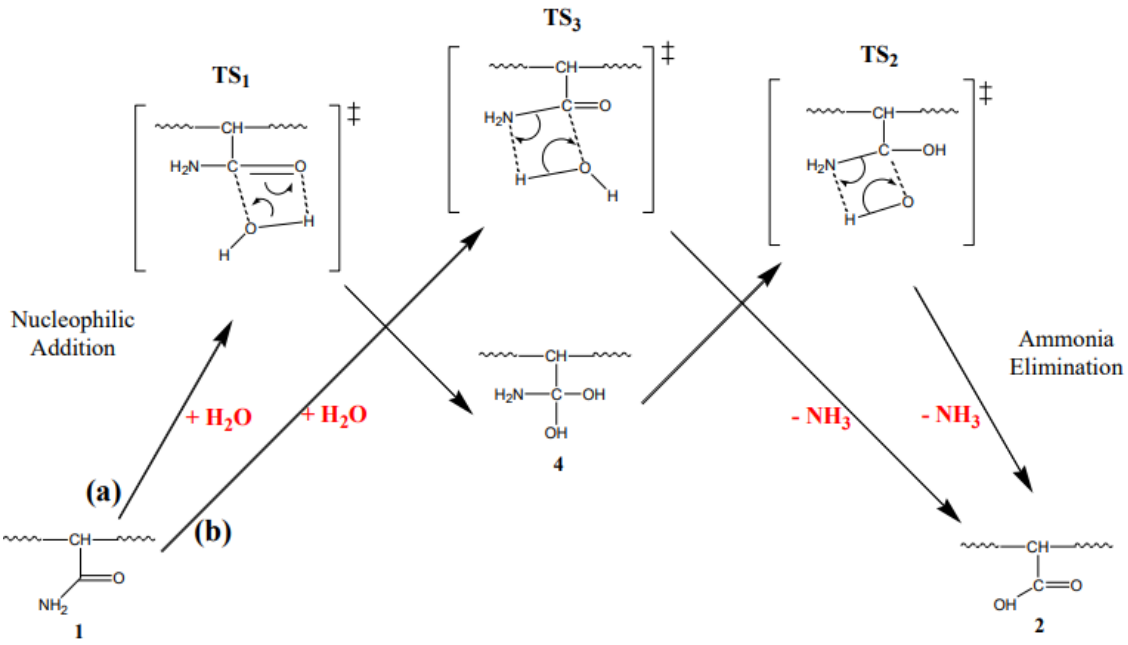

Figure 1.3. Reaction pathways of polyacrylamide hydrolysis under neutral conditions [58].

The base catalyzed mechanism is a widely studied and most common cause for degradation of polyacrylamide, where hydroxyl ion attacks on carbonyl carbon (with transition barrier of 22 kcal/mol) followed by an ammonia elimination step (with transition barrier of 31.5 kcal/mol) as shown in Figure 1.4 [58, 60]. It's a second order reaction which depends on concentration of both the amide and hydroxyl ions. The first step of hydrolysis is faster in the beginning and then slows down because of increasing

charge on the polymeric chain After attaining a high degree of hydrolysis, the polymer chains gain stretched configuration due to electrostatic repulsion effect of carboxylate functional groups and lowering the shielding effect for hydroxyl ion attack, causing polymer to degrade at very faster rate [61].

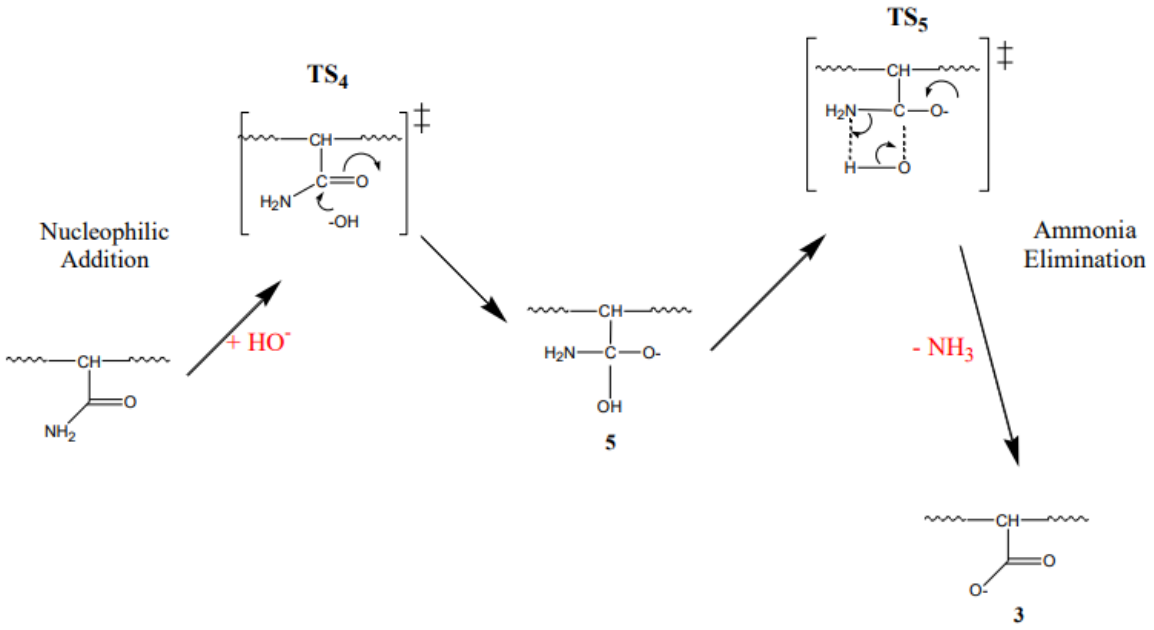

Figure 1.4. Reaction pathways of polyacrylamide hydrolysis under base catalyzed conditions [58].

In the acid catalyzed mechanism, hydrolysis results from a proton attacking the amine group or the carbonyl oxygen with activation energy barriers of over 40 kcal/mol as shown in Figure 1.5 [58]. Acid catalyzed hydrolysis is a second order reaction and strongly depends on amide and hydrogen ion concentration, where corresponding carboxylic acid groups are formed through ammonium ion elimination. The rate of degradation through such mechanisms enhances with increase in temperature.

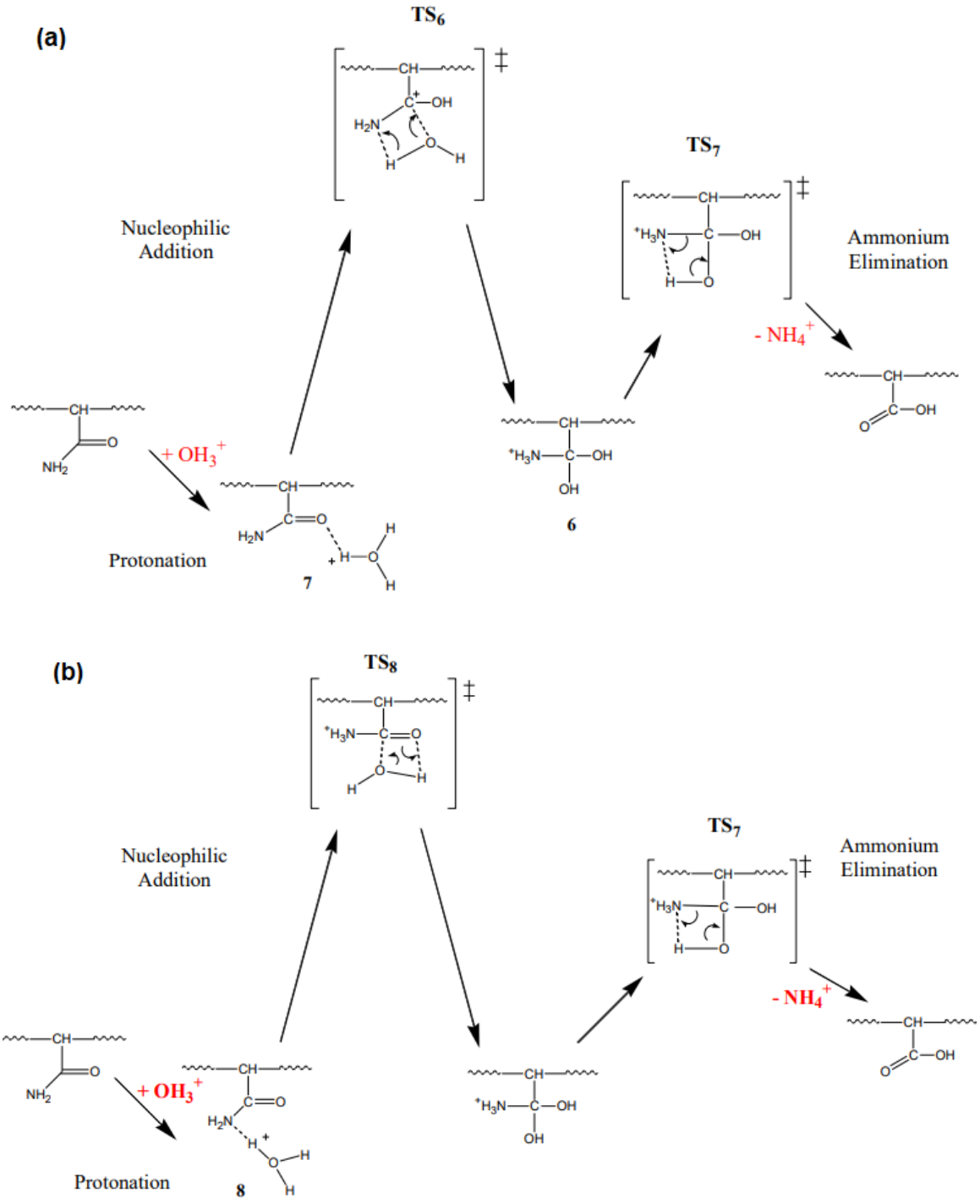

Figure 1.5. Reaction pathways of polyacrylamide hydrolysis under acid catalyzed conditions initiated through (a) O-protonation and (b) N-protonation [58].

1.6. SUBSTITUTED POLYALKYLAMIDES STABILITY AND DEGRADATION

Polyalkylamides with mono or dialkyl substitution on the nitrogen atom are more resistant to hydrolysis [61, 62]. Under strongly basic conditions, these nitrogen substitution causes the inductive effect on resonance stabilization of the amide function and thus increase in the activation energy of alkaline hydrolysis. As a result, the nucleophilic attack of the hydroxyl ion on the carbonyl carbon becomes difficult. It was also observed that with higher degrees of substitution, a lower degree of hydrolysis was attained, making these substituted polymers more stable towards degradation [61, 63]. This can be further attributed to stretched configuration of the molecule due to strong steric hindrance and high electrostatic repulsion with hydrolysis [64].

On the other hand, under acid catalyzed conditions polyacrylamides can undergo hydrolysis reactions, along with imidization reactions. Imidization reaction for creating intramolecular imide group can occur through either interaction of acid group with a neighboring amide functional group or through interaction of two amide functions. It was reported that the energy of activation for imidization is higher than the energy of activation for hydrolysis [61]. With increase in nitrogen substitution, resonance stabilization increases, and which stabilizes amide functionalities towards acid hydrolysis [65]. This increase stabilization also avoids the imidization reactions for the nitrogen substituted polymers making them more hydrolytically and thermally stable.

The alpha-methyl substitution on acrylamide monomer like in case of methacrylamide, introduces a steric hindrance along the polymer chain resulting in stretched configuration and thus less prone to hydrolysis than polyacrylamide where a 100% degree of hydrolysis can be attained. Therefore, the key for thermally and

hydrolytically stable polymers development is in line with their structures contributing towards the electrostatic repulsions and reinforced by strong steric hindrance. Polymers based on monomer structures with dialkyl substitution of nitrogen and alpha-alkyl substitution on vinyl group can be considered as a good candidate for creating thermally and hydrolytically stable hydrogels.

1.7. OTHER APPROACHES FOR DEVELOPMENT OF THERMALLY STABLE HYDROGELS

To develop thermally stable hydrogels, various routes can be followed to obtain a polymer backbone that can show better hydrolytic thermal stability.

1.7.1. Polyaromatic Water Soluble Polymers. Water soluble semi-rigid polyelectrolytes like poly (2,2'-disulfonyl-4,4'-benzidine terephthalamide) also known as PBDT (Figure 1.6) can be used to create thermally stable hydrogels owing to their semi-rigid structure and aromatic nature. It has been observed that these kinds of polyelectrolytes attribute towards self-assembly to form a well-ordered structure [66, 67]. These polyaromatic water soluble polymers can be used in synthesizing double network hydrogels, to create tough, strong and thermally stable crosslinked networks.

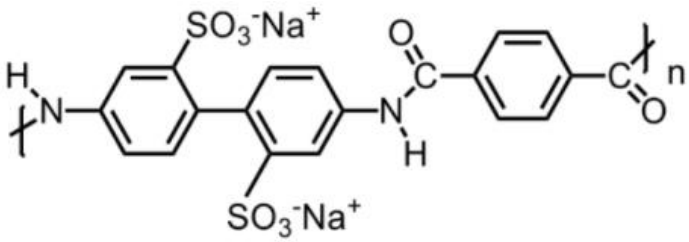

Figure 1.6. Structure of PBDT

The advantages of using a PBDT polyelectrolyte is that it has a rigid rod structure that can contribute towards stiffness of the double network hydrogels and preventing it from collapsing in high ionic strength solutions like formation of oil reservoirs. PBDT based double network hydrogels with chemically crosslinked polyacrylamide have been found to create a mechanically robust hydrogel through brittle and hard sacrificial PBDT network and stretchable polyacrylamide network [68]. Similar concepts can be adapted to create a tough strong thermally stable double network hydrogel using PBDT and second network with thermally stable crosslinked polymers.

1.7.2. Thermoresponsive Polymers with LCST-UCST Behaviour. The polymers with thermoresponsive behaviour have been intensely studied over last several decades in the fields of bioengineering, nanotechnology as an intelligent material [69, 70]. Thermoresponsive polymers exhibit volume phase transition as a function of temperature. Thermal changes are associated with coil to globule transition of polymer structure at specific temperatures, e.g., like a lower critical solution temperature (LCST), where polymer becomes water insoluble on heating, or the upper critical solution temperature (UCST) where polymer inverts from hydrophobic to hydrophilic [71]. The phase behavior of polymer-polymer systems can be controlled through the choice of monomers, molecular architecture, hydration structure, composition of the polymer and molecular size. By introducing a convenient choice of ionomer to the backbone of the LCST polymer, one can increase LCST of the copolymer system and adapt the polymer towards use in an ultra-high temperature application.

1.8. REACTIVITY RATIOS FOR COPOLYMER COMPOSITION

Copolymer composition with distribution of monomers in the final copolymer can be predicted using the understanding of reactivity ratios of monomers used. Copolymer primary structure, the order of comonomers repeat within the polymer chain, is important as the statistical distribution of monomer ordering define the final structure property relationships of copolymer obtained. Therefore, it is important to understand the statistics of monomer addition to the propagating chain in developing high performance materials [72]. A monomer's preference to homopolymerize as a ratio to its rate of polymerization with a comonomer, i.e., its reactivity ratio, during copolymerization depends on factors like steric factors, resonance stabilization of the radical site, polarity of the double bond. There are multiple methods used to measure and calculate reactivity ratios from copolymer compositions, viz; Mayo-Lewis intersection method, Fineman-Ross linearization method or the Kelen-Tudos linearization method, using known monomer feed ratios.

Mayo-Lewis method which uses terminal model of copolymerization with steady-state assumption where the concentration of active growing chain ends is constant.

$$F_1 = \frac{(r_1 f_1^2 + f_1 f_2)}{(r_1 f_1^2 + f_1 f_2 + r_2 f_2^2)} \tag{1.1}$$

$$f_1 = 1 - f_2 = \frac{M_1}{M_1 + M_2} \tag{1.2}$$

$$F_1 = 1 - F_2 = \frac{dM_1}{d(M_1 + M_2)} \tag{1.3}$$

where F_1 defines the mole fraction of monomer 1 in a copolymer over an infinitesimally small conversion, f_1 and f_2 are molar feed composition of monomers 1 and 2, r_1 and r_2 are the reactivity ratios of monomers 1 and 2 respectively.

In Fineman-Ross linearization method which is an extension of Mayo-Lewis method where generated a linear form through simple substitutions and rearrangements.

$$x\left(1-\frac{1}{y}\right)=r_1\cdot\left(\frac{x^2}{y}\right)-r_2 \tag{1.4}$$

where x = $[M_1]/[M_2]$, composition of monomer feed and y = $d[M_1]/d[M_2]$, copolymer composition after certain degree of conversion. Both Fineman-Ross and Mayo-Lewis methods depend on instantaneous copolymer equation and can introduce errors during measurements.

To overcome the shortcomings of above methods, Kelen-Tudos developed a method by adding an arbitrary positive constant to Fineman-Ross equation, which helps to spread data more evenly over the entire composition range. Kelen-Tudos equation can be written as:

$$\eta=r_1\xi-\frac{r_2}{\alpha}(1-\xi) \tag{1.5}$$

where,

$$\eta=\frac{\frac{x(y-1)}{y}}{\alpha+\frac{x^2}{y}}\text{ and }\xi=\frac{\frac{x^2}{y}}{\alpha+\frac{x^2}{y}} \tag{1.6}$$

$$\alpha=\sqrt{\left(\frac{x^2}{y}\right)_{low}\left(\frac{x^2}{y}\right)_{high}} \tag{1.7}$$

Experimental data using x and y can be used to generate a plot of η vs ξ produced a straight line with extrapolation at ξ = 0 corresponding to $-r_2/\alpha$ and ξ = 1 corresponding to r_1. The parameter α contribute towards uniform distribution of experimental data between 0 and 1 through highest and lowest values of term x^2/y obtained from experimental data.

For a given set of copolymer composition outcomes, the above methods can be used to determine reactivity ratios of monomers and accordingly hydrogel composition can be adjusted to obtain optimum structure properties in final product.

1.9. SYNTHESIS PROTOCOL FOR HYDROGELS

Hydrogels can be synthesized from synthetic or natural polymer compositions depending on end applications and properties. The term “hydrogel” is defined as a three-dimensional crosslinked network of otherwise water-soluble polymers, with providing an elastic structure. Copolymerization of monomers in presence of small amount of crosslinker can produce hydrogels which can absorb water within its three-dimensional polymer network. Hydrogels can be synthesized using polymerization techniques like bulk, solution, and suspension technique. In typical hydrogel synthesis, monomers, crosslinkers and initiator are key components, where monomers and crosslinkers are dissolved in deionized water, as a solvent medium for the polymerization reaction. Dilution also helps to control reaction temperature despite a large reaction enthalpy of polymerization.

A wide variety of monomers can be used to synthesize hydrogels with desired properties where free radical polymerization is initiated with heat, radiation, or chemical catalysis. In general, monomers and crosslinkers solution is prepared in deionized water and sparged with argon gas to remove oxygen and thus prevent air inhibition. Polymerization is initiated by addition of free radical creating thermal initiator or a redox initiator system. Reaction is continued under reaction conditions specific to initiator system used. Figure 1.7 represents the general hydrogel synthesis protocol. The hydrogel

obtained can be used as it is or can be further cut into small pieces, followed by oven drying and grinding procedure to yield dry gel particles.

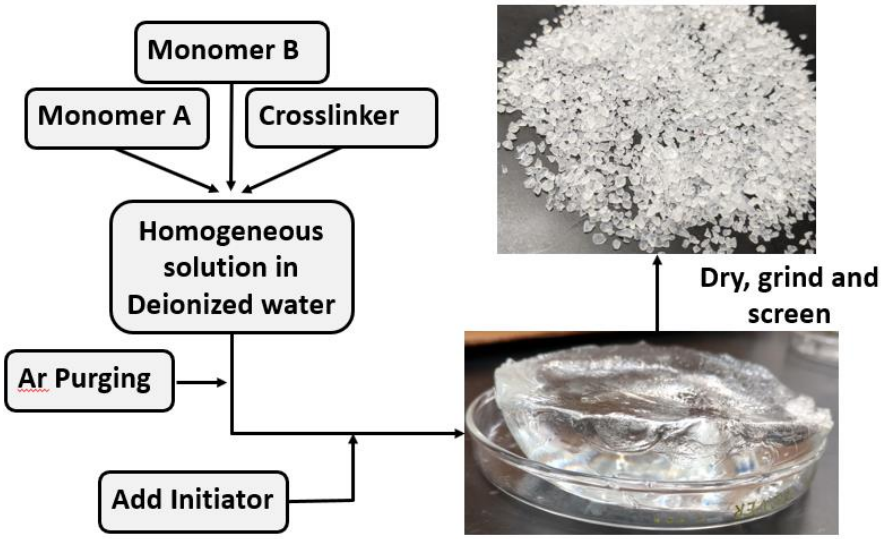

Figure 1.7. Hydrogel synthesis protocol

Hydrogel particles can be further characterized for various physiochemical properties to understand their behavior towards different stimuli. The PPG compositions developed herein were specifically developed to be used in plugging fractures present in the oil reservoirs for conformance control. Hydrogel compositions developed herein were to provide properties like resistance to temperature, strong acids, bases, electrolytes, salinity, superabsorbancy, and very high internal surface area. These properties can be utilized to support other applications such as removal of organic dyes from industrial wastewater, as a biosensor support, etc.

1.10. OTHER APPLICATIONS OF DEVELOPED HYDROGEL COMPOSITION

Considering the excellent hydrolytic thermal stability and chemical resistance, the hydrogels can be explored in several applications such as organic dyes removal from industrial wastewater, non-enzymatic biosensor supports for various analytes, tissue engineering and son on.

1.10.1. Superadsorbents for Organic Dyes Removal. Organic dyes are widely used in industries such as textile, paper, leather tanning, plastics, coatings, pharmaceutical, cosmetics, printing, ground water tracing, and many other chemical industries [73-77] creating a serious water pollution problem. These effluents constitute the pollutants which are non-biodegradable, highly toxic, and often carcinogenic and/or mutagenic in nature [78]. Therefore, variety of methods like chemical oxidation, adsorption, ion exchange, physical treatments, etc. are used in the field of water remediation. Among water treatments, adsorption is among the most promising technique for dye removal from wastewater and has attracted interests of researchers and industry owing to its advantages like simple design, low cost, insensitivity to pollutants, easy regeneration, and effectiveness [79].

Hydrogels are most widely studied material as an adsorbent for organic dye removal from wastewater owing to their excellent water absorption, high porosity, easy handling, and facile preparation resulting in a flexible network of polymer chains that helps penetration of solutes into the network [80]. The polymer backbone in these hydrogels can be designed with specific hydrophilic functional groups, such as carboxylic acids, amines, or sulfonic acids, which could be employed as complexing agents for dyes possessing opposite charge [81-84]. Hydrogels have physically well-defined, three-

dimensional structures and can swell to several times of their original volume in aqueous solutions, creating a very large surface contact area for adsorption of these organic dyes [85, 86].

Among different polymer backbone chemistries, polyacrylic acid chemistries are widely used in adsorption studies of cationic dyes [87]. Due to the presence of oxygen atoms, acrylics can complex cationic dyes. A weak acidity of carboxylic acid groups leaves these acrylic-based materials sensitive to solution pH, which affect dye adsorption capacity as a function of pH [82]. Therefore, a novel, strongly ionic hydrogel adsorbent needs to be explored to provide high adsorption capacity at lower cost with effectiveness over wide pH range.

During designing adsorption systems, understanding of adsorption process and to evaluate performance of adsorbent s through adsorption kinetics discussing the rate at which adsorption occurring and adsorption isotherms at equilibrium conditions plays pivotal role. The adsorption kinetics is a strong function of surface complexity of the adsorbent, solute concentration, chemical environment like pH, temperature, etc. Pseudo-first -order, pseudo-second-order, Elovich and Intra-particle diffusion model are most widely used models to predict the controlling mechanism of adsorption such as chemical reaction, diffusion control or mass transfer controlled.

The standard forms of equations to fit experimental data are as follows: pseudo-first order (Equation 1.8), pseudo-second order (Equation 1.9), Boyd liquid-film diffusion model (Equation 1.10), and Elovich models (Equation 1.10) [88, 89].

$$log\ (q_e - q_t) = log\ (q_e) - k_1 * t/2.303 \qquad (1.8)$$

$$t/q_t = t/q_e + 1/(k_2 * q_e^2) \quad (1.9)$$

$$-ln\,(1\text{-}F) = k_{fd}t \quad (1.10)$$

$$q_t = \ln(\alpha\beta)/\beta + \ln t/\beta \quad (1.11)$$

where q_e (mg/g) and q_t (mg/g) are the adsorption capacity at equilibrium time and time t (min), respectively. k_1 (/min), pseudo first order rate constant, k_2 (g (mg /min)), pseudo second order rate constant, k_{fd} (/min) adsorption constant corresponding to Boyd liquid-film diffusion model, α (mg /g /min), initial adsorption rate constant and β (g/mg), desorption constant related to the adsorbent surface covering and the adsorption chemical energy. F is a fractional attainment of equilibrium ($F = q_t/q_e$) at time t for liquid-film diffusion. Generally, the best-fit model is chosen based on the values of linear regression correlation coefficient R^2, where higher value of R^2 is considered as best goodness of fit.

Adsorption isotherm, another significant parameter to determine adsorption process mechanism that provides information about how the adsorbent is interacting with the solute or adsorbate and adsorption capacity. Several isotherm models are presented based on monolayer or multilayer surface phases [90], among which following are the most widely used models: Langmuir (Equation 1.12), Freundlich (Equation 1.13) and Temkin (Equation 1.14) isotherms are as follows:

$$C_e/q_e = C_e/q_m + 1/(K_L q_m) \quad (1.12)$$

$$\ln q_e = \ln K_F + \ln C_e/n \quad (1.13)$$

$$q_e = B_T \ln K_T + B_T \ln C_e \quad (1.14)$$

where C_e (mg/L) is the equilibrium concentration of MB solution used; q_e (mg/g) is the adsorption capacity at equilibrium; q_m (mg/g) maximum adsorption capacity; K_L and K_F (L/mg) are the Langmuir and Freundlich adsorption equilibrium constants respectively;

K_T (L/mg) is maximum binding energy constant; n is a heterogeneity factor indicating how favorable the adsorption process is; $B_T = RT/\beta$ and β (J/mol) is the Temkin constant related to the heat of adsorption, R is the universal gas constant (8.314 J/mol/); and T is absolute temperature (K). Langmuir adsorption isotherm model considers adsorption process as homogeneous site specific within the adsorbent, predicting monolayer adsorption [76]. On the other hand, the Freundlich adsorption isotherm assumes a heterogenous adsorption surface with unequal distribution of adsorption sites exhibiting different energies of adsorption [76]. Temkin model considers the effects of indirect solute adsorbent interactions with an assumption that adsorption of all molecules in the layer decreases linearly with increase in surface coverage and hence valid only for an intermediate range of ion concentrations [91, 92].

1.10.2. Non-enzymatic Biosensors for Organic Analytes Detection. Biosensors used in detection of biological reactions through a measurable signal have gained substantial interests across the scientific community Among various approaches used to develop biosensors, hydrogels are becoming popular alternative owing to their excellent biocompatibility, viscoelastic properties, and easy synthesis protocols. Owing to the highly porous structure of hydrogels of large internal surface area, the bioreceptors or catalysts can be incorporated to sensitively detect biological events like biochemical and/ or biological interactions to create macroscopic response through response through conductometric, amperometric tools for biosensing [93, 94]. In another approach, external stimulus responsive hydrogels can be synthesized that can be controlled through modes like change in pH, temperature, electric field, etc. [93, 95].

Electroconductive hydrogels with electronic functionality facilitating electron transport across the interface have been reported for electrochemical enzyme immobilized biosensors to detect analytes like glucose in blood samples [94, 96, 97]. Polymers used in designing this type of hydrogels are polypyrrole, polyaniline, poly(3,4-ethylenedioxythiophene) polystyrene sulfonate (PEDOT: PSS). These types of biosensors are redox active with the biosystem environment and thus responsible for electron transfer across the large surface area of electroconductive hydrogel producing current or changes the potential. Due to ionic conductivity of these hydrogels, impedance between electrode and environment decreases leads to changes in surface resistance, current, or voltage that can be monitored to gauge response at various concentrations [94].

Despite the rapid development of electrode materials, it remains challenging to develop biosensing platforms that can detect all metabolites simultaneously with high sensitivity, a wide linear range and rapid response time, detection specifically, while being compatible with simple patterning technology, which is critical for the low-cost fabrication and integration of sensor kits and multiplex sensors for healthcare monitoring, clinical diagnostics, and biomedical devices [98]. Therefore, a biosensor platform needs to develop to sense performance of analytes like glucose, dopamine, uric acid, etc. at higher sensitivities with low sensing limits.

1.11. OBJECTIVE OF THIS RESEARCH

Polyacrylamides based conventional hydrogels have been used in the industry from several decades to control excess water production problem. However, under conditions of high temperatures, salinity, acidic or basic conditions, these hydrogels

degrade readily, limiting their use in oil reservoirs with extreme harsh reservoir conditions. Therefore, to develop an ultra-high temperature resistant, chemical resistant hydrogel, a systematic approach needs to be adapted.

We describe the development of polymer hydrogel with superior thermal and salinity resistance that is characterized for use in enhanced oil recovery to solve conformance control problems in mature oilfields with high temperature of up to 150 °C and high salinity. Conformance control problems cause decreased oil production efficiency to the point of shutting down of fields but leaving untapped significant quantities of oil resources, as unswept or remaining oil. The gels described herein are designed for oil reservoirs such as the Gulf of Mexico, North Sea, Ying-qiong basin, or Mubarraz, which can have underground reservoir temperatures of more than 150 °C. The gels were developed systematically by polymer screening for hydrothermal stability followed by hydrogel synthesis, characterization, and demonstration of applicability of the product in plugging fractures. An application also of interest for this material is that, as a temperature, salt-, and acid-resistant hydrogel, it has applicability beyond oil recovery. In this case, we seek to provide removal of organic dyes from industrial wastewater, development of biosensors, etc.

The following studies are planned to achieve above stated objectives:

1. To study the polymers for their thermal and hydrolytic stability at 150 °C in their aqueous solutions at variable pH range.
2. To calculate the reactivity ratio for copolymer pair to be used for hydrogel synthesis

3. To develop hydrogel composition and optimization of the recipe for ultra-high temperature resistant preformed particle gels
4. To characterize these hydrogel compositions for physiochemical properties like effect of pH, temperature, ionic strength, types of ion on swelling capacity, morphology
5. To study thermal stability of hydrogels at 150 °C under variable brine conditions through matrices like visual observation, chemical signature retention through solid state NMR, morphology, thermogravimetric analysis, change in equilibrium swelling ratio
6. To study the chemical resistance and phase stability of hydrogels towards highly acidic, basic conditions, under supercritical CO_2 conditions
7. To study the effectiveness of PPGs in plugging open void space conduits or fractures through lab core flood tests.
8. To explore hydrogel composition in other applications, such as a superadsorbent hydrogels for methylene blue dye removal.

PAPER

I. ULTRA-HIGH TEMPERATURE RESISTANT PREFORMED PARTICLE GELS FOR ENHANCED OIL RECOVERY

Buddhabhushan Salunkhe[a], Thomas Schuman[a,*], Ali Al Brahim[b], Baojun Bai[b],

[a] *Chemistry, Missouri University of Science and Technology, Rolla, MO 65409, USA*

[b] *Petroleum Engineering, Missouri University of Science and Technology, Rolla, MO 65409, USA*

ABSTRACT

Gel treatment is one of the most efficient enhanced oil recovery techniques used for conformance control. In recent years, preformed particle gels (PPG) have gained attention for conformance control and to reduce water production. However, there are no current products available to withstand reservoir conditions with high temperature, high pressure, and high salinity. In this paper, we describe the development, characterization and detailed evaluation of a unique hydrogel composition with ultrahigh temperature resistance (HT-PPGs) for chemical enhanced oil recovery. HT-PPG described herein can swell more than 30 times its initial volume in brines of different ionic strengths. We systematically evaluated the effect of variables like temperature, pH, salinity, monovalent vs divalent ions on swelling behavior. The HT-PPGs are mechanically robust in nature with storage moduli (*G'*) of over 3000 Pa at about 90 percent water in content. Additionally, HT-PPGs showed excellent thermal stability at 150 °C for more than 12 months in monovalent and divalent ion containing brines at all swelling ratios. HT-PPGs

exhibit exceptional hydrolytic thermal stability for more than 18 months in 2% KCl brine (at water content of > 93 percent) at 150 °C. Coreflooding tests were performed in a fractured core and showed good plugging efficiency, helped to reduce the permeability of fracture and did not wash out, were not eluted, during the test. HT-PPG discussed in this work, is a unique product with excellent features which make it an ideal candidate for conformance control of reservoirs with harsh temperature, salinity conditions.

GRAPHICAL ABSTRACT

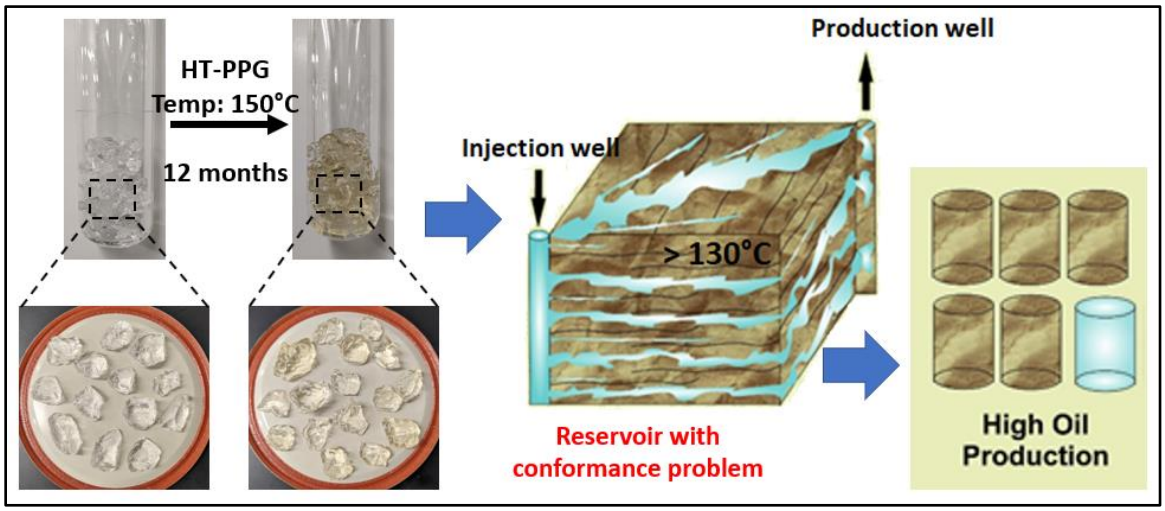

Keywords: Preformed particle gels, Thermal stability, Hydrolytic stability, Enhanced oil recovery, Conformance control

HIGHLIGHTS

- State-of-the-art ultra-high temperature resistant hydrogel (HT-PPG) developed.
- HT-PPGs exhibit excellent long-term thermal stability.

- HT-PPGs are stable for 18 months in 2% KCl (water content ~ 93 wt.-%) at 150 °C.
- HT-PPGs are mechanically robust and can swell more than 30-fold in brines.
- HT-PPGs facilitate plugging of open fractures void space conduits.
- Candidate for solving ongoing conformance problems associated with oil recovery.

1. INTRODUCTION

Excess water production is a major concern for most of mature oilfields around the world. Excess water production drastically reduces oil well productivity, causes corrosion & scale, increases environmental concerns and impacts, and can elicit sometimes severe economic challenges, which results in shutting down of production wells [1]. Controlling the excess water production has been a major obstacle for the oil industry for several decades [2]. Plugging these high permeability water thief zones, the massive heterogeneous void space conduits, is a proven cost-effective method [3]. By plugging the thief zones with a polymer or other material, it directs injection water to go through less porous regions, thereby improving oil recovery. The plugging of high permeability zones can be done by two methods, *viz*; in-situ crosslinking gels and preformed particle gels (PPGs).

In case of in-situ gel treatment, polymers and crosslinkers are simultaneously injected to the formation where gel is formed under reservoir conditions and seal off these water thief zones. Despite this characteristic, in-situ crosslinking gels can possess

drawbacks in plugging these thief zones, i.e., a lack of control over the gelation time, gelling uncertainty due to shear degradation, chromatographic fractionation, and/or dilution [1]. Several groups have presented different modifications of in-situ gels to improve their thermal stability using associative metallic crosslinkers like Cr^{3+}, organic crosslinkers like phenol–formaldehyde gels [4, 5] and polyethylene imine (PEI) based systems [6-8], hydroquinone HMTA systems [9], etc. As yet, most of these systems cannot withstand higher temperature greater than 140 °C and high salinity for more than 1 month.

On the other hand, to overcome the drawbacks of in-situ gel treatments [1, 10-13] toward solving conformance control problems, industry experts and researchers came up with a novel technology called preformed particle gels (PPGs). PPGs are three-dimensional, dried, cross-linked, polymeric granules that, on contact with/dispersion in formation water, have ability to swell from several to several hundred times their dry particle size. PPGs can be sensitive to physiochemical conditions of reservoirs like pH, multivalent ions, salinity, temperature, etc. [14, 15].

PPG technology was novel in terms of addressing problems posed by in-situ gel treatments, including sealing as damage to low permeability zones [16]. As an all-in-one package, PPGs avoid segregation via chromatographic problems, associated with traditional in-situ gels. PPGs treatments are of interest because they have decades-worth of successful field application and are inexpensive, relatively easy to synthesize and handle in the field. PPGs are used to redirect water flow from high permeability zones or fractures with residual hydrocarbon saturation towards unswept hydrocarbon rich zones [17-21].

Despite the advantages of PPGs over in-situ gels, PPGs have not provided a complete solution to conformance control problems associated with reservoir heterogeneity. Conventional PPGs are based on polyacrylamide homopolymer networks, which degrade at higher temperatures and high salinity conditions [22, 23]. Exposures to harsh conditions of high salinity, formation hardness, and temperature undergo syneresis as a result of hydrolysis of the amide groups and rapid structural degradation of its primary structure [24]. It has been observed that PPGs can suffer mechanical degradation under shear conditions. Toward improving thermal stability and other harsh conditions, several approaches, *viz.*, introduction of inorganic fillers [25], copolymerization with 2-acrylamido-2-methylpropane sulfonic acid (AMPS) or N-vinyl pyrrolidone (NVP) monomers [26] have been reported. These PPGs have proven stable at harsh reservoir conditions of temperature and salinity for periods of several months. However, to our knowledge there are no PPGs with long-term thermal stability at temperatures up to 150°C have been reported.

Recently, our group has developed high temperature stable PPGs (HT-PPGs) based on poly(dimethylacrylamide-co-styrenesulfonate) for reservoirs with harsh conditions. In this article, a systematic approach for development of a unique hydrogel composition is discussed based on screening for thermally stable polymer components. Polymers of dimethylacrylamide and sodium styrene sulfonate showed exceptional hydrolytic thermal stability compared to traditional acrylamide-based hydrogel systems, which enabled a synthesis of an HT-PPG with characteristic features. The HT-PPGs are here demonstrated to withstand temperatures of 150°C and high pressure of up to 100 psi for a minimum of 18 months with no loss of molecular integrity.

A detailed evaluation of the product in several formation brines for swelling kinetics, pH effect, rheological strength, morphology, thermal stability, and core flooding test results are presented and discussed. The mechanically and thermally robust HT-PPGs can be dispersed into formation brine and pumped into the formation. During their transport through the formation, all dispersed HT-PPGs can move together and helps in avoiding the segregation and chromatographic problems associated with traditional in-situ gels. These HT-PPGs can be a good candidate for gel treatments in reservoirs with high temperature and high salinity conditions.

2. EXPERIMENTAL

2.1. MATERIALS

All chemicals and reagents were purchased from Sigma-Aldrich (St. Louis, MO) except as noted. Poly (sodium-p-styrenesulfonate), PSSS, ~70,000 Da, polyacrylamide, PAM, ~150,000, and poly (N, N'-dimethylacrylamide), PDMA, ~100,000 Da, were obtained from Scientific Polymer Products, Inc. (Ontario, NY). 2,2'-Azobis[2-(2-imidazolin-2-yl) propane] dihydrochloride (VA-044) initiator and sodium styrene sulfonate (NaSS) monomer were used as received. N, N'-dimethylacrylamide (DMA) or divinylbenzene (DVB) monomers were passed through a basic alumina column prior to use. Ultra-high purity argon gas (99.999%) was obtained from Airgas.

2.2. POLYMER THERMAL AND HYDROLYTIC STABILITY

Aqueous solutions of polymer were prepared by dissolving PDMA, PSSS or PAM in deionized water (DI) and sparged under ultra-high purity argon gas. The concentration of polymers in aqueous solutions were adjusted to produce a final viscosity in the range of 5 to 10 cP on Brookfield DVIII viscometer at 23°C. Polymer solutions were transferred to high pressure glass tubes under argon atmosphere, sparged under argon and sealed. These samples were aged at temperatures, *viz:* 80, 130, or 150 °C, and periodic viscosity measurements were performed at variable time intervals.

2.3. HT-PPG HYDROGEL SYNTHESIS

HT-PPG hydrogels were prepared by free radical polymerization in aqueous solution using a closed kettle reactor. A typical polymerization procedure is as follows: NaSS (2.68 g, 5 mol%), DMA (24.46 g, 95 mol%) and DVB (0.034 g, 0.1 mol%) were dissolved in DI water sparged under argon gas. Polymerization was initiated by adding VA-044 initiator (0.168 g, 0.2 mol%) and reaction was continued for 24 hours at room temperature. The resulting hydrogel was cut in small cubes, dried at 60 °C in oven and pulverized before characterization and evaluation. Particle size used for analysis of swelling, thermal stability and conformance control was 1 to 2 mm (mesh size -10 +18).

2.4. FOURIER TRANSFORM INFRARED SPECTROSCOPY (FT-IR)

Spectroscopic analysis was carried out on monomers and PPGs. Polymer samples were dried in a vacuum oven chamber for 2 days prior to measurement of FTIR spectra. FTIR spectra were recorded between 4000 and 400 cm^{-1} with setting of 16 signal-

averaged scans at a resolution of 2 cm^{-1} using Nicolet iS50 FT-IR spectrometer (ThermoFischer Scientific).

2.5. SWELLING KINETICS

The swelling kinetics were performed by immersing a weighed dried hydrogel sample in the respective brine. The kinetics of change in volume of HT-PPGs with respect to time was studied until the equilibrium swelling ratio was achieved. The measurements were performed at different conditions with reference to brine of different ionic strengths, pH and temperature. The swelling ratio of PPGs can be calculated using the equation (1), where, V_t is volume of PPGs at particular time t and M_0 is the initial mass of dried PPGs [15].

$$SR = V_t / M_0 \quad (1)$$

2.6. RHEOLOGICAL STUDIES

The rheology measurements were performed using Haake MARS III rheometer with a parallel plate geometry (PP35L Ti L) with a gap of 1mm. All sets of rheological measurements were carried out in ambient room temperature conditions. Strain sweep tests were carried out using the oscillation strain-dependent experiment model at a fixed frequency of 1 Hz in order to determine the linear viscoelastic region over which storage modulus, *G'* is independent of strain amplitude. The rheology measurements were performed as the oscillation time-dependent experiment model at a fixed frequency of 1 Hz and controlled strain (γ) of 1% to measure storage modulus (*G'*) as a function of time.

2.7. THERMAL STABILITY EVALUATIONS

The thermostability tests for HT–PPGs were carried out in high pressure glass tubes with temperature resistant O-rings. In thermal stability evaluation, oxygen free environment is very critical, as it can cause oxidative polymer degradation. Samples for thermal stability evaluations were prepared precisely to create towards oxygen free environment as shown in schematic Figure 1 using cannulation transfer. Before cannulation transfer, brine solution was purged with ultra-high purity argon gas for 60 mins. The pressure tube with dry HT-PPGs was kept under argon gas for 10 mins before starting the cannulation transfer. The predetermined amount of brine solution depending on the required swelling ratio (10, half equilibrium, equilibrium, and excess brine) was transferred. The pressure tubes were further maintained under argon environment for 30 mins before sealing. HT-PPGs thermal stability was checked by monitoring the retention of swollen HT-PPGs volume on aging at 150 °C as a function of time.

2.8. CPMAS ^{13}C SOLID STATE NMR ANALYSIS

The retention of chemical signature of HT-PPG after aging was studied with solid-state CPMAS ^{13}C NMR on a Bruker Avance III 400 MHz spectrometer with a carbon frequency of 100 MHz, using a 7 mm Bruker MAS probe at a magic angle spinning rate of 5 kHz with broadband proton suppression, and CP total suppression of spinning sidebands (TOSS) pulse sequence. The TOSS pulse sequence was applied by using a series of four properly timed 180° pulses on the carbon channel at different points of a cycle before the acquisition of the FID, after an initial excitation with a 90° pulse on the proton channel. The 90° excitation pulse on the proton and the 180° excitation pulse

on carbon were set to 4.2 and 10 μs, respectively. The cross-polarization contact time and the relaxation delay were set at 2000 μs and 5 s, respectively. The number of scans was set at 2048. Spectra were referenced externally to glycine (carbonyl carbon at 176.03 ppm). Chemical shifts are reported versus TMS (0 ppm).

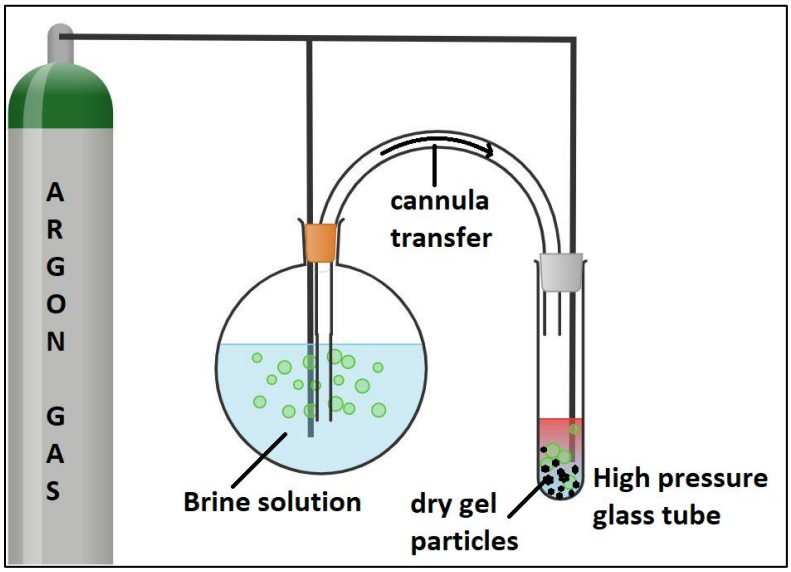

Figure 1. Set up for HT-PPG sample preparation in brines for thermal stability test

2.9. THERMOGRAVIMETRIC ANALYSIS (TGA)

Thermal stability of the PPGs before and after aging at 150 °C temperature in 2% KCl solution were studied using TGA Q50 (TA instruments), under a nitrogen atmosphere at a heating rate of 10 °C/min. Samples were scanned from room temperature to 700 °C temperature range. The swollen PPGs were frozen using liquid nitrogen and then freeze dried in vacuum for 2 days, then the obtained dried gels were ground with the help of mortar. Samples ranging from 10 to 20 mg were tested in alumina pans.

2.10. MORPHOLOGY CHARACTERIZATION

The hydrogel microstructure was characterized using Hitachi S-4700 field emission scanning electron microscope (SEM). Swollen gels were frozen in liquid nitrogen and then freeze dried at -50 °C and 30 x 10^{-3} mbar pressure for 48 hours to obtain aerogels. The freeze-dried aerogels were plunged into liquid nitrogen and carefully fractured to obtain a fresh cross-section, which was mounted on aluminum stub and sputter coated with a thin layer of gold for scanning. SEM imaging was performed at 10 kV.

2.11. LABORATORY COREFLOODING TEST

The coreflooding experiment was performed to examine the HT-PPG efficiency in plugging open fracture/ void space conduits (VSC). A sandstone core with 2 in. diameter and 5 in. length was used for the test. Initially the core was oven dried to remove any residual water in the core, then the core was vacuumed for 24 hours, and saturated with 1% NaCl. Figure 2a shows the schematic diagram of the coreflooding test, where the core was placed inside the coreholder and a confining pressure of 700 psi was applied to the core. Then, the core was flooded with 1% NaCl at different injection flow rates, the resulted stabilized pressure gradients were recorded, and the matrix permeability was calculated based on Darcy's law. Thereafter, the core was removed from the coreholder and cut uniformly into two halves where stainless steel strips with a thickness of 0.077 in. were glued on the surface of the core and the fractured core was wrapped with Teflon sheet as shown in Figure 2b. Table 1 summarizes the matrix and the fracture properties of the core used in the evaluation.

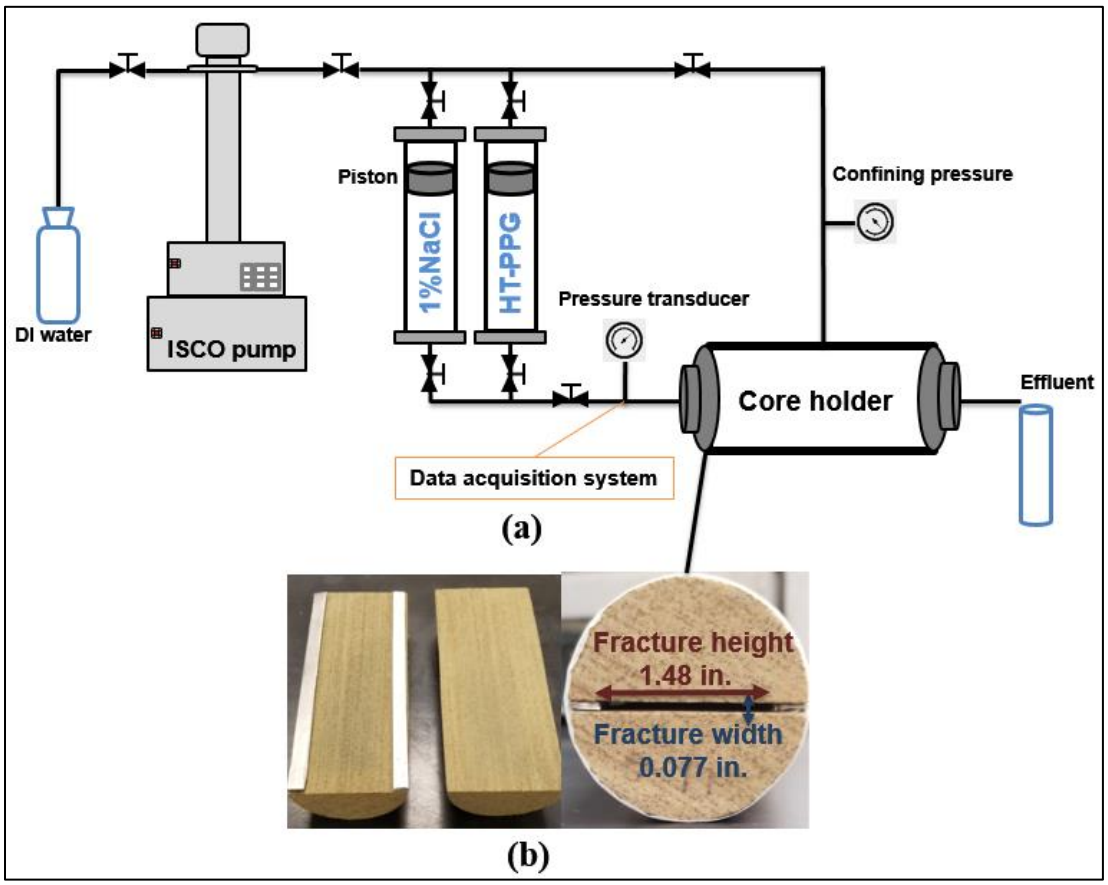

Figure 2. (a) Schematic diagram of the coreflooding test, (b) the configuration of the fractured core

Table 1. The matrix and the fracture properties of the core.

D (in.)	L (in.)	Pore volume (PV)	Porosity, % (φ)	Permeability (md)	Fracture width (in.)	Fracture height (in.)	Fracture Volume (FV)
2.0	5.0	51.9	20.2	83.9	0.077	1.48	0.57 in^3, 9.3 cm^3

The fractured core was flooded with 1% NaCl at a constant injection flow rate of 1.0 m/min until a stabilized pressure gradient was reached. Then, the HT-PPG with

swelling ratio of 1/10 in 1 % NaCl was placed inside the accumulator and injected through the fracture using 0.5 ml/min provided from the Isco pump. After the gel placement pressure gradient was stable, post water injection at different injection flow rates were carried out in order to determine the extent at which the HT-PPG reduced the effective permeability of the fracture and subsequently diverted the chase water into the matrix.

3. RESULTS AND DISCUSSION

3.1. POLYMER THERMAL AND HYDROLYTIC STABILITY

A systematic approach for development of thermally resistant hydrogels was adapted in this study. Commercially available polymers were studied for thermal and hydrolytic stability in aqueous solutions at different temperature. Polyacrylamide is a widely studied polymer which readily degrades at higher temperatures [22, 24]. Similar observations were noted in our studies, where a more than 85% viscosity loss was observed over 3 months of aging time in water at 130 °C (see Table S1 in Supporting Information). Solution viscosity loss can be correlated to the loss of molecular weight due to random thermal degradation of polymer chains [27]. The decrease in the viscosity of PAM aqueous solution is as a result of degradation which occurs through two mechanism *viz;* oxidation-reduction reaction which cause breaking of carbon-carbon bonds in polymer chain and hydrolysis reaction with almost 100% degree of hydrolysis [28].

On the contrary, PDMA and PSSS showed a better than 80% of viscosity retention after aging for 5 months at different temperatures including 150°C (see Table

S1 in Supporting Information). PDMA undergo limited degree of hydrolysis because of alkyl substitution on nitrogen. As a result, resonance stabilization stretched configuration formed causing slight increase in the viscosity. Alkyl substitution on nitrogen causes increase of activation energy for hydrolysis due to inductive effect, which makes it difficult for nucleophilic attack of hydroxyl ion on the carbonyl atom [29]. Thus, PDMA showed better thermal and hydrolytic stability than PAM.

The viscosity retention after exposure to high temperature conditions attributed to polymer molecular weight retention, confirming these polymers are stable under high temperatures and exhibit exceptional thermal and hydrolytic stability. Thermally stable polymer backbone is inevitable for high temperature resistant hydrogel development and therefore, construction of such hydrogels based on DMA and NaSS monomers chemistry can produce thermally robust materials.

3.2. HT-PPG HYDROGEL SYNTHESIS

HT-PPG, a preformed particle gel, was synthesized by copolymerization of DMA, NaSS, and a thermally stable covalent crosslinker divinylbenzene by an azo-type initiator, as depicted in Figure 3. The resulting HT-PPG gel was transparent with apparent bulk density of 1.3 g/cc and, when dried, contained less than 5% moisture content. The FT-IR spectrum of the dried gel is shown in Figure S1 of Supporting Information that confirmed the presence of NaSS at 670 cm^{-1} for aromatic C-H out of plane bending vibration, 1010 and 1130 cm^{-1} for in-plane bending and in-plane skeleton vibration of benzene ring, respectively. Additional absorptions at 1040 and 1180 cm^{-1} correspond to symmetric and asymmetric vibration absorption of SO_3^- groups,

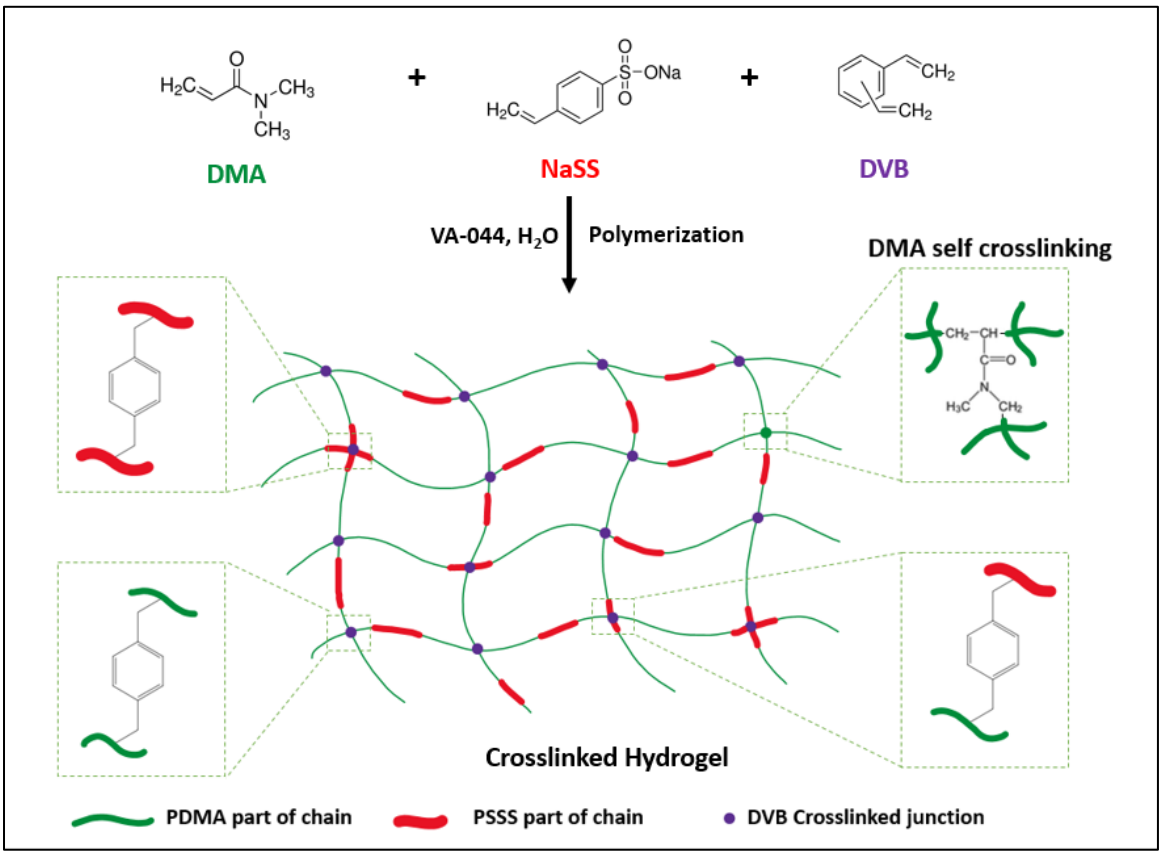

Figure 3. General synthetic scheme for HT-PPG hydrogel synthesis

respectively. Absorption by DMA at 1615 cm^{-1} confirmed the C=O stretching absorption by amide functionality present in the copolymer. The characteristic C-H bond from DMA units at around 2920 cm^{-1} was observed for vibration due to CH_3 groups. A small absorption at ~800 cm^{-1} is assigned to the presence of the DVB crosslinker.

3.3. SWELLING KINETICS

HT-PPG dry particles with the size of 1 to 2 mm were used for swelling kinetics measurements. The effects of NaCl brine on swelling kinetics and equilibrium swelling ratio was studied at 23 °C (Figure 4). It was observed that degree of salinity affects the

swelling kinetics behavior. Lower concentration brine (1% NaCl) showed relatively faster swelling kinetics than a higher concentration brine (20% NaCl). In case of 20% NaCl solution, it required 36 hours to attain an equilibrium swelling ratio whereas in 1% NaCl solution, it required merely 18 hours to achieve equilibrium swelling ratio. Osmotic pressure describes the strength of the interaction between polymer and solvent [30]. At the beginning of swelling process, diffusion of Na^+ and Cl^- ions will be faster due to the concentration gradient difference that results into faster swelling rate. Towards the end of swelling process, diffusion rate will be slowed as the polymer matrix becomes saturated with these ions, resulting in an infinitesimally small concentration gradient, which results in slower swelling rate [31]. Interestingly, brine salinity did not show major influence on

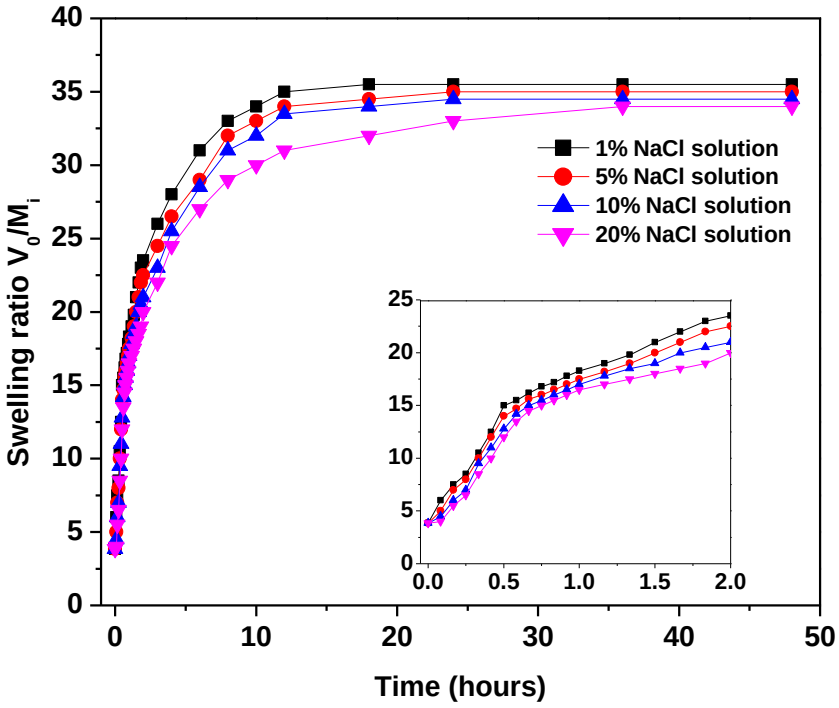

Figure 4. Swelling kinetics behavior of HT-PPG in NaCl brines at different concentrations at 23°C. Inset shows the swelling kinetics of HT-PPG in first two hours period.

the measured equilibrium swelling ratio. Equilibrium swelling ratios observed for 1% NaCl and 20% NaCl brines were near 35.5 and 34.0 (each averaged over 3 experiments), respectively. It was also noted that HT-PPG showed higher swelling ratio than some previously reported PPGs [13].

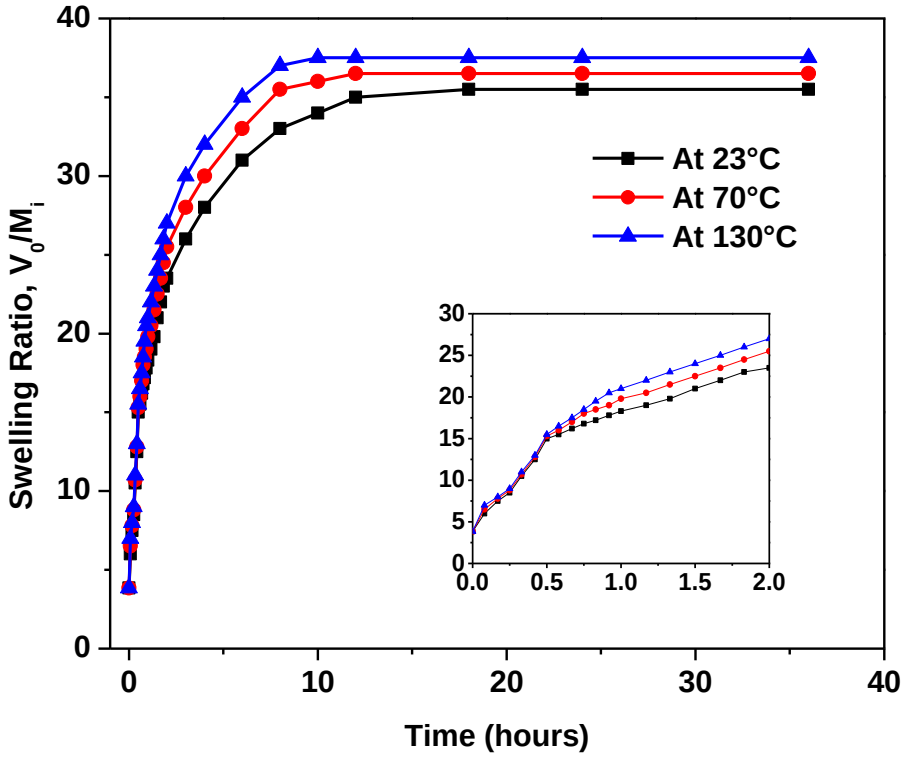

Figure 5. Swelling kinetics behavior of HT-PPG in 1% NaCl brines at 23, 70 and 130 °C. Inset shows the swelling kinetics of HT-PPG in first two hours period.

Effect of temperature on swelling kinetics of HT-PPG in 1% NaCl solution at 23, 70 and 130 °C was evaluated. Figure 5 illustrates increase of rate of swelling and equilibrium swelling ratio with increase in temperature used for swelling experiments. An equilibrium swelling ratio of 37.5 was achieved within 10 hours at 130 °C while, at a room temperature condition, it took 18 hours to reach its equilibrium swelling ratio of

35.5. Swelling process time for a hydrogel is determined by the diffusion of the polymer network into water and Flory Huggins polymer solvent interaction parameter (χ) [30, 32]. Higher diffusion rates can be expected with increase in temperature, which in turn results in faster swelling behavior [30, 33].

In order to assess swelling behavior further, HT-PPG dry particles were studied for equilibrium swelling ratio in fixed ionic strength brines as a function of pH at 23 °C. A 1% NaCl solution was used and pH was adjusted with dilute solutions of HCl and NaOH to prepare acidic and basic solutions. Figure 6 demonstrates that change in pH does not make a significant effect on equilibrium swelling ratio. Further, we studied effect of multivalent ions on swelling behavior of HT-PPG by swelling in monovalent and divalent ions containing brines were at 23 °C. Equilibrium swelling ratio found to

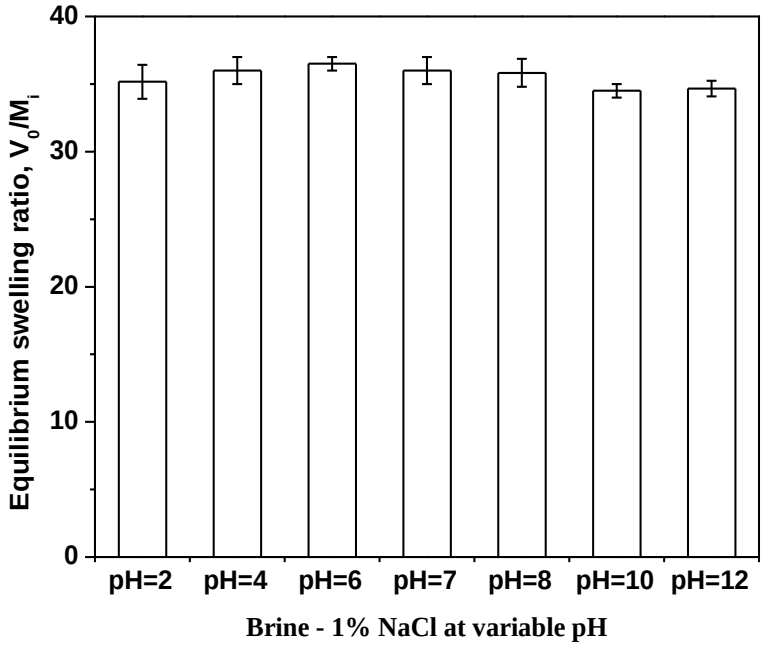

Figure 6. Equilibrium swelling ratio in 1% NaCl solution as a function of solution pH at 23 °C (n=3).

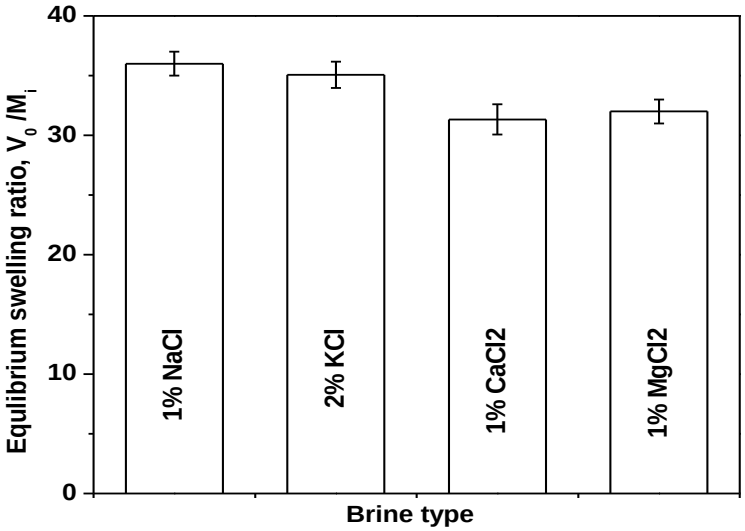

Figure 7. Equilibrium swelling ratio of HT-PPG in 1% NaCl, 2% KCl, 1% $CaCl_2$ and 1% $MgCl_2$ at 23 °C (n=3).

decrease slightly in presence of divalent ions (Ca^{2+}, Mg^{2+}) than monovalent ions (Na^+, K^+) as shown in Figure 7. This can be attributed to weak binding of monovalent ions compare to the multivalent ions which interact strongly with the oppositely charged polyelectrolyte structures. Presence of multivalent ions bring change in thermodynamic interactions among polymer-solvent system where conformation change from expanded coil to slightly contracted state occurs causing lowering of swelling degree. These findings are in accordance with the observations found in Horkay, et al. [34] and Sircar, et al. [35], where divalent ions can increase the mixing free energy, causing lower degree of swelling.

3.4. RHEOLOGY MEASUREMENTS

The strength of PPGs is of great importance to be used as a plugging agent for conformance control which is essential to decrease reservoir heterogeneity and increase

oil recovery. The linear viscoelastic region was determined to set the parameters for the measurements. It was noticed that there was no deviation from the linear region up to 10% of shear strain and 10 Hz frequency (Figure 8). This confirmed the chosen parameters of 1Hz frequency at controlled strain (γ) of 1% holds good for storage modulus measurements. The HT-PPGs dry particles with 0.85 to 1 mm size with variable swelling ratio in 1% NaCl brine was studied for storage modulus measurements as shown in Figure 9. At swelling ratio of 10, elastic modulus of over 3100 Pa was obtained while it was reduced to 900 Pa at equilibrium swelling ratio of 35.5. At equilibrium swelling ratio, polymer network chains are in fully extended conformation, where polymer concentration per unit volume of hydrogel is lower as compared to hydrogels at limited/ lower swelling ratio, thus lowering the elastic modulus at equilibrium swelling ratio.

To further investigate the robust nature of HT-PPGs, compression test was performed on Instron 4469 Universal testing machine. As shown in Figure S2a, HT-PPG can be compressed to a 80% strain without breaking and can recover to its original shape within 15 minutes after removing the pressure. Compressive modulus of 0.3 MPa was obtained from the compression stress-strain curve (Figure S2b). This demonstrated the outstanding mechanical properties and robust structure of HT-PPGs that displayed uniform stress distribution throughout the crosslinked polymer matrix under compression load. HT-PPGs demonstrated better mechanical strength than previously reported robust nanofiller induced preformed particle gels [14]. This further confirmed the robust mechanical strength of HT-PPG is merely result of strong and stable polymer backbone.

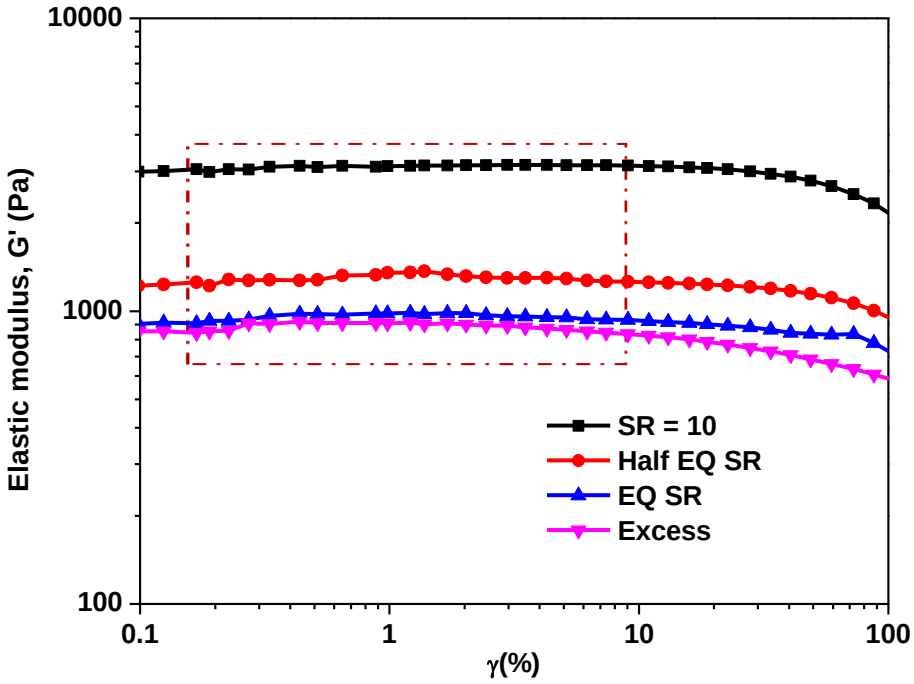

Figure 8. Effect of change in strain (γ) on storage modulus (G') of HT – PPG in 1% NaCl brine at variable swelling ratio, 23 °C (linear viscoelastic region is shown by dotted rectangle).

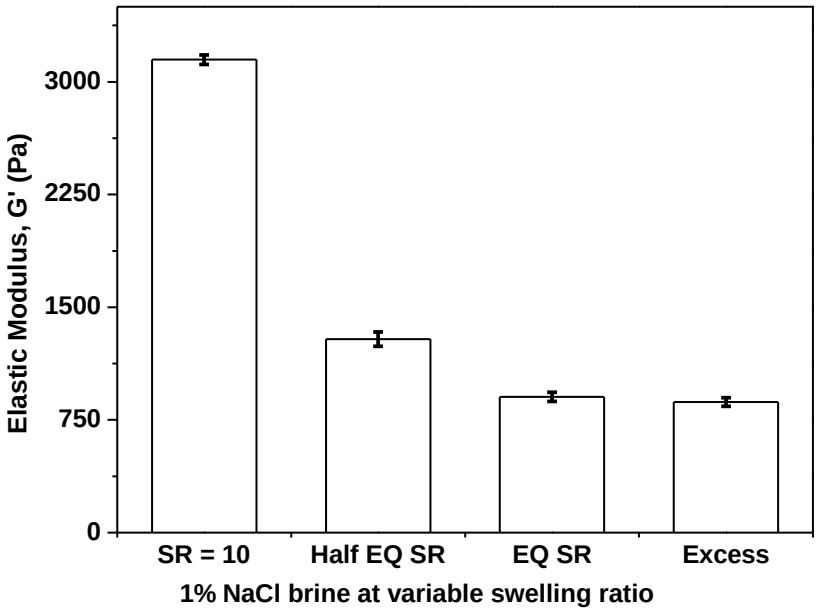

Figure 9. Effect of swelling ratio (SR) on storage modulus (G') of HT – PPG in 1% NaCl brine at 23 °C, (n=3).

3.5. THERMAL STABILITY EVALUATIONS

HT-PPG thermal stability was evaluated for more than 370 days in different brine solutions at variable swelling ratios. The change in swelling ratio was monitored periodically and any observations for hysteresis behavior or visual sign of degradation were noted. Figure 10 represents percent retention of hydrogel volume as a function of exposure time in different brine compositions. As seen in Figure 10a, HT-PPGs are stable with no change in initial volume of hydrogel for more than 370 days at 150 °C for 1% NaCl brine, at swelling ratio of 10 and half equilibrium swelling ratio (Half EQ SR). At higher swelling ratios, i.e., equilibrium swelling ratio (EQ SR) and excess brine, gels are stable for more than 370 days with less than 5% of volume change, which can be attributed to the surface water. Similar observations were noted with 2% KCl and 1% $CaCl_2$ brines, where HT-PPGs are stable for more than 370 days up to half EQ SR (Figure 10b, 10c). For equilibrium swelling ratio and excess brine conditions less than 10 and 12.5% hydrogel volume change was observed after 370 days of aging.

Aged HT-PPGs were recovered from pressure tubes after 12 months and did not show signs of degradation. Integrity, shape, size and edges of gel particles, were maintained over 12 months of aging at 150 °C in different brine solutions at all swelling ratios. Figure 11 shows the appearance of swollen gel particles before and after aging at 150 °C for EQ SR and confirmed that the structural integrity of gel particles retained during the thermal aging. This can be attributed to the thermally stable polymer backbone of Poly (DMA) and Poly (NaSS), which retains its chemical signature after aging. Some aged particles showed slight brown color presumably as a result of oxidation process induced by slight amount of oxygen left behind in the pressure tubes during sample

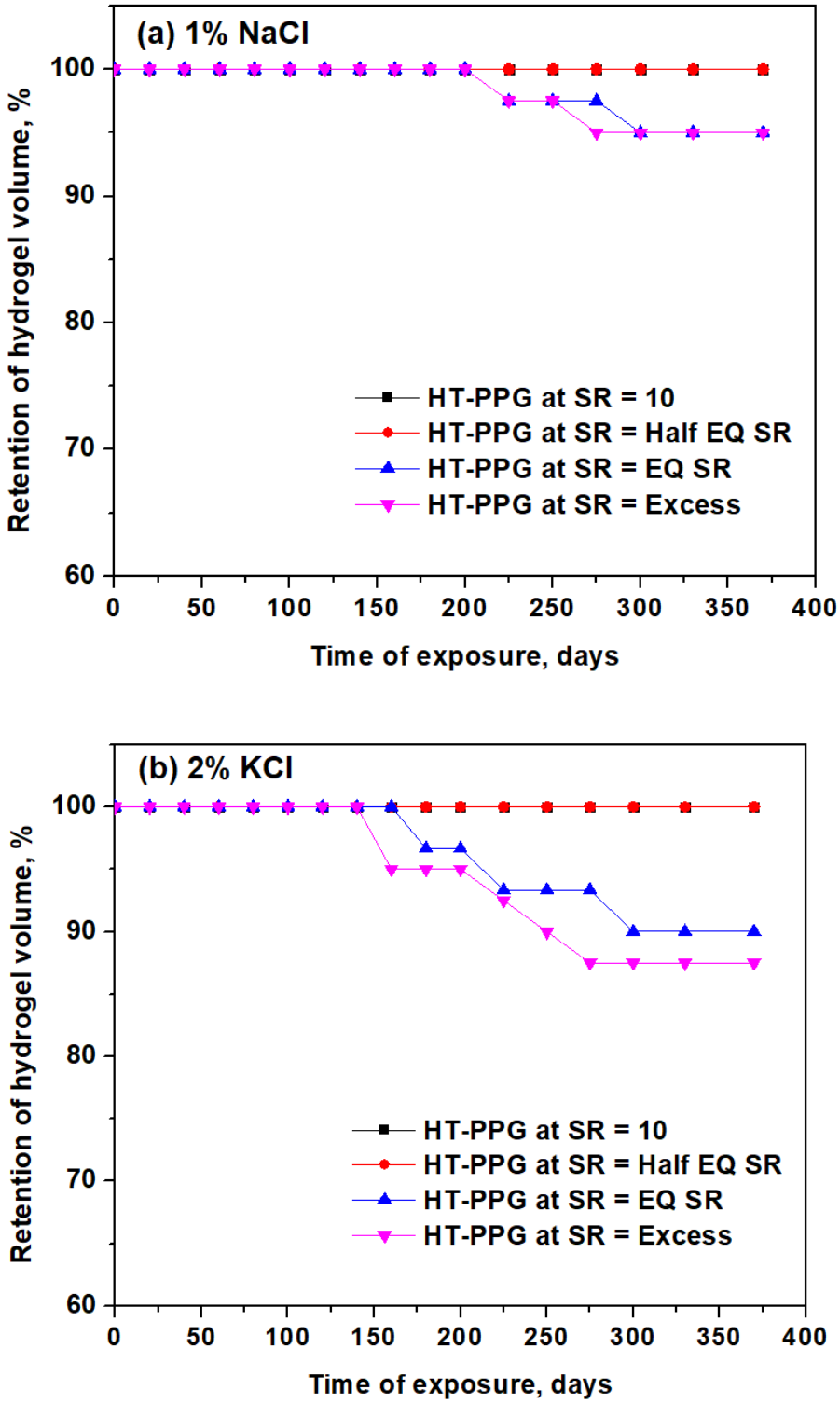

Figure 10. Hydrolytic thermal stability of HT-PPG at swelling ratio of 10, half EQ SR, EQ SR and in excess brine with respect to time for (a) 1% NaCl, (b) 2% KCl and (c) 1% $CaCl_2$ brine at 150 °C temperature.

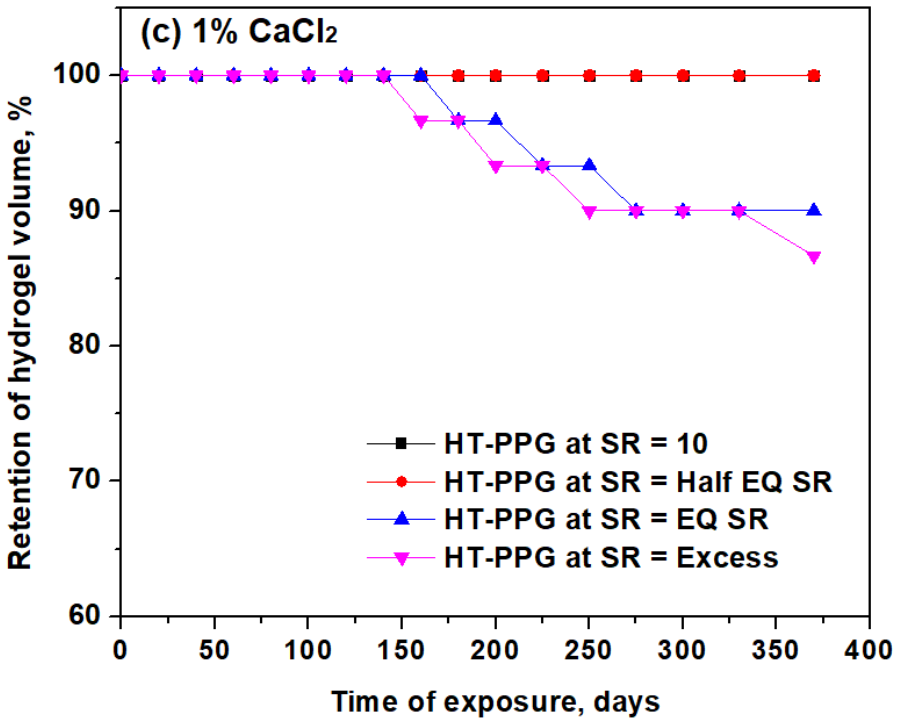

Figure 10. Hydrolytic thermal stability of HT-PPG at swelling ratio of 10, half EQ SR, EQ SR and in excess brine with respect to time for (a) 1% NaCl, (b) 2% KCl and (c) 1% $CaCl_2$ brine at 150 °C temperature. (Cont.)

preparation. HT-PPGs chemistry showed long-term stability to thermal and ionic environments.

A 2% KCl solution is a commonly used injection brine in well treatments as it can inhibit shale hydration [36]. Oil producing companies can apply lower swelling ratios of 10 to 15 in 2% KCl for gel injection treatments [37] to provide higher strength and minimize injection variance while filling a void space to ensure complete space filling by gel via consumption of the injection and void fluid through injected gel particles. Therefore, one of the conditions performed to assess long term thermal stability of HT-PPG was a 2% KCl brine at swelling ratio of 15.

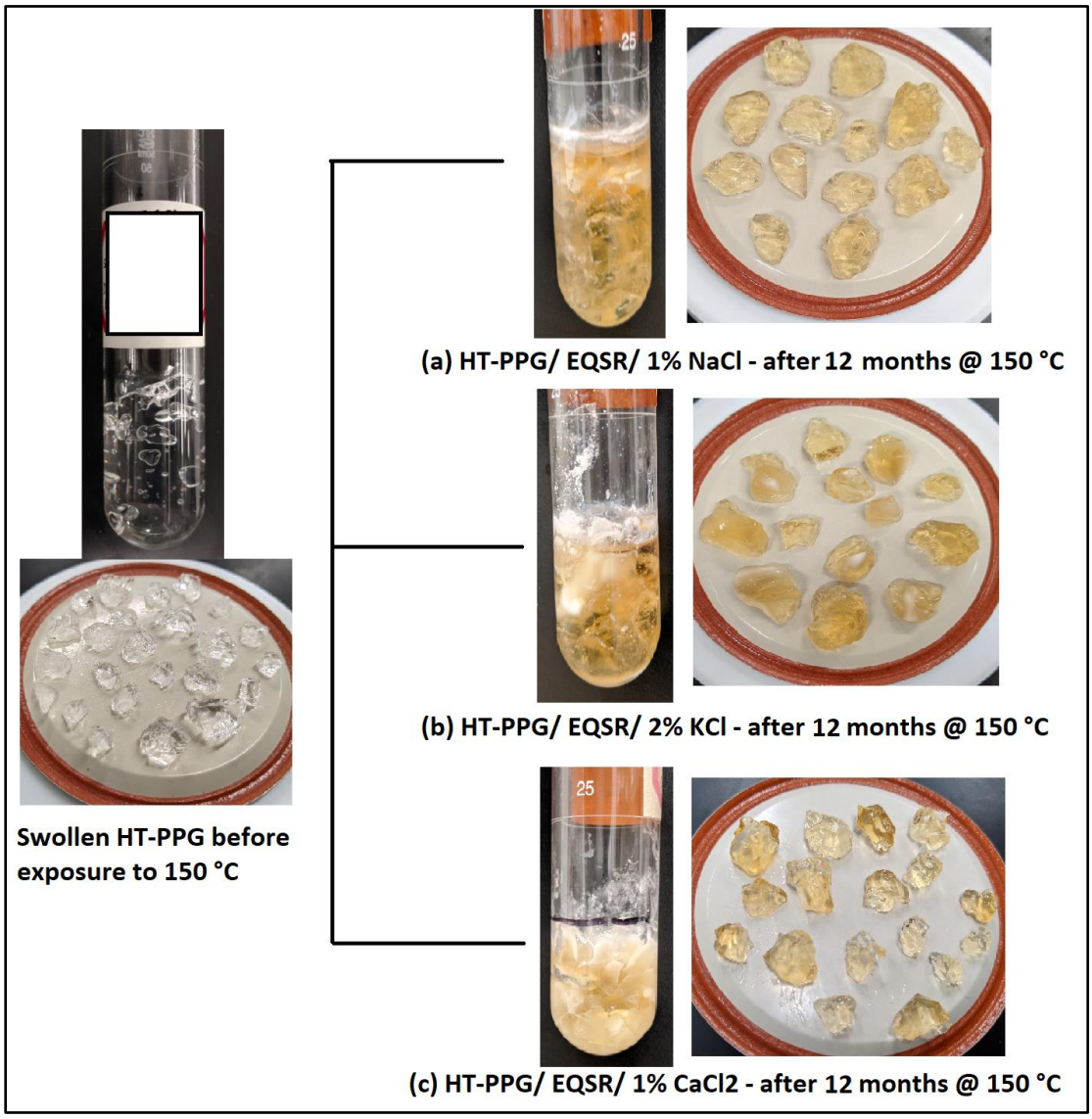

Figure 11. Thermal stability evaluation of HT-PPG in variable brines at equilibrium swelling ratios (EQ SR), aged at 150 °C temperature for 12 months

The product evaluation was performed similarly to that discussed earlier, with periodic measurements for volume change and checking for visual signs for degradation. HT-PPG showed stability towards 2% KCl brine and 150 °C temperature for more than 18 months with no sign of degradation or syneresis as shown in Figure 12. Color change of gels can be attributed to a residual amount of oxygen in glass tubes causing oxidative

thermal oxidation or seal degradation leakage. Despite steam-durable o-ring seals being used, some degradation at the longest exposure times was observed. Testing under oxygen exposure replicated the color change.

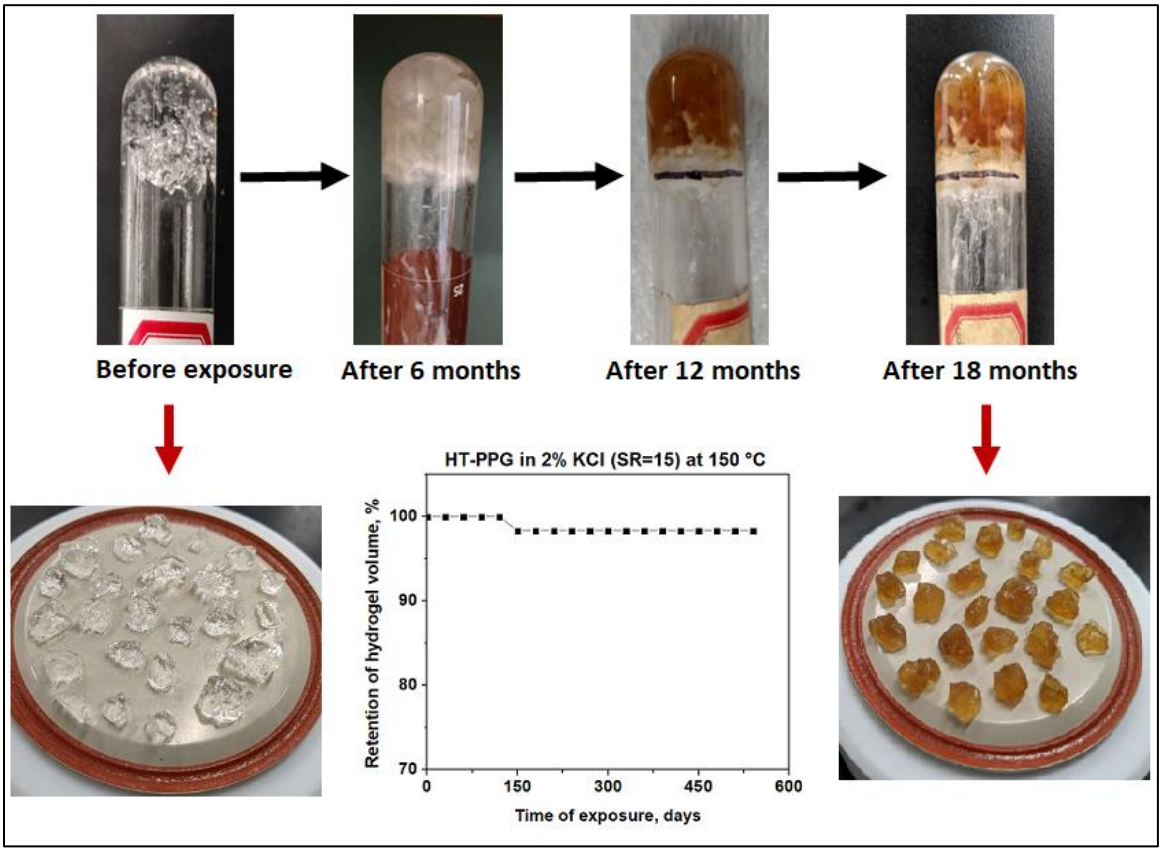

Figure 12. Thermal stability evaluation of HT-PPG in 2% KCl at SR = 15 and temperature of 150 °C. HT-PPGs recovered after 18 months of aging shows retention of structural integrity and form of gel particles. Plot for retention of hydrogel volume with respect to time does not show significant syneresis (original hydrogel volume change) or water loss.

Many polymers undergo significant changes when exposed to heat, oxygen, and water. The deterioration mechanisms for thermal degradation (when heat is the driving force) are different from hydrolytic thermal degradation (when heat and water are both

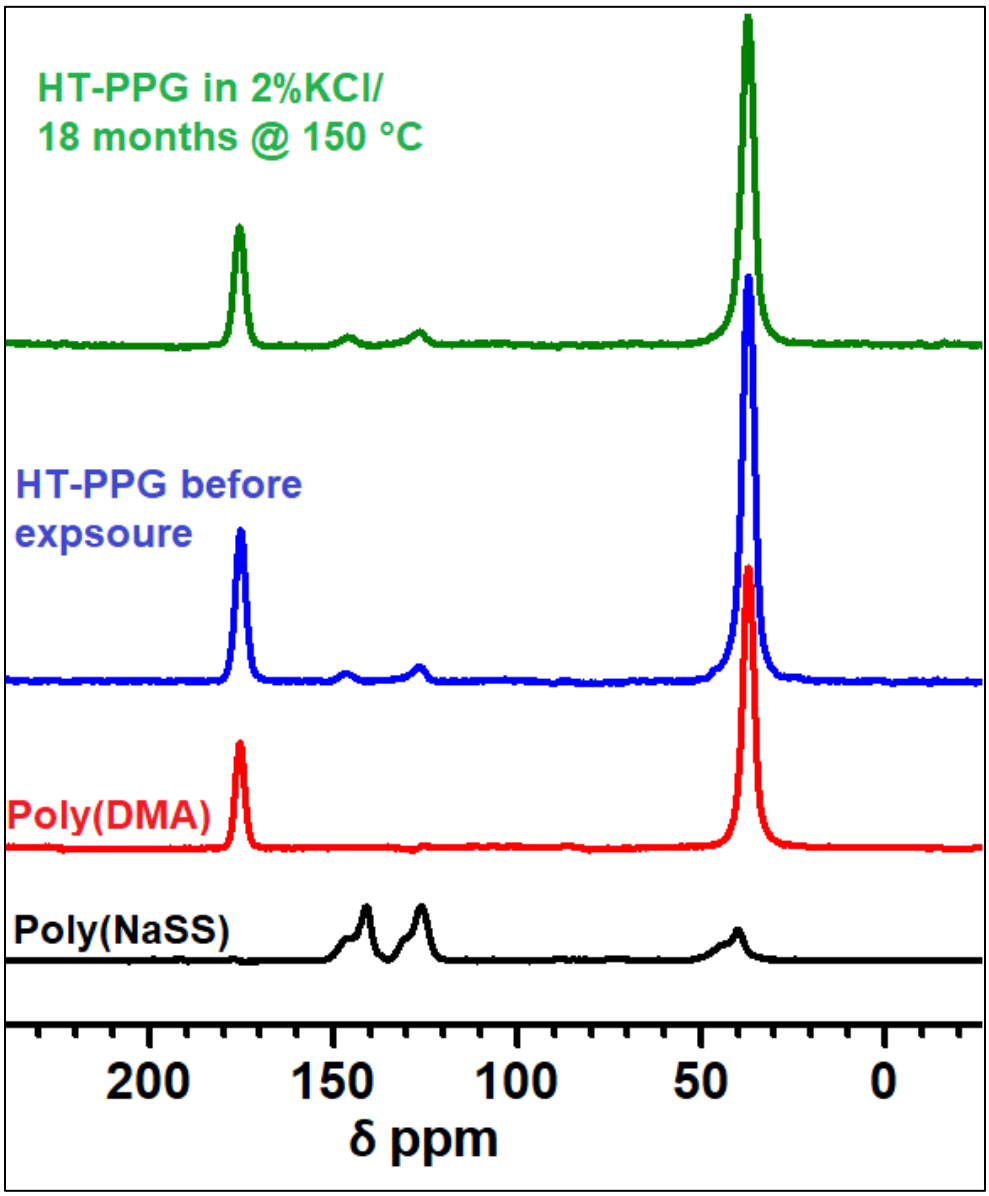

Figure 13. Solid-state CPMAS ^{13}C NMR for polymers Poly (NaSS), Poly (DMA), HT-PPG before aging as control sample and HT-PPG aged in 2% KCl (SR=15) at 150 °C for 18 months

present) of polymers just as the presence of oxygen has a strong chemical influence on degradation mechanisms. Each phenomenon can be quite different, having their own significances with respect to information one tries to infer from these analyses. While

water and heat are present in oil reservoir conditions, reservoir environments are anaerobic.

In case of gel treatment for conformance control, PPGs are applied in contact with multivalent brines during their use and hence it is important to study their hydrolytic thermal stability under similar conditions. If HT-PPGs degrade under on hydrolytic thermal conditions (in the presence of heat and water), volatile small molecules or non-volatile moieties such as oligomeric units, cyclized compounds, etc., should be produced. Each compound should have a unique chemical shift which pertains to their polymeric chemical structure and composition. Therefore, if HT-PPGs are truly degrading during long term aging at 150 °C in presence of high ionic strength brines, it will generate new compounds. On freeze-drying of these aged HT-PPGs, a dry aerogel mass is obtained that comprises the leftover polymer matrix along with nonvolatile degradation products. These degradation products may be seen via solid-state CPMAS ^{13}C NMR in the form of new distinct peak associated with their new chemical makeup.

To illustrate the retention of chemical composition that provides bulk properties of HT-PPG after aging at 150 °C, solid-state CPMAS ^{13}C NMR was performed on a Bruker Avance III 400 MHz spectrometer. HT-PPG sample before exposure as control sample and aged sample in 2% KCl (SR=15) at 150 °C for 18 months were freeze dried to remove water. Commercial samples of Poly (DMA) and Poly (NaSS) polymers were used and ^{13}C signals corresponding to their respective structure were used for peak assignments in HT-PPGs. Solid-state ^{13}C NMR, Figure 13, showed that HT-PPG aged sample was chemically identical to HT-PPG control sample. This further confirmed that

HT-PPG compositions remain stable on aging at 150 °C and retain their chemical signature.

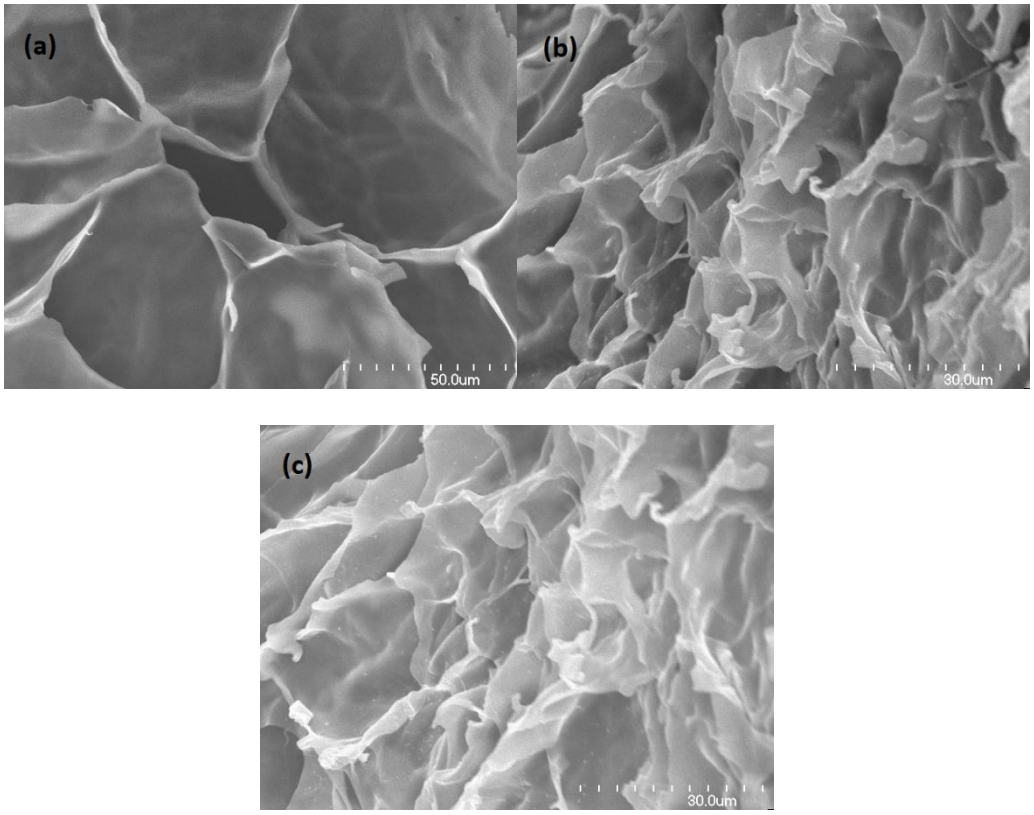

Figure 14. SEM images of (a) fully swollen HT-PPG before aging, (b) HT-PPG in 2%KCl, SR=15, aged at 150 °C for 6 months and (c) HT-PPG in 2%KCl, SR=15, aged at 150 °C for 12 months

To further demonstrate the gel structural integrity and stability after aging at higher temperature, morphology studies were performed using scanning electron microscopy (SEM) analysis. SEM images of HT-PPGs samples aged for 6 months and 12 months were acquired and compared with HT-PPG before aging (Figure 14). Polymer crosslinked network with open and interconnected pore structure was observed in an unexposed sample of fully swollen HT-PPG (Figure 14a) and was used as a control. As

seen from Figure 14(b) and 14(c), the crosslinked network pore structure was retained for both 6 months aged sample and 12 months aged sample which confirms that polymer matrix is stable to high temperature and ionic environments.

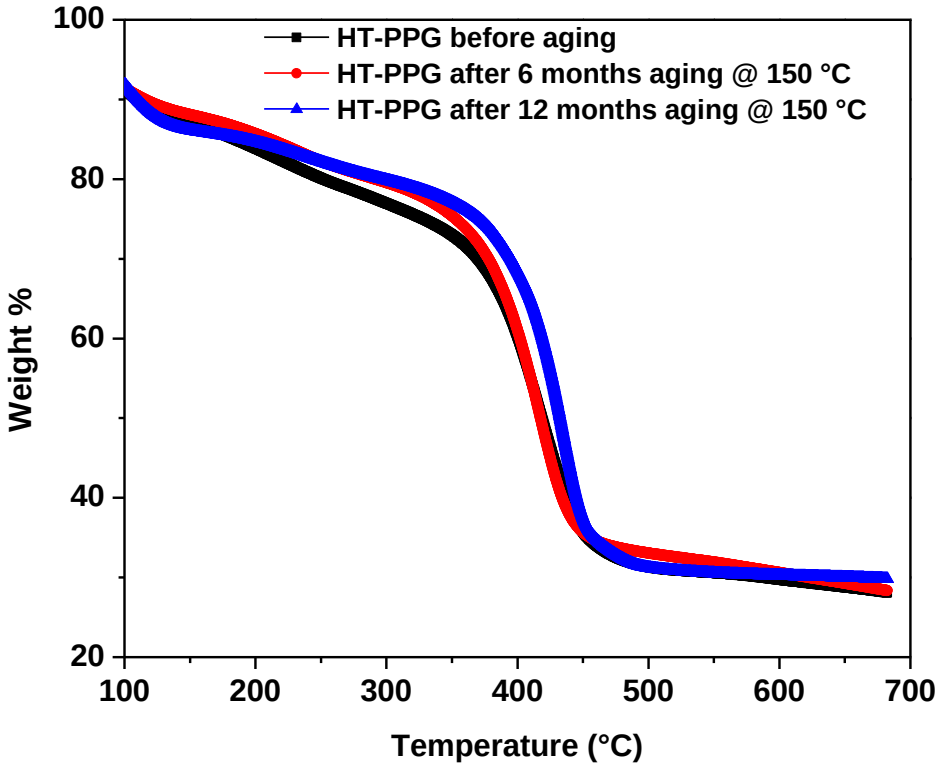

Figure 15. Thermogravimetric analysis results for HT-PPG samples.

TGA analyses were performed on freeze-dried samples of HT-PPGs swollen in 2% KCl at SR=15, before aging and after 6 and 12 months of aging to 150 °C. As seen in Figure 15, percent weight loss up to 225 °C temperature was associated with free and adsorbed water present in the samples. Above a 225°C temperature, organic molecule degradation mass losses were observed. It can be observed that there are no new inflections or peaks for the onset of degradation temperature for the high temperature

aged HT-PPG samples when compared to the HT-PPG before aging. It was also noted that the onset of degradation temperature was slightly shifted to higher temperature as HT-PPG time of aging increased. This observation can be ascribed to additional crosslinking induced during the long-term exposure, making the network stronger and resistant to thermal degradation.

When hydrogel crosslinked polymer matrix undergoes degradation, it loses its pore network connectivity and pore cellular structure [38]. Corresponding with lost crosslink density, a larger pore size distribution is observed along with an increase in swelling ratio and suggest change in bulk properties [39]. Freeze dried samples of aged HT-PPGs in 2% KCl brine were studied for swelling capacity, which showed slightly lower equilibrium swelling ratios than the control sample (Figure S3). We attribute the measured change to a reduced effective mass of dry HT-PPG particles because of non-volatile, precipitated salt during the freeze-drying process. A similar behavior can also be related to additional crosslinking of the polymer matrix during long term exposure to brine at higher temperature.

Therefore, it was concluded that HT-PPG compositions are thermally, hydrolytically stable and maintained their chemical and structural integrity for more than 18 months. This further confirmed that HT-PPGs can be used to solve conformance control problems in reservoirs of high salinity and high temperature.

3.6. CORE FLOOD TEST

Figure 16 depicts the three regions of injection flooding processes conducted to evaluate the plugging efficiency of HT-PPG in 1% NaCl brine at swelling ratio of 10.

Firstly, the fractured core was flooded with 1 % NaCl at 1 cm^3/min to determine the permeability of the open fracture prior to the gel treatment. The resulted pressure gradient was low due to the high conductivity of the fracture. The swollen HT-PPGs were then placed inside the fracture at a constant injection flow rate of 0.5 cm^3/min. The pressure gradient during the HT-PPG injection continuously increased as the gel particles were transporting and packing the fracture. Once the gel particles extruded from the effluent, the pressure gradient dropped from 180 psi/ft (4.07 MPa/m) until reaching a stabilized pressure gradient of 90 psi/ft (2.3 MPa/m).

Before a post-water injection process was conducted, the tubes connected to the core holder were cleaned while maintaining the fractured core with the packed gel under a confining pressure of 700 psi (4.83 MPa). Four different injection flow rates were applied during the 2^{nd} water flooding (0.1, 0.5, 0.75 and 1.0 cm^3/min) to investigate the efficiency of the packed gel in the fracture. At 0.1 cm^3/min, the pressure gradient increased indicating the resistance of the HT-PPG to the chase water until the water breakthrough occurred at 60 psi/ft (1.36 MPa/m), the injection flow rate was maintained until the pressure gradient was stabilized at 33.4 psi/ft (0.76 MPa/m). Subsequently, the injection flowrate was increased to 0.5 cm^3/min, the pressure gradient further increased and stabilized at 47.6 psi/ft (1.08 MPa/m) demonstrating greater resistance to water flood exerted by the packed gel. However, when the injection flow rates were further increased to 0.75 and 1.0 cm^3/min, no changes to the stabilized pressure gradients were observed and remained stable at 48.5 psi/ft (1.1 MPa/m), likely indicating that the chase water created a path through or around the packed gel.

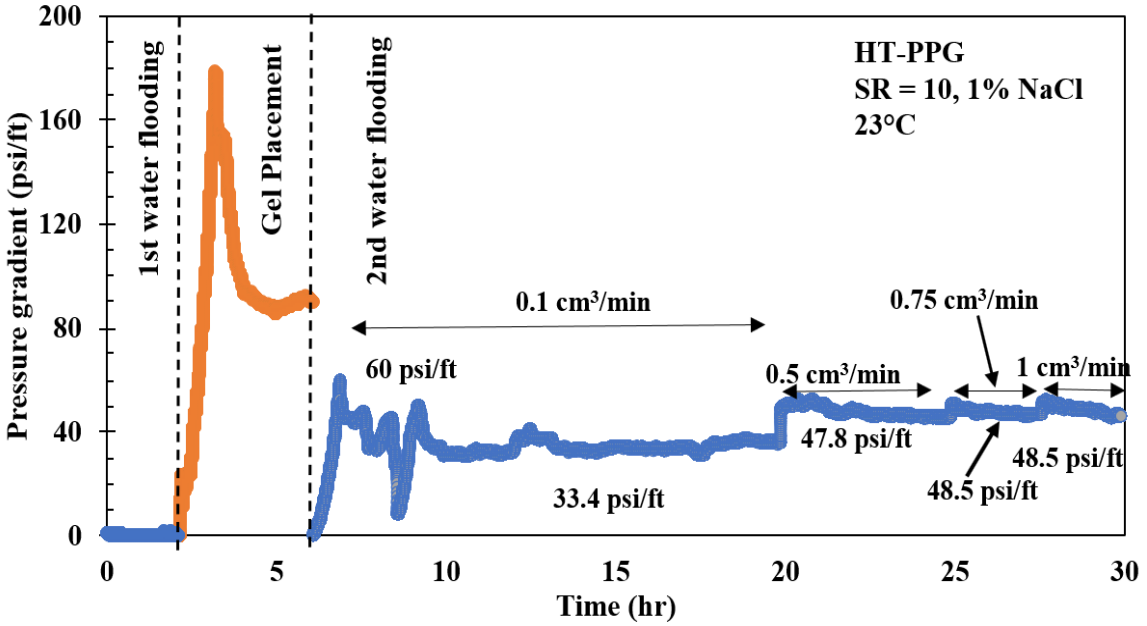

Figure 16. The pressure gradient vs. time of the coreflooding test illustrating the 1st water flooding, gel placement and 2nd water flooding

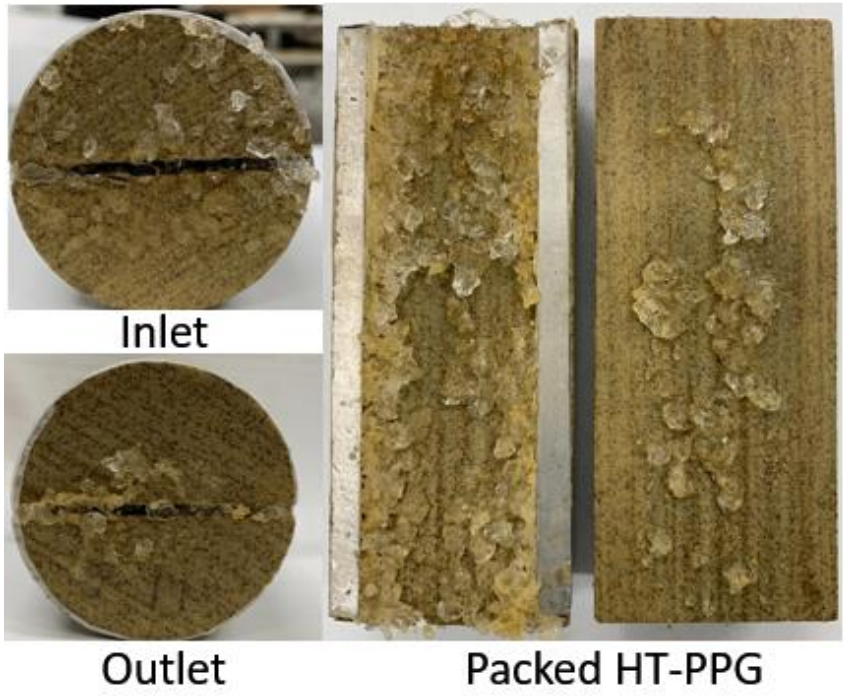

Figure 17. The fractured core after the test showing the packed HT-PPG

The fractured core was then removed from the core holder to inspect the condition of the packed HT-PPG inside the fractured. Figure 17 shows the HT-PPG adhered to the surface of the fracture core confirming that the HT-PPG reduced the permeability of the open fracture core.

4. CONCLUSIONS

Robust, ultra-high temperature resistant hydrogel compositions were synthesized from monomers DMA and NaSS with DVB crosslinker after a polymer screening process. The use of the thermally stable crosslinker DVB further helped to generate stable, covalent crosslinks within the hydrogel making it both strong and chemically stable. The effect of different parameters like salinity, temperature, pH and type of ions on swelling behavior of robust HT-PPG was studied. The HT-PPG showed a greater than 30-fold equilibrium volume swelling ratio for a variety of brine conditions, including divalent ions. HT-PPG has characteristics of excellent high temperature stability of 150 °C for more than 18 months, which makes it a candidate for solving conformance control problems in reservoirs of high salinity and high temperature. HT-PPG composition's thermal, hydrolytic stability along with retention of chemical and structural integrity was confirmed by solid-state ^{13}C NMR, morphology through SEM, TGA analyses and equilibrium swelling ratio post aging. A core flood evaluation supports HT-PPG's applicability for treating petroleum reservoirs displaying void space conduit problems. Core flood tests confirmed good plugging efficiency by the HT-PPGs to reduce the

permeability of open fractures. Scale up and commercialization of this product is underway.

This work can be further explored by conducting a series of coreflooding tests using different fracture and conduit models to see how the technology can be best designed and used for water control in high temperature high salinity reservoirs. HT-PPG technology can be further studied for supercritical CO_2 stability, for oil recovery involving gas injections. The novel hydrogels described here will open an avenue to explore exciting applications like hydrogel coatings on biomedical devices requiring steam sterilization stable material, electrochemical applications and other engineering applications.

ACKNOWLEDGEMENTS

The authors would like to acknowledge funding from our JIP Consortium members ConocoPhillips, Occidental Petroleum, Daqing Xinwantong Technology Developing Company, Ltd. and Petrochina that supported this work. We would like to thank Dr. Chariklia Sotiriou-Leventis and A B M Shaheen ud Doulah for helping us to perform compression test on Instron instrument.

SUPPORTING INFORMATION

1. POLYMER THERMAL AND HYDROLYTIC STABILITY

Table S1. Polymer thermal stability data assessed through TGA and viscosity measurements of polymer aqueous solutions viscosity change on aging.

Polymer	Onset of TGA degradation (°C)	Viscosity (in cP) measurements at 25 °C				
		Initial	Time of aging	Aging Temperature (°C)		
				80	130	150
PAM	230	9.9	3 months	NA	1.4	NA
PDMA	400	5.8	5 months	6.5	6.8	6.9
PSS	430	10.6	5 months	10	9.2	8.5

2. FTIR

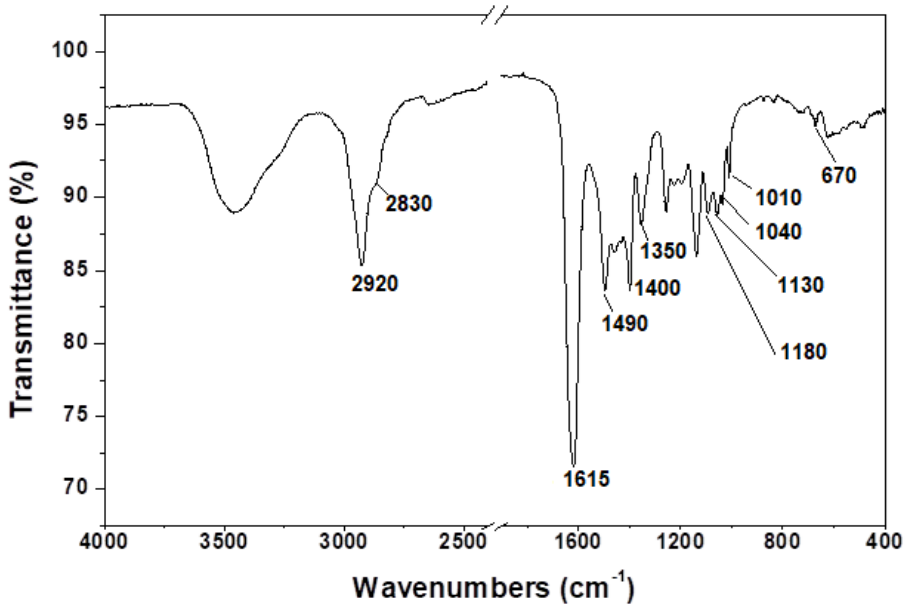

Figure S1. FT-IR spectrum of HT-PPG hydrogel, crosslinked copolymer of DMA and NaSS

3. COMPRESSION TEST RESULTS FOR HT-PPG

The compression test was performed with a universal testing machine (Instron 4469 model), at 25°C at a speed of 2 mm/min with 500 N load cell. The HT-PPGs (n=3), at water content of 90 wt.%, in the form of cylinders with dimensions 20 mm diameter

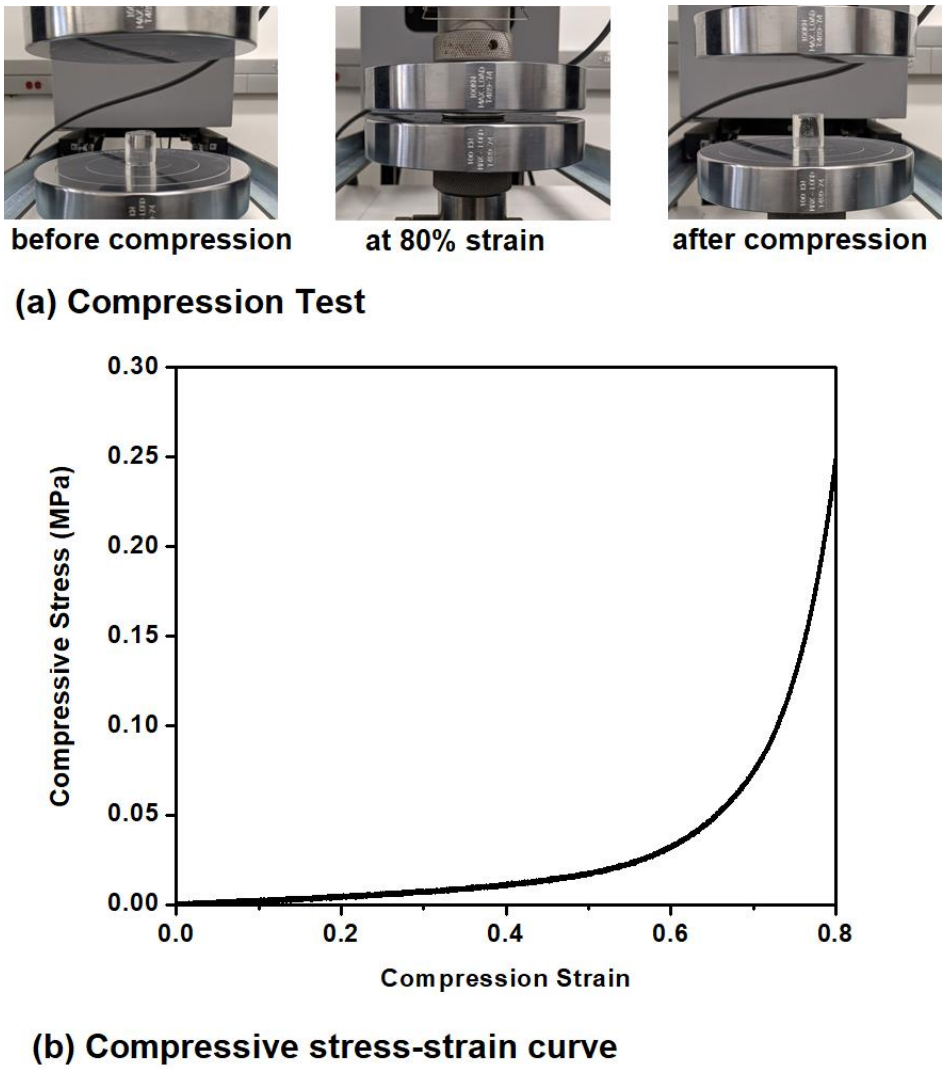

Figure S2. Demonstration of robust nature of HT-PPGs. (a) HT-PPG can sustain high compression of 80% strain without rupturing and recover to original shape on removal of pressure. (b) Compressive stress-strain curve for HT-PPGs

and 20 mm height (dimensions were measured using a digital caliper) were compressed up to 80% strain. Compression stress was determined based on the measured load per unit initial surface area for each sample. The compression strength of 0.25 MPa at a strain of 0.8.

4. EQUILIBRIUM SWELLING RATIO COMPARISON

Equilibrium swelling ratio of HT-PPG samples before and after aging were determined. Aged sample of HT-PPG in 2% KCl (SR=15) at 150 °C was recovered and freeze dried. Equilibrium swelling ratio was determined by immersing these weighed dried samples in 2% KCl for 48 hours. The final weights of swollen HT-PPGs were measured and compared with the original control sample (shown in Figure S3).

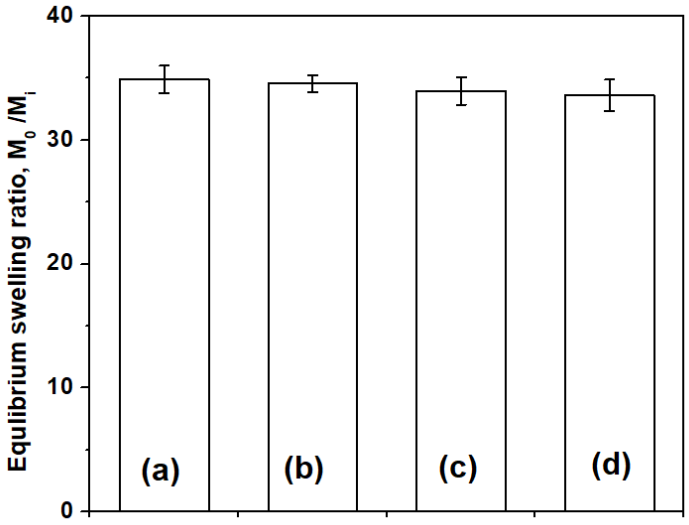

Figure S3. Equilibrium swelling ratio of HT-PPG in 2% KCl, before aging and after aging at 150 °C and 23 °C (n=3). (a) Control sample, (b) sample (SR=15) that exposed for 6 months, (c) sample (SR=15) that exposed for 12 months and (d) sample (SR=15) that exposed for 18 months

REFERENCES

[1] B. Bai, L. Li, Y. Liu, Z. Wang, H. Liu, Preformed Particle Gel for Conformance Control: Factors Affecting Its Properties and Applications, SPE Reserv. Eval. Eng. 10 (2004). https://doi.org/10.2118/89389-MS.

[2] T. Babadagli, Development of mature oil fields — A review, J. Pet. Sci. Eng. 57(3) (2007) 221-246. https://doi.org/https://doi.org/10.1016/j.petrol.2006.10.006.

[3] B. Bai, Y. Liu, J.-P. Coste, L. Li, Preformed Particle Gel for Conformance Control: Transport Mechanism Through Porous Media, SPE Reserv. Eval. Eng. 10(02) (2007) 176-184. https://doi.org/10.2118/89468-PA.

[4] S.L. Bryant, M. Bartosek, T.P. Lockhart, Laboratory evaluation of phenol-formaldehyde/polymer gelants for high-temperature applications, J. Pet. Sci. Eng. 17(3) (1997) 197-209. https://doi.org/https://doi.org/10.1016/S0920-4105(96)00079-4.

[5] H. Jia, W.-F. Pu, J.-Z. Zhao, R. Liao, Experimental Investigation of the Novel Phenol−Formaldehyde Cross-Linking HPAM Gel System: Based on the Secondary Cross-Linking Method of Organic Cross-Linkers and Its Gelation Performance Study after Flowing through Porous Media, Energy Fuels. 25(2) (2011) 727-736. https://doi.org/10.1021/ef101334y.

[6] H. Jia, J.-Z. Zhao, F.-Y. Jin, W.-F. Pu, Y.-M. Li, K.-X. Li, J.-M. Li, New Insights into the Gelation Behavior of Polyethyleneimine Cross-Linking Partially Hydrolyzed Polyacrylamide Gels, Ind. Eng. Chem. Res. 51(38) (2012) 12155-12166. https://doi.org/10.1021/ie301818f.

[7] G.A. Al-Muntasheri, H.A. Nasr-El-Din, I.A. Hussein, A rheological investigation of a high temperature organic gel used for water shut-off treatments, J. Pet. Sci. Eng. 59(1) (2007) 73-83. https://doi.org/https://doi.org/10.1016/j.petrol.2007.02.010.

[8] G.A. Al-Muntasheri, H.A. Nasr-El-Din, P.L.J. Zitha, Gelation Kinetics and Performance Evaluation of an Organically Crosslinked Gel at High Temperature and Pressure, SPE J. 13(03) (2008) 337-345. https://doi.org/10.2118/104071-PA.

[9] Y. Liu, C. Dai, K. Wang, M. Zhao, G. Zhao, S. Yang, Z. Yan, Q. You, New insights into the hydroquinone (HQ)-hexamethylenetetramine (HMTA) gel system for water shut-off treatment in high temperature reservoirs, J. Ind. Eng. Chem. 35 (2016) 20-28. https://doi.org/10.1016/j.jiec.2015.09.032.

[10] A.K. Alhuraishawy, B. Bai, A. Imqam, M. Wei, Experimental study of combining low salinity water flooding and preformed particle gel to enhance oil recovery for fractured carbonate reservoirs, Fuel. 214 (2018) 342-350. https://doi.org/https://doi.org/10.1016/j.fuel.2017.10.060.

[11] G. Chauveteau, A. Omari, R. Tabary, M. Renard, J. Rose, Controlling Gelation Time and Microgel Size for Water Shutoff, SPE/DOE Improved Oil Recovery Symposium, Society of Petroleum Engineers, Tulsa, Oklahoma, 2000, p. 8. https://doi.org/10.2118/59317-MS.

[12] A. Goudarzi, H. Zhang, A. Varavei, P. Taksaudom, Y. Hu, M. Delshad, B. Bai, K. Sepehrnoori, A laboratory and simulation study of preformed particle gels for water conformance control, Fuel. 140 (2015) 502-513. https://doi.org/https://doi.org/10.1016/j.fuel.2014.09.081.

[13] J. Pu, J. Zhou, Y. Chen, B. Bai, Development of Thermotransformable Controlled Hydrogel for Enhancing Oil Recovery, Energy Fuels. 31(12) (2017) 13600-13609. https://doi.org/10.1021/acs.energyfuels.7b03202.

[14] Y. Long, Z. Wang, H. Ding, J. Geng, B. Bai, Investigation and Characterization of a Robust Nanocomposite Preformed Particle Gel for Enhanced Oil Recovery, Energy Fuels. 33(6) (2019) 5055-5066. https://doi.org/10.1021/acs.energyfuels.9b00778.

[15] J. Pu, B. Bai, A. Alhuraishawy, T. Schuman, Y. Chen, X. Sun, A Recrosslinkable Preformed Particle Gel for Conformance Control in Heterogeneous Reservoirs Containing Linear-Flow Features, SPE J. 24(04) (2019) 1714-1725. https://doi.org/10.2118/191697-PA.

[16] B. Bai, M. Wei, Y. Liu, Field and Lab Experience With a Successful Preformed Particle Gel Conformance Control Technology, SPE Production and Operations Symposium, Society of Petroleum Engineers, Oklahoma City, Oklahoma, USA, 2013, p. 17. https://doi.org/10.2118/164511-MS.

[17] B. Bai, H. Zhang, Preformed-Particle-Gel Transport Through Open Fractures and Its Effect on Water Flow, SPE J. 16(02) (2011) 388-400. https://doi.org/10.2118/129908-PA.

[18] A. Imqam, B. Bai, M. Al Ramadan, M. Wei, M. Delshad, K. Sepehrnoori, Preformed-Particle-Gel Extrusion Through Open Conduits During Conformance-Control Treatments, SPE J. 20(05) (2015) 1083-1093. https://doi.org/10.2118/169107-PA.

[19] A. Imqam, Z. Wang, B. Bai, The plugging performance of preformed particle gel to water flow through large opening void space conduits, J. Pet. Sci. Eng. 156 (2017) 51-61. https://doi.org/https://doi.org/10.1016/j.petrol.2017.04.020.

[20] L. Wang, Y. Long, H. Ding, J. Geng, B. Bai, Mechanically robust re-crosslinkable polymeric hydrogels for water management of void space conduits containing reservoirs, Chem. Eng. J. 317 (2017) 952-960. https://doi.org/https://doi.org/10.1016/j.cej.2017.02.140.

[21] A. Imqam, Z. Wang, B. Bai, Preformed-Particle-Gel Transport Through Heterogeneous Void-Space Conduits, SPE J. 22(05) (2017) 1437-1447. https://doi.org/10.2118/179705-PA.

[22] B. Xiong, R.D. Loss, D. Shields, T. Pawlik, R. Hochreiter, A.L. Zydney, M. Kumar, Polyacrylamide degradation and its implications in environmental systems, NPJ Clean Water. 1(1) (2018) 17. https://doi.org/10.1038/s41545-018-0016-8.

[23] A.Y. Kwok, G.G. Qiao, D.H. Solomon, Synthetic hydrogels. 1. Effects of solvent on poly(acrylamide) networks, Polymer. 44(20) (2003) 6195-6203. https://doi.org/https://doi.org/10.1016/S0032-3861(03)00671-2.

[24] T. van Vliet, H.J.M. van Dijk, P. Zoon, P. Walstra, Relation between syneresis and rheological properties of particle gels, Colloid Polym. Sci. 269(6) (1991) 620-627. https://doi.org/10.1007/BF00659917.

[25] P. Tongwa, R. Nygaard, B. Bai, Evaluation of a nanocomposite hydrogel for water shut-off in enhanced oil recovery applications: Design, synthesis, and characterization, J. Appl. Polym. Sci. 128(1) (2013) 787-794. https://doi.org/10.1002/app.38258.

[26] H.R. Saghafi, A. Naderifar, S. Gerami, M.A. Emadi, Improvement in thermo-chemical stability of nanocomposite preformed particle gels for conformance control in harsh oil reservoir conditions, The Can. J. Chem. Eng. 94(10) (2016) 1880-1890. https://doi.org/10.1002/cjce.22577.

[27] T. Sato, D.A. Katila, Oxidative Degradation of Cellulose Derivatives In Aqueous Solution of Chromic Acid, Polym. J. 10(4) (1978) 433-436. https://doi.org/10.1295/polymj.10.433.

[28] H. Kheradmand, J. François, V. Plazanet, Hydrolysis of polyacrylamide and acrylic acid-acrylamide copolymers at neutral pH and high temperature, Polymer. 29(5) (1988) 860-870. https://doi.org/https://doi.org/10.1016/0032-3861(88)90145-0.

[29] J. Moens, G. Smets, Alkaline and acid hydrolysis of polyvinylamides, J. Polym. Sci. 23(104) (1957) 931-948. https://doi.org/https://doi.org/10.1002/pol.1957.1202310436.

[30] P.J. Flory, Principles of Polymer Chemistry, Cornell University Press1953.

[31] D.C. Lin, J.F. Douglas, F. Horkay, Development of minimal models of the elastic properties of flexible and stiff polymer networks with permanent and thermoreversible cross-links, Soft Matter. 6(15) (2010) 3548-3561. https://doi.org/10.1039/B925219N.

[32] P.J. Flory, J. Rehner, Statistical Mechanics of Cross-Linked Polymer Networks II. Swelling, J. Chem. Phys. 11(11) (1943) 521-526. https://doi.org/10.1063/1.1723792.

[33] M.L. Huggins, THERMODYNAMIC PROPERTIES OF SOLUTIONS OF LONG-CHAIN COMPOUNDS, Annals of the New York Academy of Sciences. 43(1) (1942) 1-32. https://doi.org/10.1111/j.1749-6632.1942.tb47940.x.

[34] F. Horkay, I. Tasaki, P.J. Basser, Effect of Monovalent−Divalent Cation Exchange on the Swelling of Polyacrylate Hydrogels in Physiological Salt Solutions, Biomacromolecules. 2(1) (2001) 195-199. https://doi.org/10.1021/bm0056153.

[35] S. Sircar, J.P. Keener, A.L. Fogelson, The effect of divalent vs. monovalent ions on the swelling of Mucin-like polyelectrolyte gels: Governing equations and equilibrium analysis, J. Chem. Phys. 138(1) (2013) 014901. https://doi.org/10.1063/1.4772405.

[36] X. Shi, L. Wang, J. Guo, Q. Su, X. Zhuo, Effects of inhibitor KCl on shale expansibility and mechanical properties, Petroleum. 5(4) (2019) 407-412. https://doi.org/https://doi.org/10.1016/j.petlm.2018.12.005.

[37] G. Targac, C. Gallo, D. Smith, C.-K. Huang, S. Autry, J. Peirce, L. Baohong, Case History of Conformance Solutions for West Sak Wormhole/Void Space Conduit with a New Reassembling Pre-formed Particle Gel RPPG, SPE Annual Technical Conference and Exhibition, Society of Petroleum Engineers, Virtual, 2020, p. 18. https://doi.org/10.2118/201302-MS.

[38] H. Tan, C.M. Ramirez, N. Miljkovic, H. Li, J.P. Rubin, K.G. Marra, Thermosensitive injectable hyaluronic acid hydrogel for adipose tissue engineering, Biomaterials. 30(36) (2009) 6844-6853. https://doi.org/https://doi.org/10.1016/j.biomaterials.2009.08.058.

[39] M.S. Rahman, M.M. Islam, M.S. Islam, A. Zaman, T. Ahmed, S. Biswas, S. Sharmeen, T.U. Rashid, M.M. Rahman, Morphological Characterization of Hydrogels, in: M.I.H. Mondal (Ed.), Cellulose-Based Superabsorbent Hydrogels, Springer International Publishing, Cham. (2019) pp. 819-863. https://doi.org/10.1007/978-3-319-77830-3_28.

II. DEVELOPMENT AND EVALUATION OF ULTRA-HIGH TEMPERATURE RESISTANT PREFORMED PARTICLE GELS FOR CONFORMANCE CONTROL IN NORTH SEA RESERVOIRS

Buddhabhushan Salunkhe[a], Thomas Schuman[a,*], Ali Al Brahim[b], Baojun Bai[b],

[a] *Chemistry, Missouri University of Science and Technology, Rolla, MO 65409, USA*

[b] *Petroleum Engineering, Missouri University of Science and Technology, Rolla, MO 65409, USA*

ABSTRACT

Preformed particle gels (PPGs), a 3-D, cross-linked, dried polymer particles which can swell to several hundred times on contact with formation water. PPGs have been extensively used to control water production problem for reservoirs with conformance problems. The current state of the art PPGs are polyacrylamide-based hydrogel compositions which lacks long term thermal stability under high temperatures and salinity conditions. There are many oil reservoirs across the globe exhibiting conditions of temperatures higher than 120 °C with high salinity. A novel ultrahigh temperature resistant PPG composition (HT-PPG) was designed to fill up the technology gap between existing polyacrylamide-based PPGs technology that degrades readily over 110 °C temperatures. HT-PPG exhibited excellent thermal stability for greater than 18 months in North Sea formation and formation water environments at 130 °C. HT-PPG described herein showed swelling capacities of up to 30 times in different salinity North Sea brines. HT-PPGs physiochemical properties like swelling, swelling rate, rheological behavior as a function of temperature and salinity. HT-PPGs showed excellent elastic

modulus (G') of about 3200 Pa in formation water of at 90% water content. Thermostability of HT-PPGs was assessed at 130 °C and 150 °C in North Sea brines with different salinity conditions. HT-PPGs found to be stable for more than 18 months without losing molecular integrity. Thermostability was further confirmed through different matrices such as CPMAS ^{13}C NMR, thermogravimetric analysis (TGA) and morphology. Laboratory core flood experiments were performed to demonstrate the plugging efficiency of open fractures and effectiveness in reducing the permeability. HT-PPG comprehensive evaluation confirms its novelty for excellent hydrothermal stability, thus can be used to control water production problem for mature reservoirs exhibiting conditions of high salinity and high temperature.

1. INTRODUCTION

Excess water production problem is an utmost issue for mature oilfields across the world, making oil recovery uneconomical and leads to shutting down of these oil wells. Excessive water production causes corrosion and scale formation, introduces additional operations for handling and disposal for the produced water, creates environmental concerns along with severe economic challenges (Babadagli 2007). Among different approaches to tackle excess water production concern, polymer gel treatment is a proven, cost-effective technology with considerable success in improving sweep efficiency (Bai et al. 2007). Preformed particle gel (PPG) technology was developed with improved swelling capacities for conformance control problem. In last few decades, intensive research has been done on preformed particle gels for conformance control through

studying the behavior of PPGs through fractures (Zhang and Bai 2011), gel placement (Wang et al. 2019, Elsharafi and Bai 2012, Saghafi 2018, Sang et al. 2014), plugging performance (Imqam et al. 2017a, Elsharafi and Bai 2012, 2016, Goudarzi et al. 2015), and factors affecting PPGs properties (Bai et al. 2007, Mousavi Moghadam et al. 2012, Tongwa et al. 2013, Durán-Valencia et al. 2014) and flow conformance/transport mechanisms (Bai et al. 2004, Bai et al. 2007, Leng et al. 2021).

Conventional PPGs used for conformance control are commonly products based on the acrylamide monomer with crosslinker and initiator, which is processed into hydrogel and available as a dried particle. These PPGs are a three-dimensional network polymer chains, dried, as cross-linked particles processed at surface facilities with size of few micrometers to millimeter (Imqam and Bai 2015, Bai et al. 2007, Coste et al. 2000). The fact that PPGs are already crosslinked and processed, eliminates problems associated with in-situ gels like gelation time control, shear degradation, and chromatographic fractionation (Bai et al. 2004, Alhuraishawy et al. 2018, Chauveteau et al. 2000, Goudarzi et al. 2015). PPG technology has gained interest in last two decades in field application owing to its simple synthesis protocol and material handling in the field, that redirects water flow from higher permeability zones into unswept, oil rich zones as evident from thousands of successful field jobs (Bai et al. 2013, Imqam et al. 2017a, 2017b, Zaitoun et al. 2007, Mustoni et al. 2010).

Overall PPGs exhibit multiple advantages over in-situ gels in treating oil wells for conformance control, however, their success depends strongly on oil field characteristics e.g. temperature of oil reservoirs, hardness and salinity of formation water, pH and mineral compositions. Under conditions of high temperature and salinity conditions,

conventional PPGs can show syneresis phenomena which can be attributed to their rapid degradation due to poor thermal and hydrolytic stability under harsh reservoir conditions (Xiong et al. 2018, Kwok et al. 2003). The degradation products are likely to contain ketone, aldehyde, carboxylate groups along with monomeric units that can retained in porous media through adsorption onto mineral surfaces (Lu et al. 2012, Touzé et al. 2015, Lande et al. 1979, van Vliet et al. 1991). There are many oil reservoirs located around the world, e.g., North Sea, China, Gulf of Mexico, with harsh temperature and salinity conditions. Apart from that, regions like the North Sea have stringent environmental regulations (Cordes et al. 2016) for injection of chemicals into the oil reservoirs. Currently, there are no reports of non-toxic polymer products with long-term thermal stability at temperatures up to 150 °C. However, there is immediate need for development of environmentally friendly products with more than year-long hydrothermal stability.

Our research group recently reported a novel design of an ultra-high temperature resistant preformed particle gels (HT-PPGs) with poly(dimethylacrylamide-co-styrenesulfonate) chemistry beneficial in treating oil reservoirs with temperatures up to 150 °C (Salunkhe et al. 2021). These HT-PPGs are intended to be nontoxic to aquatic life and these chemistries are not reported in the ECHA (European Chemicals Agency) database. A commercial product based on this technology has been manufactured by collaborator Daqing Xinwantong Company and was provided for further evaluation. This paper presents a detailed evaluation of HT-PPGs in North Sea formation brines for physiochemical properties such as swelling rates, elastic modulus (G') measurements, along with thermal stability evaluation results. Lab core flood experiments were demonstrated to confirm plugging performance of HT-PPGs in North Sea brine. Owing

to excellent features of HT-PPG, they make an ideal candidate for excess water production control and to resolve problems associated with conformance for mature oil reservoirs exhibiting high temperature and salinity conditions.

2. EXPERIMENTAL SECTION

2.1. MATERIALS

HT-PPG product was provided by Daqing Xinwantong Company and used as received for evaluation without further processing. HT-PPGs are dry, transparent white particles with apparent bulk density of 1.31 g/cm^3 and less than 5% water content. All other chemicals and reagents were purchased from Sigma-Aldrich (St. Louis, MO).

2.2. SWELLING KINETICS

The weighed dried HT-PPG was immersed in synthetic North Sea brines that were prepared in lab and their ionic composition is presented in Table 1. Swelling kinetics measurements were performed through monitoring change in volume of HT-PPGs with respect to temperature and time until equilibrium swelling ratio (EQSR) was achieved. The swelling ratio (SR) of HT-PPGs can be obtained using the equation (1), where, V_t is volume of swollen HT-PPGs at particular time t and M_0 is the initial mass of dried PPGs at time t = *0* and can be expressed as mL/g of dried HT-PPG

$$SR = V_t / M_0. \quad (1)$$

2.3. RHEOLOGICAL STUDIES

The rheology properties of swollen HT-PPGs were measured on HAAKE MARS III rheometer (Germany) with a gap of 1 mm using a parallel plate geometry (PP35L Ti L). The oscillation strain-dependent experiment model at a fixed frequency of 1 Hz was used to perform strain sweep measurements. The linear viscoelastic region was obtained through experiments showing constant *G'* measuremnets as function of strain amplitude. All measurements were performed at ambient room temperature conditions. The oscillation time-dependent experiment model was used at a fixed frequency of 1 Hz and controlled strain (γ) of 1% to measure Elastic modulus (*G'*) as a function of time.

Table 1. Simulated Composition for North Sea formation water and seawater (Javanmard et al. 2018)

Ions	Formation brine (ppm)	Seawater (ppm)
Na^+	27286	10744
K^+	249	400
Mg^{2+}	592	1094
Ca^{2+}	1466	410
Sr^{2+}	140	20
Ba^{2+}	1	-
Cl^-	46300	19350
HCO_3^-	-	65
SO_4^{2-}	290	2000

2.4. THERMAL STABILITY EVALUATIONS

The glass tubes (high-pressure resistant) with temperature resistant O-rings were used to age HT-PPG North Sea formation brines swollen samples at high temperatures of 130 and 150 °C. All measurements were performed in 5 replicates samples and the cumulative observations were noted down as a function of aging time. All samples were precisely prepared under identical conditions, by creating oxygen free environments using cannulation transfer technique as shown in Figure 1. The sample preparation was done under argon gas inert atmosphere. Thermal stability of HT-PPGs at 130 and 150 °C was assessed by monitoring the volume changes (volume at time t (V_t)/ initial volume (V_0)) for swollen HT-PPGs on aging.

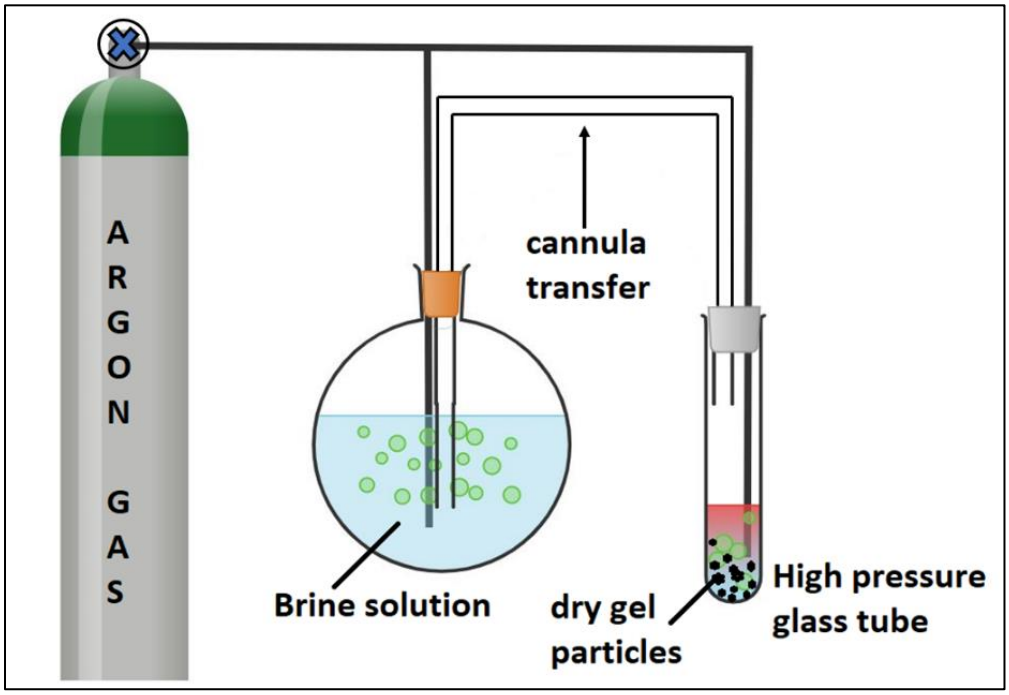

Figure 1. HT-PPG test sample preparation for assessing thermal stability

2.5. CPMAS ^{13}C SOLID STATE NMR ANALYSIS

Solid-state Cross-Polarization Magic Angle Spinning Carbon-13 Nuclear Magnetic Resonance, (CPMAS) ^{13}C NMR spectroscopy was performed on a Bruker Avance III 400 MHz spectrometer as described previously (Salunkhe et al. 2021). A carbon frequency of 100 MHz was used for a 7 mm Bruker MAS probe at a magic angle spinning rate of 5 kHz with broadband proton suppression, and CP total suppression of spinning sidebands (TOSS) pulse sequence. TOSS pulse sequence was introduced by a series of four properly timed 180° pulses on the carbon channel at different points of a cycle before the acquisition of the free induction decay (FID) after an initial excitation with a 90° pulse on the proton channel. The 90° excitation pulse on the proton and the 180° excitation pulse on carbon were set to 4.2 and 1 x 10^{-5} s, respectively. The cross-polarization contact time and the relaxation delay were set at 2 x 10^{-3} s and 5 s, respectively. The experiment was conducted at 2048 scans. Glycine (carbonyl carbon at 176.03 ppm was used as external reference standard and chemical shifts data was collected with respect to tetramethylsilane (TMS) at 0 ppm.

2.6. MORPHOLOGY OF HT-PPG

The swollen HT-PPG microstructure was characterized using Helios Nanolab 600 Dual Beam scanning electron microscope (SEM) operating at 5 kV. Freeze dried samples of swollen HT-PPGs were prepared and a fresh cross-section was obtained by carefully fracturing the sample in liquid nitrogen. The fractured sample was sputter coated with gold coating before SEM imaging.

2.7. THERMOGRAVIMETRIC ANALYSIS (TGA)

Thermogravimetric analysis was performed on HT-PPG aged sample at 150 ℃ temperature in North Sea brines and compared with HT-PPG control sample (with no aging). All the experiments were conducted on TGA Q50 (TA instruments), at a heating rate of 10 °C/min under a nitrogen atmosphere. The aged HT-PPGs were frozen under liquid nitrogen and further freeze dried under high vacuum. The dried gels obtained thereafter were analyzed for weight loss as a function of temperature and compared with the HT-PPG control (unaged). Alumina pans were used to perform TGA analysis with sample size of 10 to 20 mg.

2.8. LABORATORY COREFLOODING TEST

To investigate the plugging performance of HT-PPG, dynamic Coreflooding experiment were conducted in the open fracture. The sandstone core was oven dried at 120 °C to remove residual water, followed by vacuuming for 24 hours. The core was saturated with North Sea formation water for overnight before initiating coreflood experiment. The pore volume and porosity were calculated by weighing saturated core. The experimental setup for coreflood test is depicted in Figure 2a, the core was placed inside a core holder and a confining pressure was applied. The core waterflooding was performed using North Sea formation water at variable injection flow rates and corresponding stabilized pressure gradients were recorded at the steady state condition. The permeability of matrix was calculated using Darcy's law. A saturated fractured core was split into two equal halves and fracture was supported by gluing a stainless-steel strip of thickness 0.077 inches over the core surface (Figure 2b). This assembled core with

fracture was wrapped in a Teflon sheet and the fracture volume was obtained. Table 2 depicts the dimensions and fractured core properties used in coreflood experiment.

The fractured core was confined back into core holder and flooded with North Sea formation water at 1.0 mL/min injection flow rate. The core was flooded until a stabilized pressure gradient was observed, representing the first water flooding. HT-PPG dried particles (1.68 - 2.0 mm) were swollen at swelling ratio of 10 in North Sea formation water and placed inside an accumulator. The swollen HT-PPGs were injected using Isco pump through the core setup at a flow rate of 0.5 mL/min until gel placement steady pressure gradient was attained. Thereafter, second water flooding was performed by post water injection at different injection flow rates of 0.1, 0.25, 0.5, 0.75 and 1 mL/min and reduction in effective permeability of the open fracture by HT-PPG was determined.

Table 2. The fractured core properties.

Core diameter (D), in.	Core length (L), in.	Pore vol-ume (PV)	Porosity, (φ), %	Permeability (k), md	Fracture width, in.	Fracture height, in.	Fracture Volume (FV)
2.0	5.0	49.02	19.51	86	0.077	1.48	0.57 in^3, 9.3 cm^3

The residual resistance factor (F_{rr}) is a ratio of the mobility of water before (λ_b) and after the gel placement (λ_a) (Jennings et al. 1971) and can be calculated from equation (2). K_b represents the initial permeability of the fractured core including both the

matrix and the fracture parts, and K_a is the permeability of the fractured core to formation brine after the HT-PPG placement. μ_w is the viscosity of the injected brine.

$$F_{rr} = \frac{\lambda_b}{\lambda_a} = \frac{K_b/\mu_w}{K_a/\mu_w} = (\Delta P_a / \Delta P_b) \text{ at given q.} \quad (2)$$

where, ΔP_b, pressure drop along the fractured core (atm) was calculated using Darcy's law, equation (3), q (mL/sec) is a volumetric injection flow rate, A is the cross-sectional area of the fractured core (cm^2), μ is the viscosity of the brine (cp) and L is the length of the fractured core (cm).

$$q = \frac{K_b A \Delta P}{\mu L}. \quad (3)$$

The *Frr* can be expressed in terms of pressure gradient along the fractured core once the steady state condition is achieved as a function of the injection flow rate.

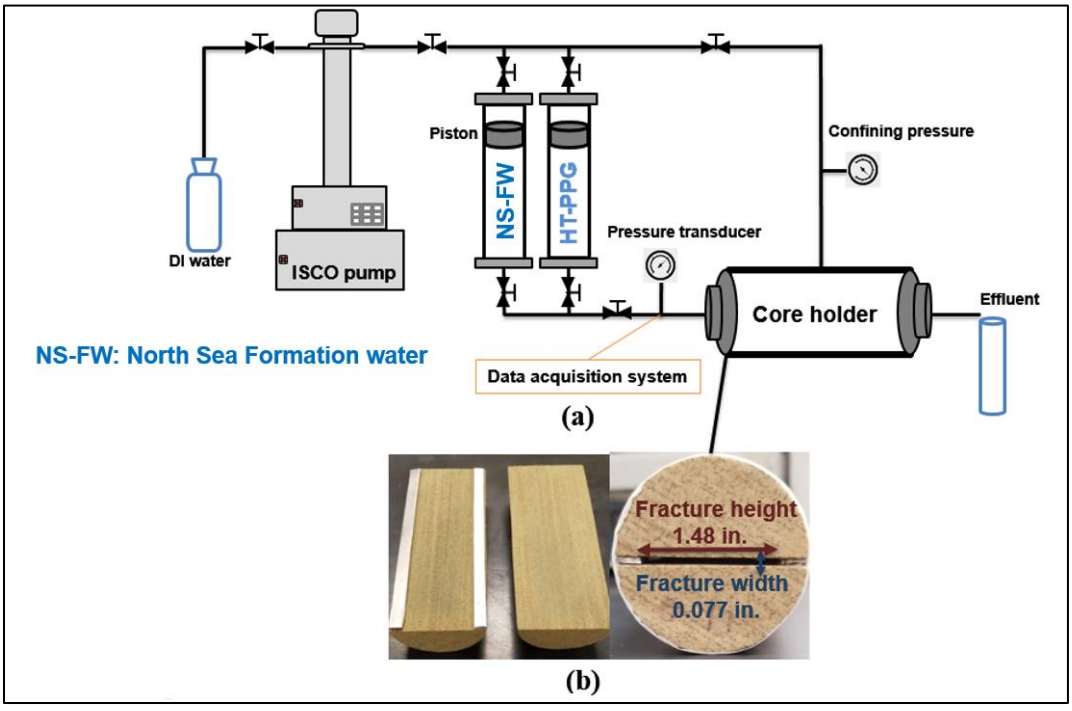

Figure 2. (a) Schematic diagram of the coreflooding experiment, (b) the parameters of the fractured core.

3. RESULTS AND DISCUSSIONS

3.1. SWELLING KINETICS

All measurements for swelling kinetics were performed on HT-PPG dry particles of size 1 to 2 mm using North Sea brines. Figure 3 shows the effect of temperature on swelling behavior of HT-PPG at room temperature and at 130 °C temperature. It was observed that salinity slightly influences the rate of swelling and degree of swelling for HT-PPG. In case of North Sea seawater brine, with total dissolved solids of 34,000 ppm, an equilibrium swelling ratio of up to 30 times the original volume can be obtained at room temperature and a ratio to 33 times at 130 °C. Similarly, in case of North Sea formation water, with total dissolved solids of 76,000 ppm, an equilibrium swelling ratio of up to 28 times the original volume was observed at room temperature and that up to 32 times observed at 130 °C.

These increases can be attributed to higher diffusion rates of ions with increase in temperature, in turn results in faster swelling behavior (Flory 1953, Huggins 1942, Flory and Rehner 1943). This further illustrated the effect of temperature on swelling behavior, where with increase in temperature, the rate of swelling and equilibrium swelling ratio increases. It was also observed that, in case of North Sea seawater brine, equilibrium swelling ratio can be attained in 12 hours at room temperature and in 8 hours at 130 °C. Similarly, equilibrium swelling ratio was achieved in 18 hours at room temperature and in 8 hours at 130 °C, when North Sea formation water was used for swelling.

From Figure 3, it is also evident that at the beginning of swelling process, faster swelling rates were observed, because of faster diffusion of ions in gels as a function of

concentration gradient difference. Towards the end of swelling process, diffusion process will slow down because of saturation of hydrogel matrix with the ions present in the brine, that results into low swelling rate (Lin et al. 2010).

3.2. RHEOLOGY MEASUREMENTS

The elastic modulus (*G'*) of HT-PPG was measured to determine the mechanical strength. These measurements were performed with parameters of 1 Hz frequency at a controlled strain (γ) of 1% using oscillation time dependent experiment model. The linear viscoelastic region was determined and accordingly the parameters for measurements were set up for storage modulus measurements. Figure 4(a) represents the oscillation time dependent model experiment for North Sea seawater brine at variable swelling ratio. At swelling ratio of 10 (brine content = ~ 90.9%), over 3100 Pa of elastic modulus was

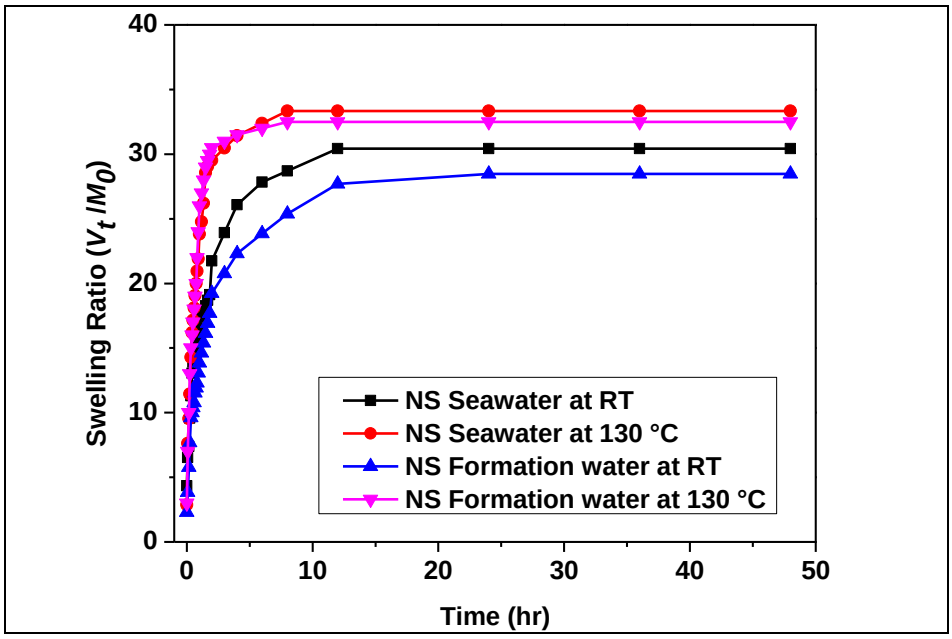

Figure 3. Swelling kinetics behavior of HT-PPG in North Sea brines at room temperature (23°C) and 130 °C

obtained which reduces to over 600 Pa at equilibrium swelling ratio (brine content = ~ 96.7%). The reduction of strength at equilibrium swelling ratio can be attributed to fully extended conformation of polymer network chains at equilibrium swelling ratio, where net polymer concentration per unit volume is lower as compared to HT-PPG swollen at swelling ratio of 10.

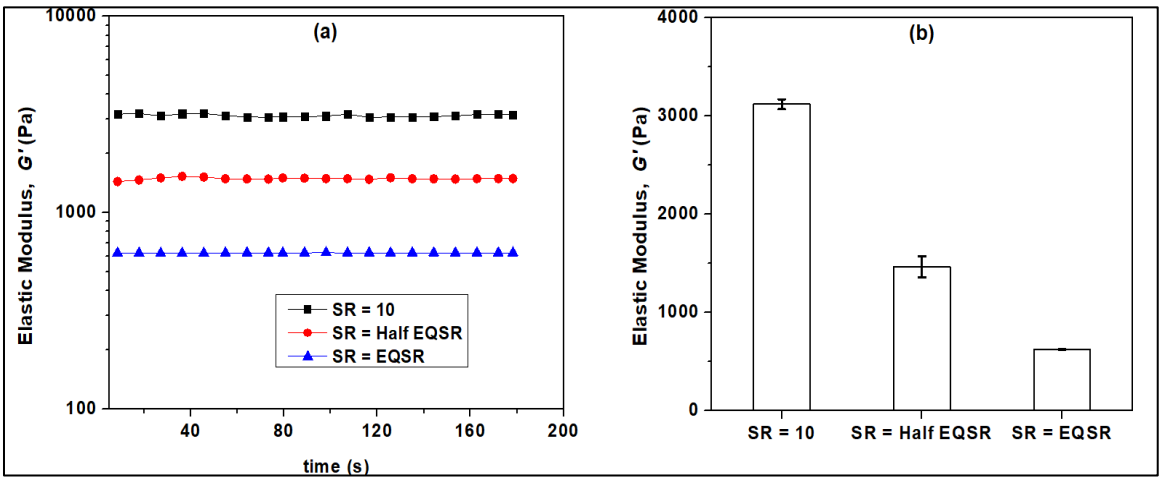

Figure 4. (a) Time sweep profiles for Elastic modulus (G') of HT-PPG in North Sea seawater brine at swelling ratio of 10, half equilibrium swelling ratio (Half EQSR) and equilibrium swelling ratio (EQSR), (b) Elastic modulus (G') of HT-PPG for N=3, at variable swelling ratio.

Similarly, Figure 5(a) represents the oscillation time dependent model experiment for North Sea formation water at variable swelling ratio. At a swelling ratio of 10 (brine content = ~ 91 %), an elastic modulus of over 3200 Pa was obtained, which was reduced to just over 650 Pa at an equilibrium swelling ratio (brine content = ~ 97 %).

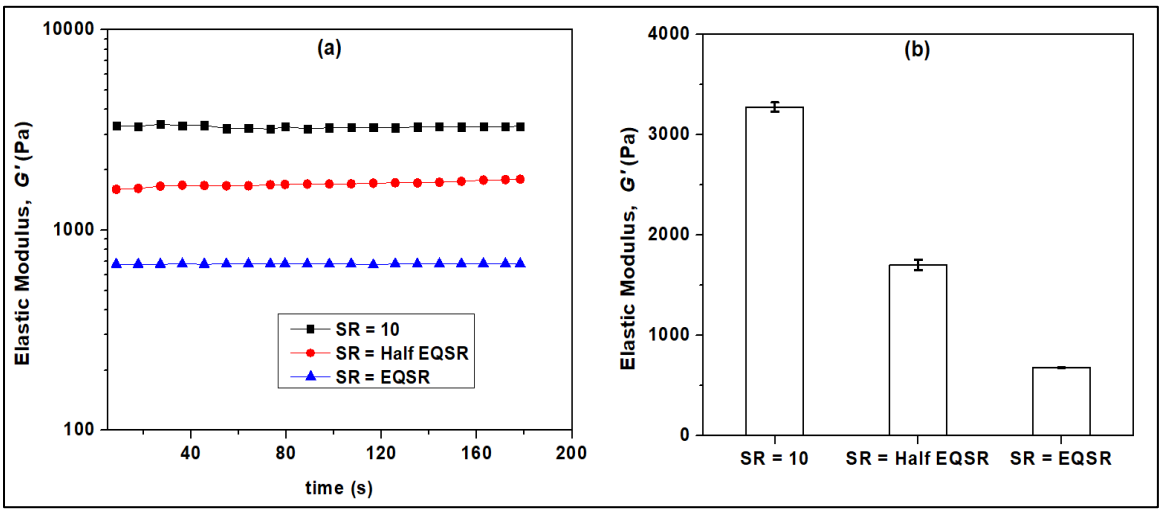

Figure 5. (a) Time sweep profiles for Elastic modulus (G') of HT-PPG in North Sea formation water at swelling ratio of 10, half equilibrium swelling ratio (Half EQSR) and equilibrium swelling ratio (EQSR), (b) Elastic modulus (G') of HT-PPG for N=3, at variable swelling ratio.

3.3. THERMOSTABILITY EVALUATIONS FOR HT-PPG IN NORTH SEA BRINES

Thermal and hydrolytic stability of HT-PPG was evaluated in North Sea brines by monitoring hysteresis behavior (change in hydrogel original volume) and observing visual signs of degradation as a function of aging time. The HT-PPG samples with swelling ratio of 10, half EQSR and EQSR was aged for more than 18 months at 150 °C. HT-PPG swollen in North Sea seawater at swelling ratio of 10 (brine content = ~ 90.9%) did not show any syneresis while at half EQSR ((brine content = ~ 93.7%) condition showed approximately 5% volume change after aging for 18 months at 150 °C (Figure 6a). Similar observations were noted for HT-PPG swollen in North Sea formation water, where HT-PPG were stable for more than 18 months aging at 150 °C for swelling ratio of 10 (brine content = ~ 90.9%) while in case of half EQSR (brine content = ~ 93.3%) approximately 7% volume change was observed (Figure 6b). On the other hand, samples

swollen in North Sea seawater at EQSR (brine content = ~ 96.7%) showed around 20% change in volume after 16 months and that in North Sea formation water EQSR (brine content = ~ 96.5%), less than 75% change in volume was observed after 12 months of aging at 150 °C. Similar observations were made for HT-PPG aged at 130 °C under similar conditions (Figure 6c and 6d).

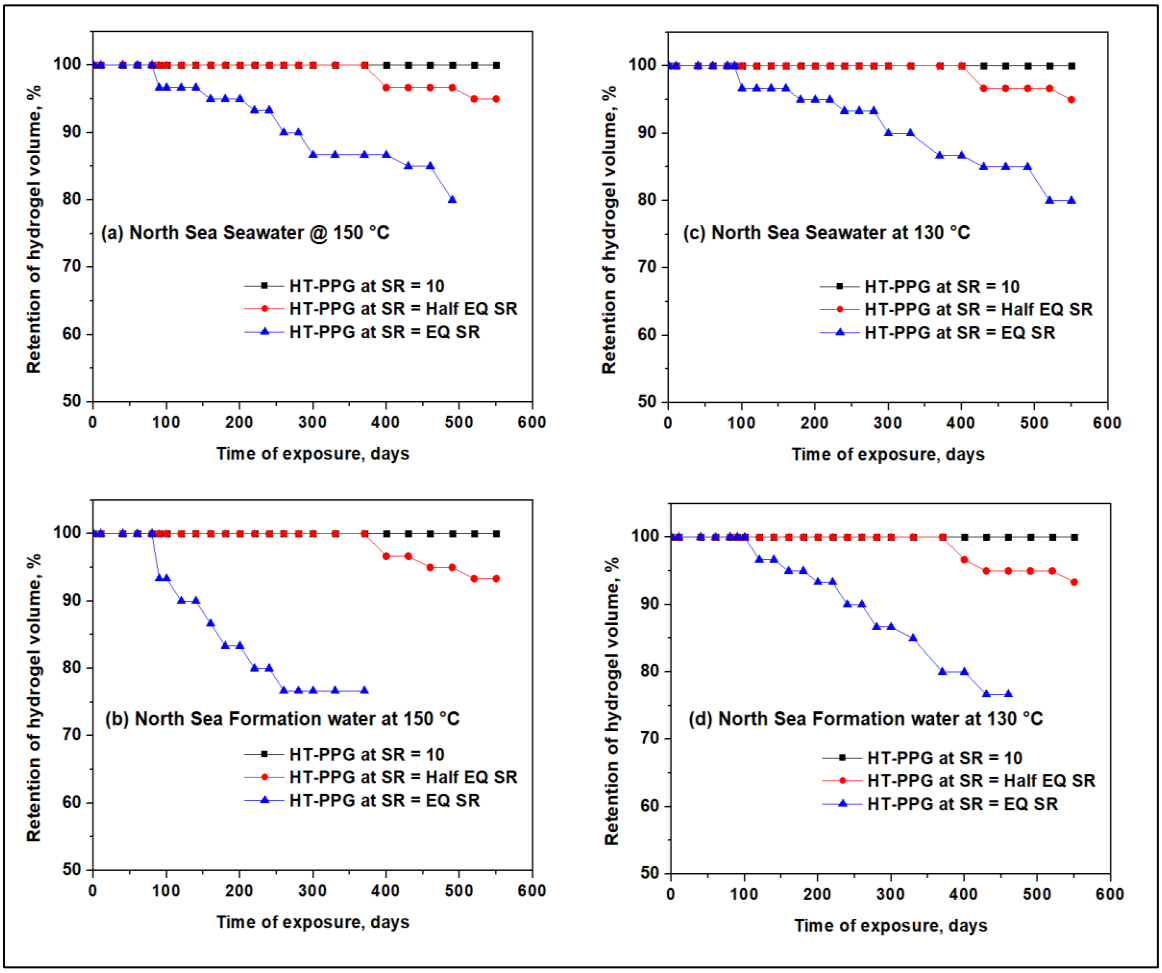

Figure 6. Hydrolytic thermal stability of HT-PPG for swelling ratio of 10, Half EQSR and EQSR with respect to time for (a) North Sea Seawater at 150 °C, (b) North Sea Formation water at 150 °C, (c) North Sea Seawater at 130 °C and (d) North Sea Formation water at 130 °C

HT-PPGs were monitored for change in shape, size and degradation after 18 months of aging. As seen in Figure 7 for 150 °C aging and Figure 8 for 130 °C aging, HT-PPG recovered at half EQSR did not show any visual degradation signs, the shape, size, and structural integrity of HT-PPG was retained during thermal aging. HT-PPGs chemistry confirms the long-term thermal stability towards hydrothermal and strongly ionic environments. A slight change of hydrogels color is attributed towards a small amount of residual oxygen left behind in glass tubes. We also observed at longer exposure times that steam-durable o-ring seals were degrading near the longest exposure times and which might have introduced the air inhibition toward the end of our testing regimen.

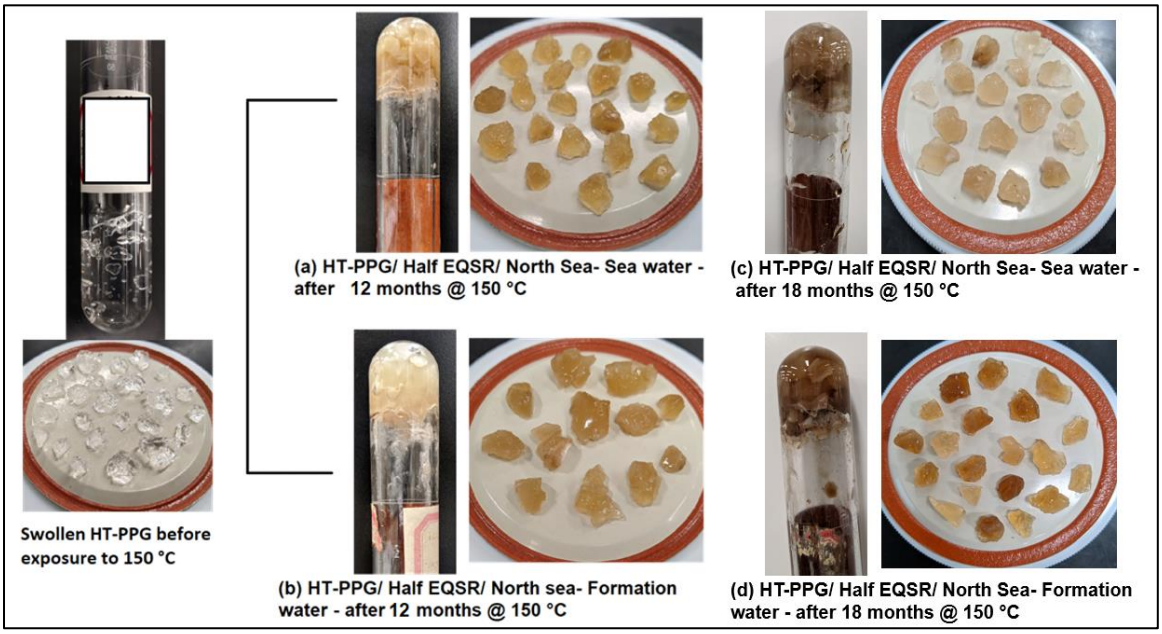

Figure 7. Thermal stability observations of HT-PPG at Half EQSR aged in (a) North Sea Seawater and (b) North Sea Formation water for 12 months at 150 °C temperature, (c) North Sea Seawater and (d) North Sea Formation water for 18 months at 150 °C temperature.

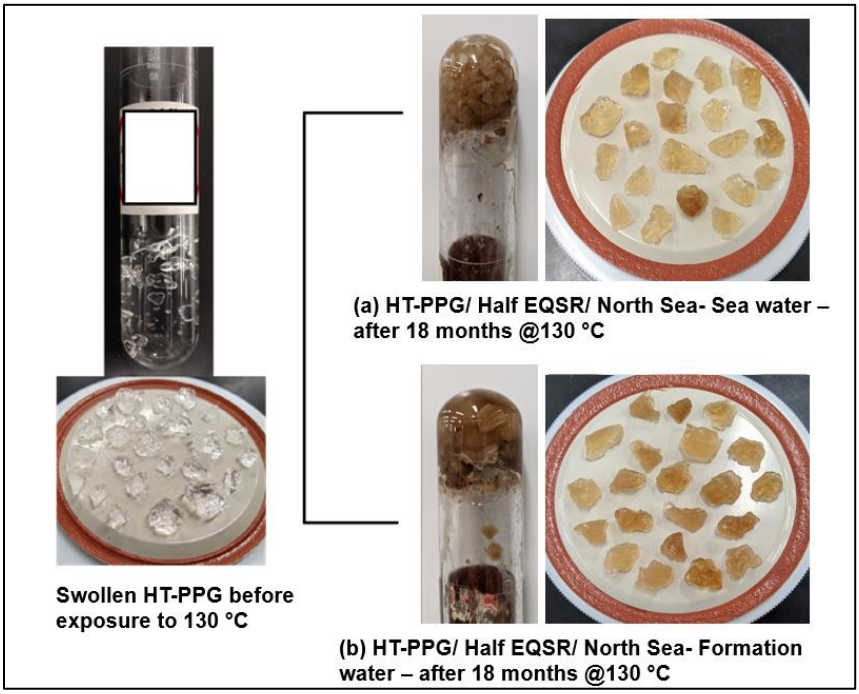

Figure 8. Thermal stability observations of HT-PPG at Half EQSR aged in (a) North Sea Seawater and (b) North Sea Formation water for 18 months at 150 °C temperature.

The chemical composition of HT-PPG after aging for 12 months at 150 °C in North Sea seawater and formation water can be studied through ^{13}C NMR technique. Solid-state CPMAS ^{13}C NMR was performed on a Bruker Avance III 400 MHz spectrometer. If HT-PPGs are undergoing degradation, they will form degradation products, which can be captured as a new compositional signal in NMR. Figure 9 represents the retention of chemical structure for HT-PPG aged sample when ^{13}C NMR signals were compared to the control HT-PPG sample. Signal around 173.5 ppm confirmed presence of carbonyl carbon from dimethylacrylamide while signals around 145 ppm and 125 ppm confirmed retention of aromatic ring of sodium styrenesulfonate after aging. Signals in the range of 30 to 40 ppm ascribed to combined signal from aliphatic backbone of copolymer of poly (dimethylacrylamide-co-sodium styrenesulfonate). Thus, aged HT-

PPG samples in North Sea brines are chemically identical to HT-PPG control sample and thermally stable for more than 12 months at 150 °C and in accordance with our previous reports (Salunkhe et al. 2021).

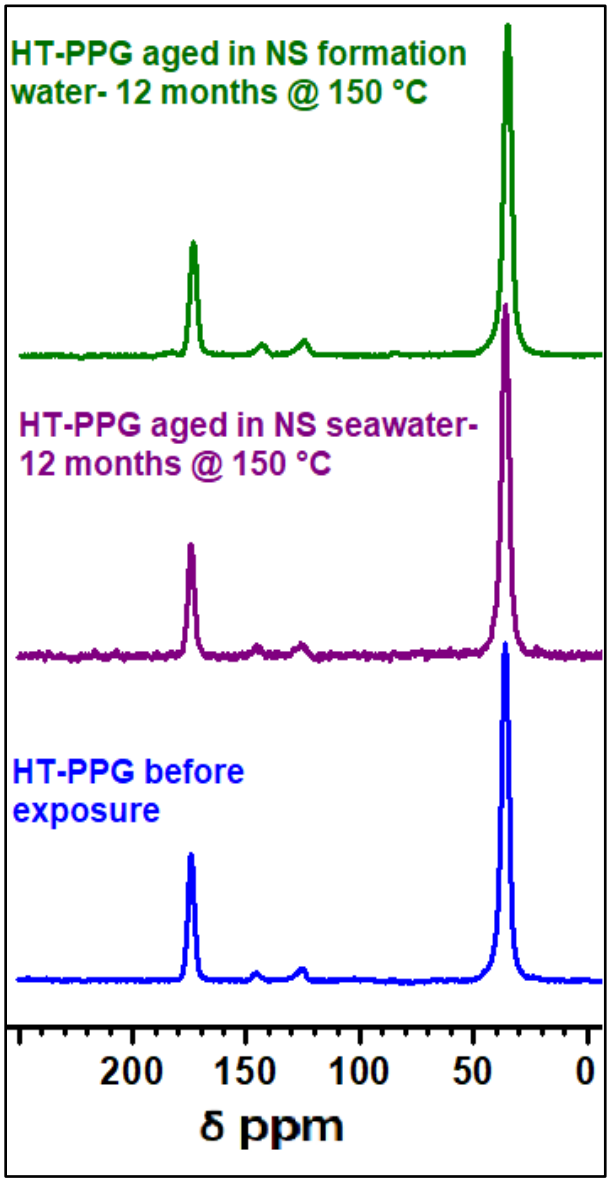

Figure 9. Solid-state CPMAS ^{13}C NMR for HT-PPG before aging as control sample, HT-PPG aged North Sea seawater and HT-PPG aged North Sea formation water at 150 °C for 12 months.

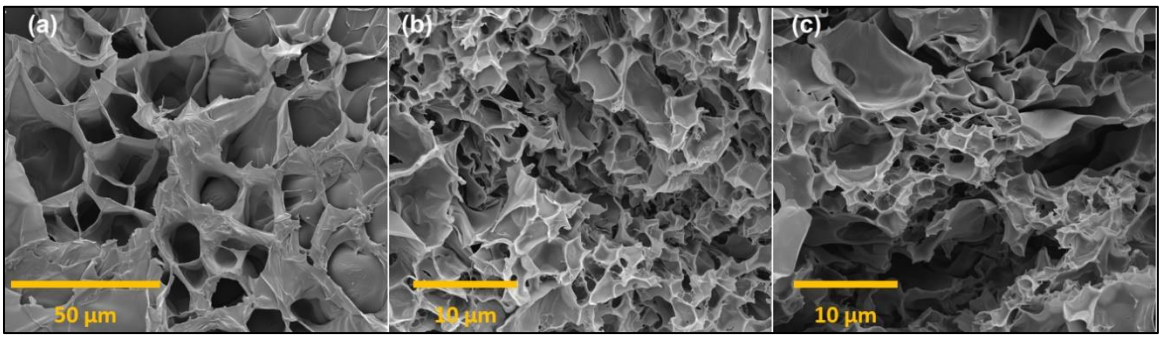

Figure 10. SEM images of (a) fully swollen HT-PPG before aging, (b) HT-PPG in North Sea seawater at half EQSR, aged at 150 °C for 12 months and (c) HT-PPG in North Sea formation water at half EQSR, aged at 150 °C for 12 months.

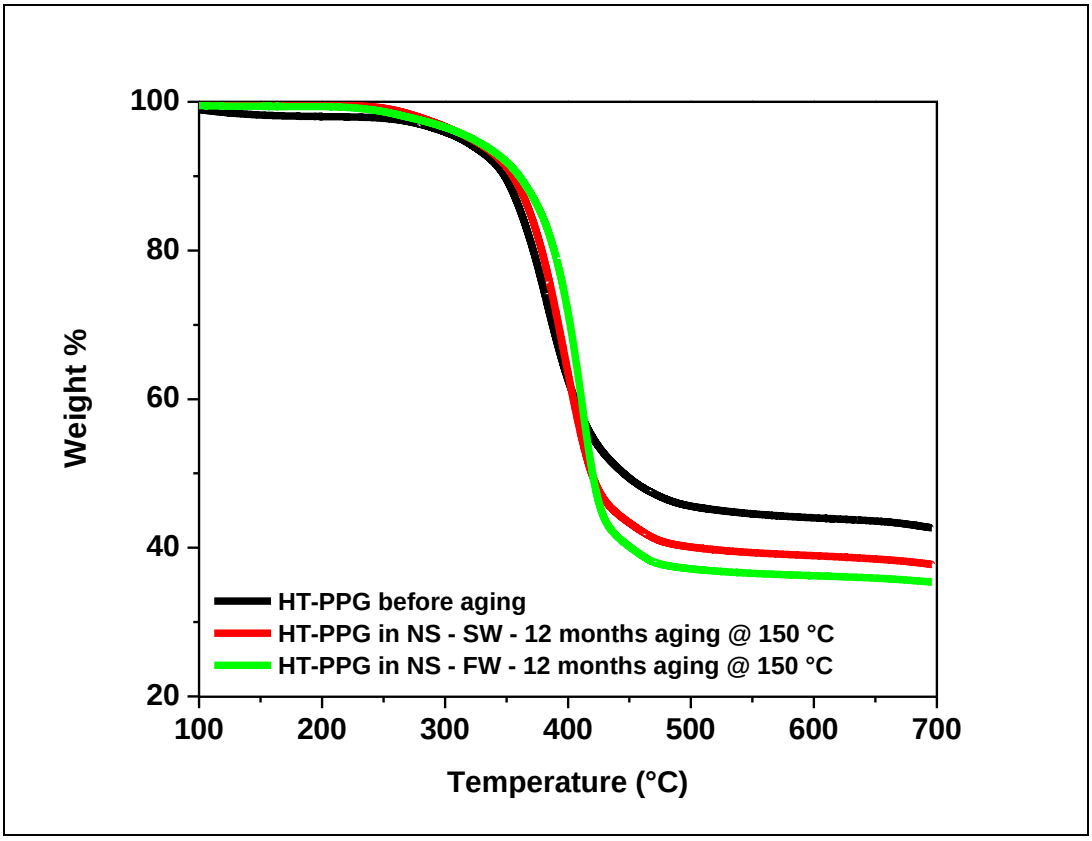

Figure 11. Thermogravimetric analysis results for HT-PPG samples representing percent weight loss as a function of temperature

Gel structural integrity was observed through scanning electron microscopy images for HT-PPG aged samples. As seen from Figure 10 (b), for HT-PPG aged sample in North Sea seawater for 12 months and 10 (c), for HT-PPG aged sample in North Sea formation water for 12 months, the crosslinked polymer network structure is retained after aging. Retention of gel microstructure confirmed structural stability of the gel matrix against higher temperature and ionic environment degradation.

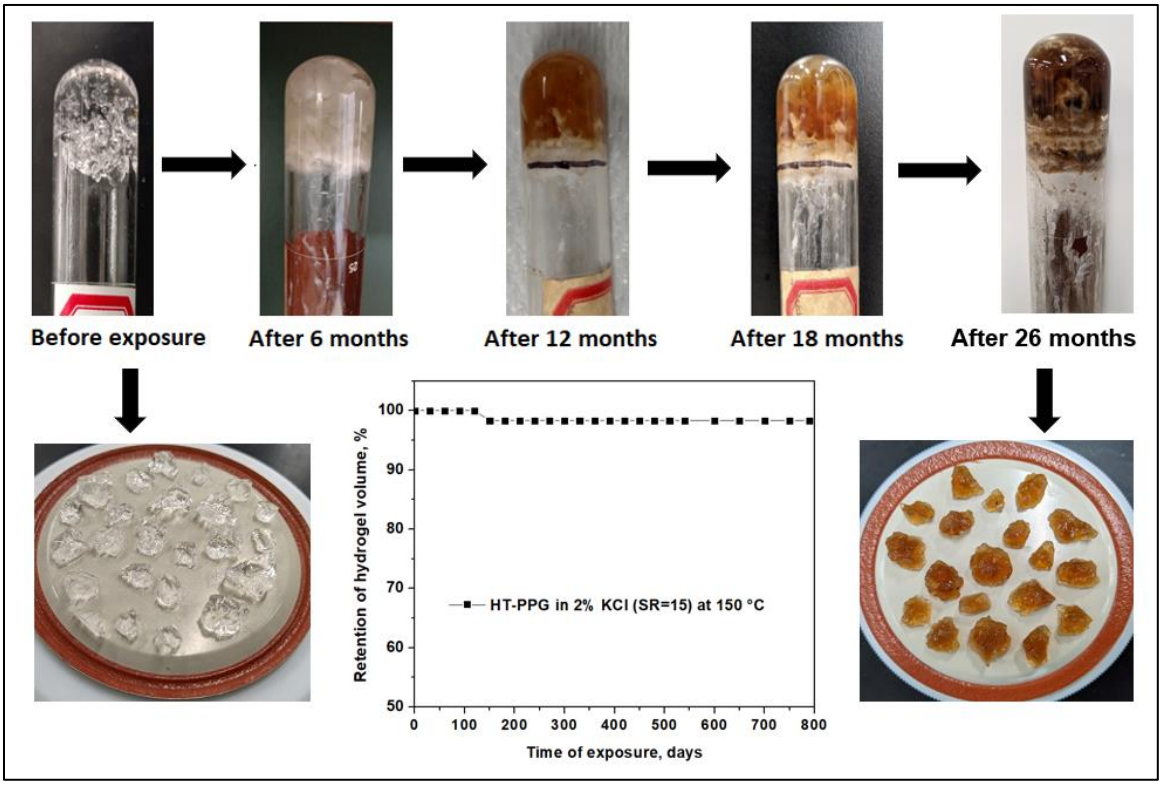

Figure 12. Thermal stability evaluation of HT-PPG in 2% KCl at SR =15 and temperature of 150 ◦C. HT-PPGs recovered after 26 months of aging shows retention of structural integrity and form of gel particles.

Freeze-dried HT-PPG aged samples in North Sea seawater and formation water for 12 months were analyzed using Thermogravimetric analyses (TGA) and compared

with the control sample of HT-PPG. As seen in Figure 11, no new peaks or inflections points were observed for these HT-PPG aged samples in North Sea brines when compared with HT-PPG control sample. This further confirmed that HT-PPG compositions are thermally stable at 150 °C for more than 12 months.

We also performed HT-PPG thermal stability in 2% KCl solution as it is commonly used: the injection brines in some of oilfields by oil producing companies seeking to inhibit shale hydration. Swollen HT-PPG with a swelling ratio of 15 (brine content = ~ 94 %) in 2% KCl were exposed for more than 2 years (Figure 12). HT-PPG found to be stable at 150 °C temperature for up to 26 months without showing any signs of syneresis or degradation which further confirmed the robustness of HT-PPG towards harsh reservoir conditions.

3.4. COREFLOOD TEST

Fractured core model depicts the performance of HT-PPG after the gel placement using residual resistance factor that determines the extent of permeability reduction to formation water. Figure 13 shows three regions of core flood experiment, first water flooding, gel placement and second water flooding representing stabilized pressure gradient as a function of time and flowrate. It was observed that injection brine (formation water) preferentially flooded the fractured core during the first water flooding, creating a low-pressure gradient owing to the open fracture heterogeneity. During the placement of swollen HT-PPG, pressure gradient was gradually increased implying transport of HT-PPG and thus eventually packing the open fracture in the core. The gel particles injection was continued until produced at effluent, where the pressure gradient

was reduced from 420 psi/ft to a stabilized pressure gradient of 135.4 psi/ft. Before initiating the second water flooding process, the tubes connecting to the core holder were cleaned.

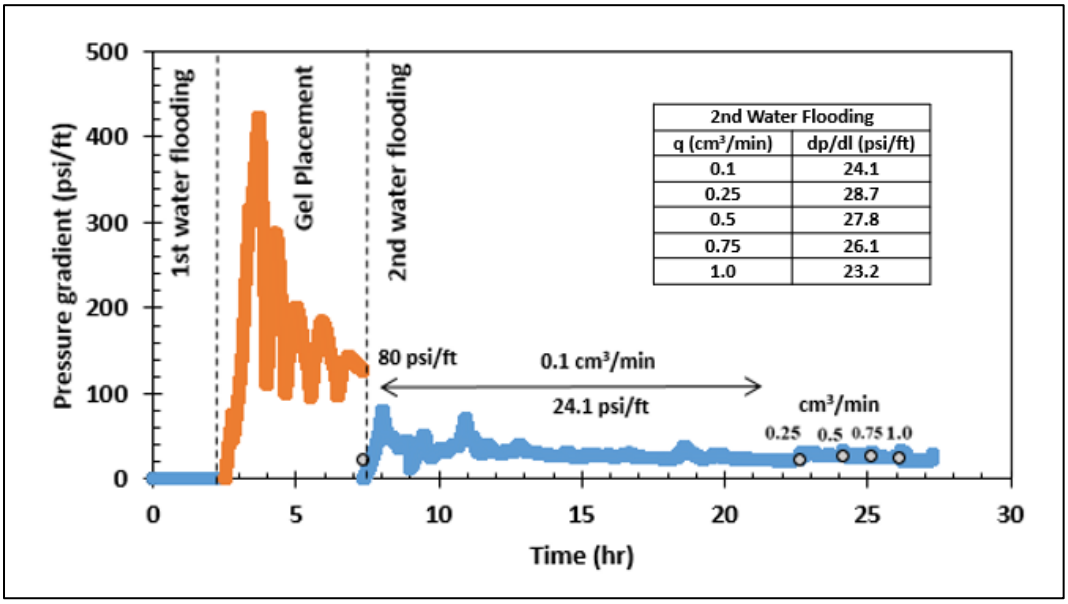

Figure 13. The pressure gradient vs. time of the coreflooding test illustrating the 1st water flooding, gel placement and 2nd water flooding

Second water flooding process was conducted at different injection flow rates viz; 0.1, 0.25, 0.5, 0.75 and 1.0 mL/min to investigate the efficiency of the packed gel in the fracture. In the beginning of second water flooding at 0.1 mL/min injection flow rate, the pressure gradient increased rapidly. This can be ascribed to the resistance of HT-PPG to the chase water resulting into water breakthrough at 80 psi/ft. The water injection was continued at 0.1 mL/min until stabilized pressure gradient of 24.1 psi/ft was attained. The injection flow rates were further increased to 0.25, 0.5, 0.75 and 1 mL/min and

corresponding stabilized pressure gradients of 28.7, 27.8, 26.1 and 23.2 psi/ft were obtained.

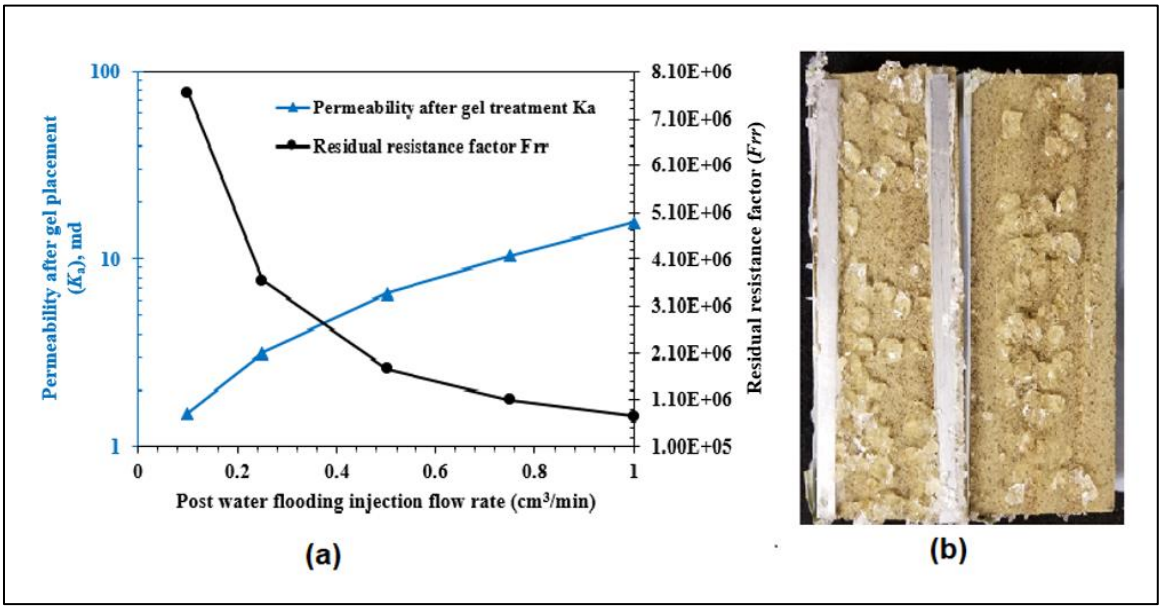

Figure 14. (a) The Residual resistance factor (Frr) and fracture permeability (*K*after) at variable brine injection rates, (b) The fractured core after the test showing the packed HT-PPG.

Residual resistance factor, Frr was calculated from the stabilized pressure gradient values to determine the extent of the permeability reduction to injection water of the fractured core after the gel placement. Frr is an important parameter to confirm plugging efficiency performance data obtained in core-flooding test. Frr and fracture permeability after blocking (*K*after) at variable brine injection rates is shown in Figure 14a. The Frr values decreased with the increase in brine injection flow rateswhich is a very common trend for gel blocking. It was noted that no gel washout was observed when we increased the brine injection rates. The high Frr values confirmed the good plugging efficiency by

HT-PPG to reduce the permeability of open fractures. After the coreflood experiment, the fractured core was removed and assessed for the condition of packed HT-PPG. The gel particles found to be adhered the surface of the fracture core (Figure 14b) which reaffirmed that HT-PPG successfully reduced the permeability of the open fracture.

4. CONCLUSIONS

- HT-PPG systems exhibiting long term hydrothermal stability were evaluated. The effect of parameters like salinity and temperature was evaluated, where HT-PPG were observed to swell up to 30 times their original volume.
- HT-PPG exhibited excellent swollen gel strengths with elastic moduli of over 3000 Pa at a swelling ratio of 10 times, confirming a robust nature.
- Thermal and hydrolytic stability of HT-PPG were studied in detail, where HT-PPG were found to be stable for more than 18 months in both North Sea seawater and formation water at 130 and 150 °C.
- Thermal stability observations were further confirmed using Solid-state CPMAS ^{13}C NMR spectroscopy, where aged samples were found to be chemically identical to the control sample. SEM and TGA analyses reaffirmed the thermal stability of HT-PPG post-aging with no loss of molecular integrity.
- HT-PPG can reduce the permeability of open fractures to mili-Darcy level and thus can be used to control the conformance of a reservoir with open fractures or conduits.

- Overall, HT-PPG is a novel product with excellent features that make it an ideal candidate for treating conformance problems associated with reservoirs of high temperature and salinity conditions.

ACKNOWLEDGEMENT

The authors would like to acknowledge funding from our Preformed Particle Gel Conformance Control Consortium company members: ConocoPhillips, Occidental Petroleum, Daqing Xinwantong Technology Developing Company, Ltd. and Petrochina that supported this work.

REFERENCES

Alhuraishawy, Ali K., Bai, Baojun, Imqam, Abdulmohsin et al. 2018. Experimental study of combining low salinity water flooding and preformed particle gel to enhance oil recovery for fractured carbonate reservoirs. *Fuel* **214**: 342-350. http://www.sciencedirect.com/science/article/pii/S0016236117313066.

Babadagli, Tayfun. 2007. Development of mature oil fields — A review. *Journal of Petroleum Science and Engineering* **57** (3): 221-246. http://www.sciencedirect.com/science/article/pii/S0920410506002464.

Bai, Baojun, Li, Liangxiong, Liu, Yuzhang et al. 2004. Preformed Particle Gel for Conformance Control: Factors Affecting Its Properties and Applications. *SPE Reservoir Evaluation & Engineering* **10**.

Bai, Baojun, Liu, Yuzhang, Coste, Jean-Paul et al. 2007. Preformed Particle Gel for Conformance Control: Transport Mechanism Through Porous Media. *SPE Reservoir Evaluation & Engineering* **10** (02): 176-184. https://doi.org/10.2118/89468-PA.

Bai, Baojun, Wei, Mingzhen, and Liu, Yuzhang. 2013. Field and Lab Experience With a Successful Preformed Particle Gel Conformance Control Technology. Paper presented at the SPE Production and Operations Symposium, Oklahoma City, Oklahoma, USA, 2013/3/23/. SPE. https://doi.org/10.2118/164511-MS.

Chauveteau, G., Omari, A., Tabary, R. et al. 2000. Controlling Gelation Time and Microgel Size for Water Shutoff. Paper presented at the SPE/DOE Improved Oil Recovery Symposium, Tulsa, Oklahoma, 2000/1/1/. SPE. https://doi.org/10.2118/59317-MS.

Cordes, Erik E., Jones, Daniel O. B., Schlacher, Thomas A. et al. 2016. *Review*. Environmental Impacts of the Deep-Water Oil and Gas Industry: A Review to Guide Management Strategies (in English). *Frontiers in Environmental Science* **4** (58). https://www.frontiersin.org/article/10.3389/fenvs.2016.00058.

Coste, J.-P., Liu, Y., Bai, B. et al. 2000. In-Depth Fluid Diversion by Pre-Gelled Particles. Laboratory Study and Pilot Testing. *Proc.*, SPE/DOE Improved Oil Recovery Symposium. https://doi.org/10.2118/59362-MS.

Durán-Valencia, Cecilia, Bai, Baojun, Reyes, Horacio et al. 2014. Development of enhanced nanocomposite preformed particle gels for conformance control in high-temperature and high-salinity oil reservoirs. *Polymer Journal* **46** (5): 277-284. https://doi.org/10.1038/pj.2013.99.

Elsharafi, Mahmoud O. and Bai, Baojun. 2012. Effect of Weak Preformed Particle Gel on Unswept Oil Zones/Areas during Conformance Control Treatments. *Industrial & Engineering Chemistry Research* **51** (35): 11547-11554. https://doi.org/10.1021/ie3007227.

Elsharafi, Mahmoud O. and Bai, Baojun. 2016. Influence of strong preformed particle gels on low permeable formations in mature reservoirs. *Petroleum Science* **13** (1): 77-90. https://doi.org/10.1007/s12182-015-0072-3.

Flory, P.J. 1953. *Principles of Polymer Chemistry*: Cornell University Press.

Flory, Paul J. and Rehner, John. 1943. Statistical Mechanics of Cross-Linked Polymer Networks II. Swelling. *The Journal of Chemical Physics* **11** (11): 521-526. https://doi.org/10.1063/1.1723792.

Goudarzi, Ali, Zhang, Hao, Varavei, Abdoljalil et al. 2015. A laboratory and simulation study of preformed particle gels for water conformance control. *Fuel* **140**: 502-513. http://www.sciencedirect.com/science/article/pii/S0016236114009508.

Huggins, Maurice L. 1942. THERMODYNAMIC PROPERTIES OF SOLUTIONS OF LONG-CHAIN COMPOUNDS. *Annals of the New York Academy of Sciences* **43** (1): 1-32. https://nyaspubs.onlinelibrary.wiley.com/doi/abs/10.1111/j.1749-6632.1942.tb47940.x.

Imqam, Abdulmohsin and Bai, Baojun. 2015. Optimizing the strength and size of preformed particle gels for better conformance control treatment. *Fuel* **148**: 178-185. https://www.sciencedirect.com/science/article/pii/S0016236115000368.

Imqam, Abdulmohsin, Wang, Ze, and Bai, Baojun. 2017a. The plugging performance of preformed particle gel to water flow through large opening void space conduits. *Journal of Petroleum Science and Engineering* **156**: 51-61. http://www.sciencedirect.com/science/article/pii/S0920410516310579.

Imqam, Abdulmohsin, Wang, Ze, and Bai, Baojun. 2017b. Preformed-Particle-Gel Transport Through Heterogeneous Void-Space Conduits. *SPE-191697-PA* **22** (05): 1437-1447. https://doi.org/10.2118/179705-PA.

Javanmard, Hoda, Seyyedi, Mojtaba, and Nielsen, Sidsel M. 2018. On Oil Recovery Mechanisms and Potential of DME–Brine Injection in the North Sea Chalk Oil Reservoirs. *Industrial & Engineering Chemistry Research* **57** (46): 15898-15908. https://doi.org/10.1021/acs.iecr.8b04278.

Jennings, R.R., Rogers, J.H., and West, T.J. 1971. Factors Influencing Mobility Control By Polymer Solutions. *Journal of Petroleum Technology* **23** (03): 391-401. https://doi.org/10.2118/2867-PA.

Kwok, Alan Y., Qiao, Greg G., and Solomon, David H. 2003. Synthetic hydrogels. 1. Effects of solvent on poly(acrylamide) networks. *Polymer* **44** (20): 6195-6203. http://www.sciencedirect.com/science/article/pii/S0032386103006712.

Lande, Sheldon S., Bosch, Stephen J., and Howard, Philip H. 1979. Degradation and Leaching of Acrylamide in Soil. *Journal of Environmental Quality* **8** (1): 133-137. https://acsess.onlinelibrary.wiley.com/doi/abs/10.2134/jeq1979.00472425000800010029x.

Leng, Jianqiao, Wei, Mingzhen, and Bai, Baojun. 2021. Review of transport mechanisms and numerical simulation studies of preformed particle gel for conformance control. *Journal of Petroleum Science and Engineering*: 109051. https://www.sciencedirect.com/science/article/pii/S0920410521007087.

Lin, David C., Douglas, Jack F., and Horkay, Ferenc. 2010. *10.1039/B925219N*. Development of minimal models of the elastic properties of flexible and stiff polymer networks with permanent and thermoreversible cross-links. *Soft Matter* **6** (15): 3548-3561. http://dx.doi.org/10.1039/B925219N.

Lu, Mang, Wu, Xuejiao, and Wei, Xiaofang. 2012. Chemical degradation of polyacrylamide by advanced oxidation processes. *Environmental Technology* **33** (9): 1021-1028. https://doi.org/10.1080/09593330.2011.606279.

Mousavi Moghadam, Asefe, Vafaie Sefti, Mohsen, Baghban Salehi, Mahsa et al. 2012. Preformed particle gel: evaluation and optimization of salinity and pH on equilibrium swelling ratio. *Journal of Petroleum Exploration and Production Technology* **2** (2): 85-91. https://doi.org/10.1007/s13202-012-0024-z.

Mustoni, J. L., Norman, C. A., and Denyer, P.. 2010. Deep Conformance Control by a Novel Thermally Activated Particle System to Improve Sweep Efficiency in Mature Waterfloods of the San Jorge Basin. *Proc.*, SPE Improved Oil Recovery Symposium. https://doi.org/10.2118/129732-MS.

Saghafi, Hamid Reza. 2018. Retention characteristics of enhanced preformed particle gels (PPGs) in porous media: Conformance control implications. *Journal of Petroleum Science and Engineering* **166**: 962-968. https://www.sciencedirect.com/science/article/pii/S0920410518302900.

Salunkhe, Buddhabhushan, Schuman, Thomas, Al Brahim, Ali et al. 2021. Ultra-high temperature resistant preformed particle gels for enhanced oil recovery. *Chemical Engineering Journal* **426**: 130712. https://www.sciencedirect.com/science/article/pii/S1385894721022981.

Sang, Qian, Li, Yajun, Yu, Long et al. 2014. Enhanced oil recovery by branched-preformed particle gel injection in parallel-sandpack models. *Fuel* **136**: 295-306. https://www.sciencedirect.com/science/article/pii/S0016236114007169.

Tongwa, Paul, Nygaard, Runar, and Bai, Baojun. 2013. Evaluation of a nanocomposite hydrogel for water shut-off in enhanced oil recovery applications: Design, synthesis, and characterization. *Journal of Applied Polymer Science* **128** (1): 787-794. https://onlinelibrary.wiley.com/doi/abs/10.1002/app.38258.

Touzé, S., Guerin, V., Guezennec, A. G. et al. 2015. Dissemination of acrylamide monomer from polyacrylamide-based flocculant use--sand and gravel quarry case study (in eng). *Environmental science and pollution research international* **22** (9): 6423-30.

van Vliet, T., van Dijk, H. J. M., Zoon, P. et al. 1991. Relation between syneresis and rheological properties of particle gels. *Colloid and Polymer Science* **269** (6): 620-627. https://doi.org/10.1007/BF00659917.

Wang, Ze, Bai, Baojun, Sun, Xindi et al. 2019. Effect of multiple factors on preformed particle gel placement, dehydration, and plugging performance in partially open fractures. *Fuel* **251**: 73-81. https://www.sciencedirect.com/science/article/pii/S0016236119305824.

Xiong, Boya, Loss, Rebeca Dettam, Shields, Derrick et al. 2018. Polyacrylamide degradation and its implications in environmental systems. *npj Clean Water* **1** (1): 17. https://doi.org/10.1038/s41545-018-0016-8.

Zaitoun, Alain, Tabary, Rene, Rousseau, David et al. 2007. Using Microgels to Shut Off Water in a Gas Storage Well. *Proc.*, International Symposium on Oilfield Chemistry. https://doi.org/10.2118/106042-MS.

Zhang, Hao and Bai, Baojun. 2011. Preformed-Particle-Gel Transport Through Open Fractures and Its Effect on Water Flow. *SPE-191697-PA* **16** (02): 388-400. https://doi.org/10.2118/129908-PA.

III. EXPERIMENTAL DATA ON WATER SOLUBLE POLYMERS THERMAL AND HYDROLYTIC STABILITY, REACTIVITY RATIOS OF MONOMERS AND Frr CALCULATION FOR THERMALLY STABLE PREFORMED PARTICLE GELS THEREFROM

Buddhabhushan Salunkhe[a], Thomas Schuman[a,*], Ali Al Brahim[b], Baojun Bai[b],

[a] *Chemistry, Missouri University of Science and Technology, Rolla, MO 65409, USA*

[b] *Petroleum Engineering, Missouri University of Science and Technology, Rolla, MO 65409, USA*

*Corresponding Author: Thomas Schuman, 335 Schrenk Hall, Department of Chemistry, Missouri University of Science and Technology, Rolla, MO 65409, USA
Tel. - +1 573 341 6236, Email - tschuman@mst.edu

ABSTRACT

Experimental data on water soluble polymer thermal and hydrolytic stability in acidic, neutral and basic pH conditions in aqueous solution is presented. Thermal and hydrolytic stability of polymer aqueous solutions were monitored in variable pH medium by aging at 130 °C temperature for different aging time. Polymer viscosity measurements were performed periodically for 3 months. Furthermore, this data can serve as a basis of monomer selection for thermally stable hydrogels for applications like oil recovery, hydrogel coatings for steam sterilized medical devices and other applications. Reactivity ratios were determined for monomers associated to the most stable polymers using ^{1}H NMR analysis. Monomer reactivity ratios for DMA (M_1) and NaSS (M_2) depicted to be $r_1 = 0.031$ and $r_2 = 5.379$ using Fineman-Ross method and $r_1 = 0.028$ and $r_2 = 5.495$ using Kelen-Tudos method. The performance of preformed particle gels developed based

on these monomers, in plugging the open fractures is explained using residual resistance factor (Frr) calculation.

Keywords: Thermal stability of polymers, Hydrolytic stability of polymers, Viscosity measurements, Thermogravimetric analysis (TGA), Reactivity ratio, Residual resistance factor (Frr)

1. SPECIFICATIONS TABLE

Subject	Chemistry
Specific subject area	Polymer thermal and hydrolytic stability in aqueous solutions, reactivity ratios of monomers, residual resistance factor (Frr) calculation
Type of data	Table Image Graph Figure
How data were acquired	Polymer thermal and hydrolytic stability was determined by viscosity measurements on Brookfield DV3T viscometer. For reactivity ratio, copolymer composition was analysed using ^{1}H NMR technique. Residual resistance factor (Frr) calculations were explained based on lab scale core flooding test performed in sandstone core.
Data format	Raw, Analyzed

Parameters for data collection	Change in viscosity as a function of time for polymer thermal and hydrolytic stability. For reactivity ratios, copolymer composition as a function of comonomers feed ratio was studied using Fineman-Ross method and Kelen-Tudos method. Frr, calculations were done based on pressure gradient values obtained during a core-flooding test.
Description of data collection	For hydrolytic thermal stability of polymer aqueous solutions, viscosity at 23 °C was determined for samples that were exposed to 130 °C temperature for variable time in acidic, basic and neutral pH. The change in viscosity was correlated to polymer molecular weight change and determine polymer backbone stability. For reactivity ratios, polymerization was conducted at different co-monomers feed, and by collecting the copolymer at early stage of polymerization (preferably less than 10% conversion) and analysed using ^{1}H NMR. For Frr calculation, permeability values were obtained from stable pressure gradient values following Darcy law.
Data source location	Institution: Missouri University of Science and Technology City/Town/Region: Rolla, Missouri Country: United States of America
Data accessibility	With the article
Related research article	B. Salunkhe, T. Schuman, A A Brahim, B. Bai, Ultra-High Temperature Resistant Preformed Particle Gels for Enhanced Oil Recovery, Chem. Eng. J. In Press.

1.1. VALUE OF THE DATA

- The dataset represents viscosity measurements data to determine thermal and hydrolytic stability when polymer aqueous solutions were prepared in acidic, neutral and basic medium.
- The data on reactivity ratios of p-Sodium styrene sulfonate and N, N'-Dimethylacrylamide was reported and can be beneficial for researchers who are interested in synthesizing copolymer compositions based on these monomers for variety of applications. This is the first report of reactivity ratio data for this monomer combination.
- Residual resistance factor (Frr) calculation are critical and small errors can give rise to large errors in Frr values. Dataset for Frr explained herein can aid a direction for petroleum engineers to conduct experiments to understand plugging efficiency of open fractures.

1.2. DATA DESCRIPTION

Data for thermal and hydrolytic stability of a polymer aqueous solutions is represented in Figure 1. The dataset represents the viscosity values of polymer aqueous solutions recorded as a function of time (# of days exposed at 130 °C) when prepared in medium of pH 2 (acidic), pH 7 (neutral) and pH 13 (basic). The obtained viscosity values for polyacrylamide and polyacrylic acid depicts that these polymers are hydrolytically and thermally unstable at 130 °C in all pH media. For Polyvinylpyrrolidone polymer, viscosity increase as a function of time in all pH media was noted, which can be attributed to partial hydrolysis of polymers. Polydimethylacrylamide showed increase in

viscosity as a function of time under acidic condition, on the other hand, under neutral and basic condition, less significant changes to the initial reported viscosity values were observed. Poly (sodium styrenesulfonate) polymer solutions showed almost similar viscosity values over the period of exposure under all pH conditions, depicting the thermal and hydrolytic stability of this polymer. Actual values for all polymer solutions are reported in attached excel file. This dataset can be useful in screening of polymers for applications involving variable moisture, pH and temperature conditions.

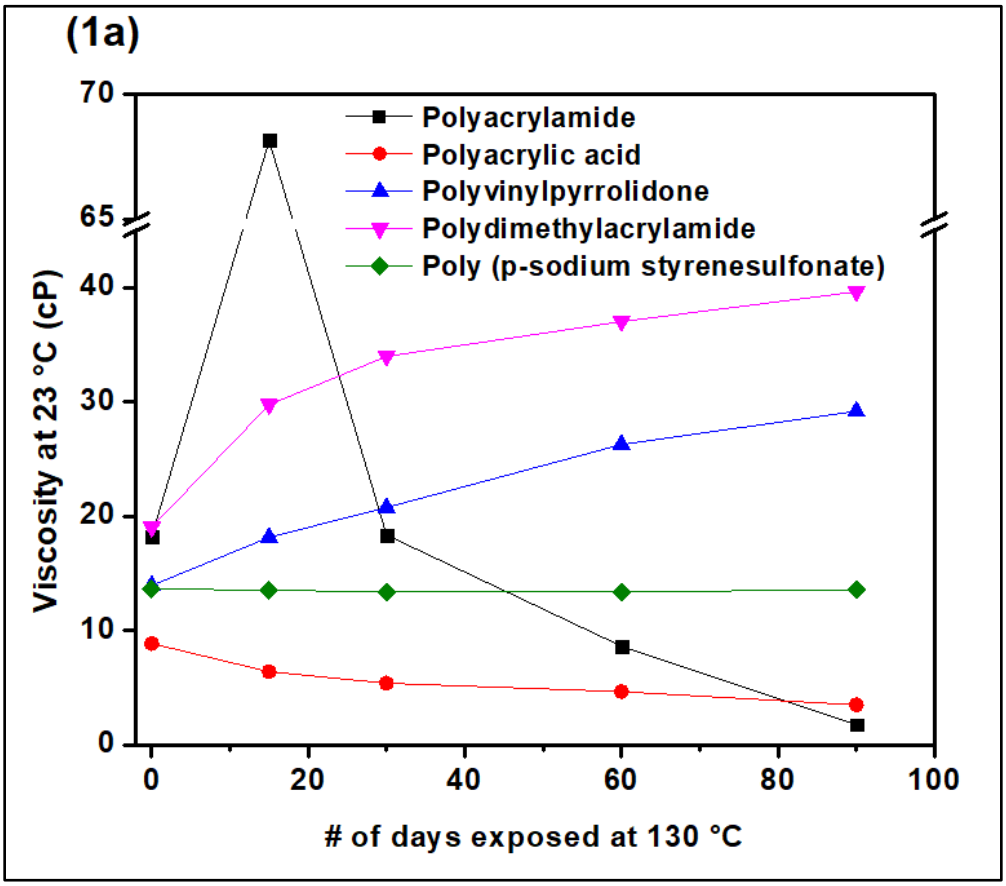

Figure 1. Thermal and hydrolytic stability of polymer aqueous solutions when exposed at 130 °C for different timeframes. The plot represents viscosity (cP) for polymer aqueous solutions prepared in acidic solution of pH=2 (figure 1a), neutral pH=7 (figure 1b) and basic pH=13 (figure 1c) as a function of aging time (days)

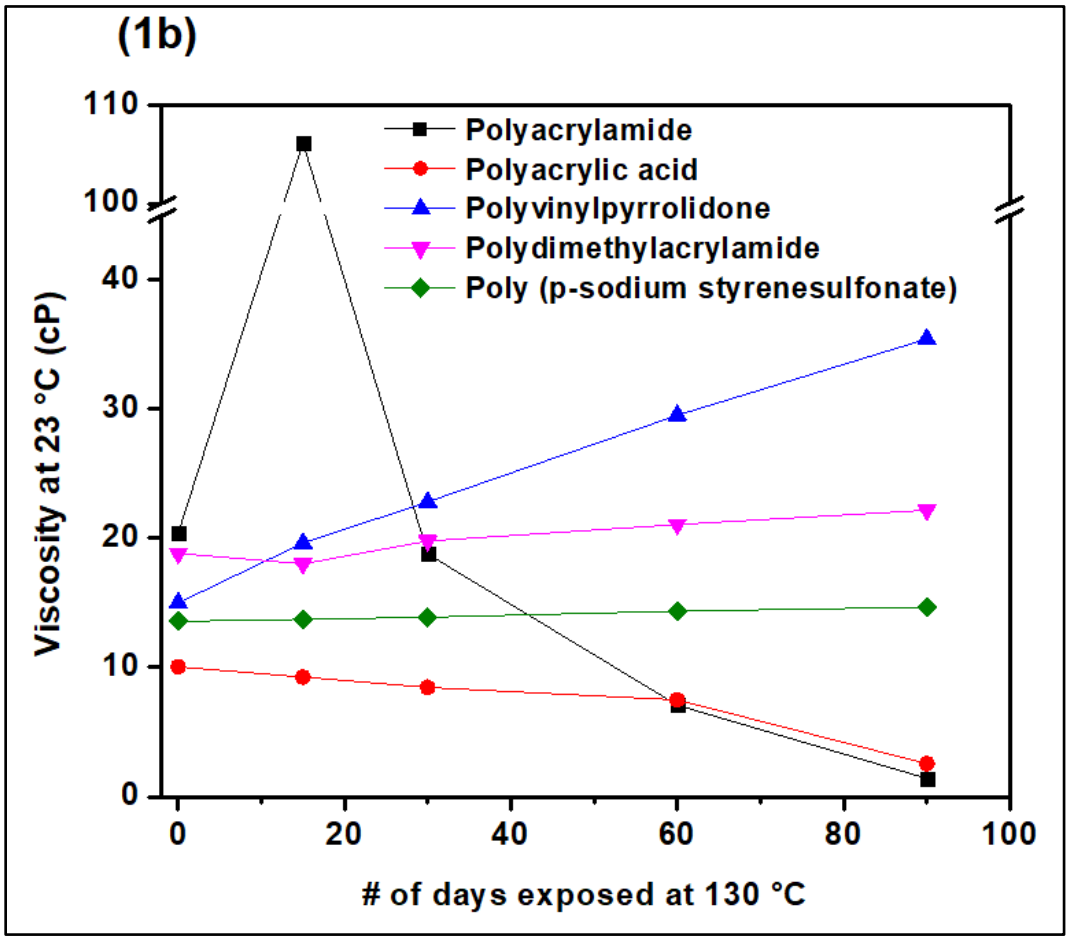

Figure 1. Thermal and hydrolytic stability of polymer aqueous solutions when exposed at 130 °C for different timeframes. The plot represents viscosity (cP) for polymer aqueous solutions prepared in acidic solution of pH=2 (figure 1a), neutral pH=7 (figure 1b) and basic pH=13 (figure 1c) as a function of aging time (days) (Cont.)

Figure 2 shows the reactivity ratio plots for monomers dimethylacrylamide and p-(sodium styrenesulfonate) using Fineman-ross method (Figure 2a) and Kelen-Tudos method (Figure 2b). The monomer reactivity ratios estimated to be r_1 = 0.031 and r_2 = 5.379 using Fineman-Ross method and r_1 = 0.028 and r_2 = 5.495 using Kelen-Tudos method where M_1 and M_2 monomers are for DMA and NaSS, respectively. These parameters indicate that NaSS has very high reactivity than that of DMA.

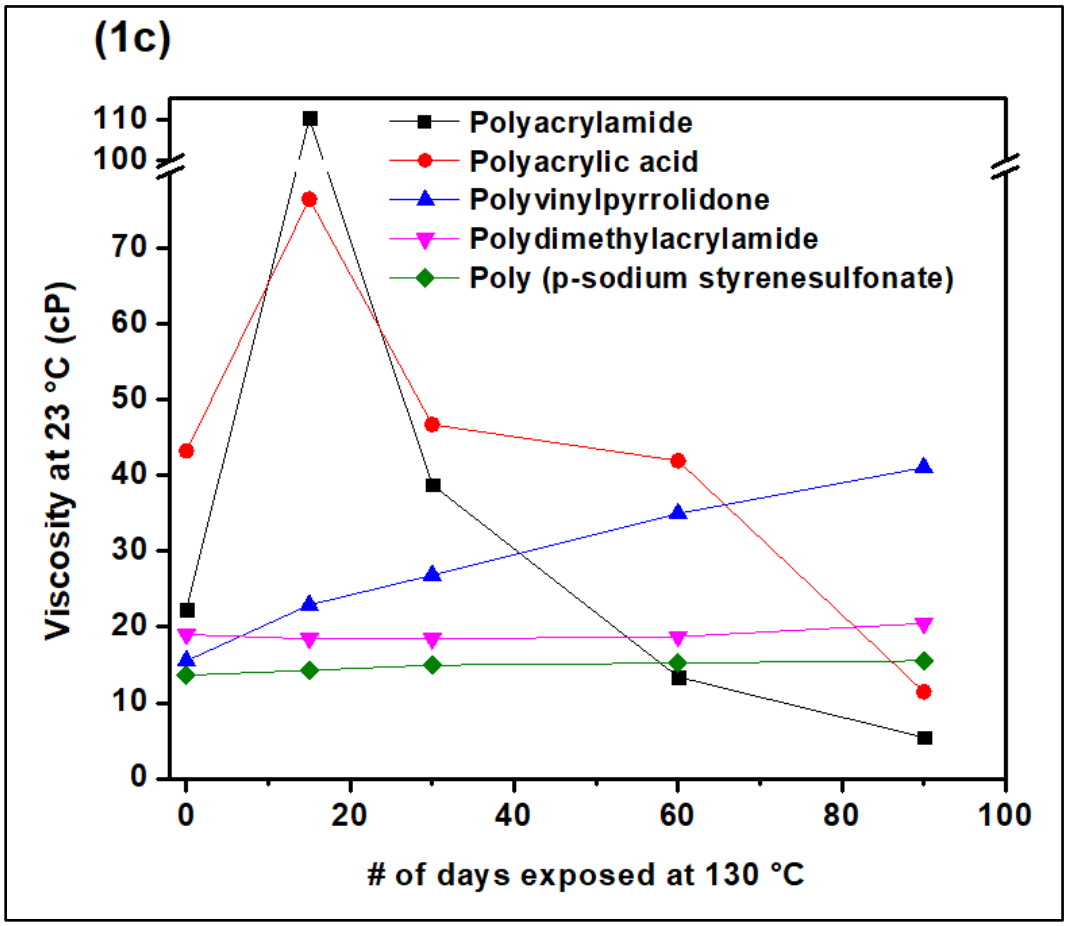

Figure 1. Thermal and hydrolytic stability of polymer aqueous solutions when exposed at 130 °C for different timeframes. The plot represents viscosity (cP) for polymer aqueous solutions prepared in acidic solution of pH=2 (figure 1a), neutral pH=7 (figure 1b) and basic pH=13 (figure 1c) as a function of aging time (days) (Cont.)

The Residual resistance factor (F_{rr}) is an important parameter to confirm plugging efficiency performance data obtained in core-flooding test. F_{rr} was calculated in order to determine the extent of the permeability reduction to water of the fractured core after the gel placement. Residual resistance factor (Frr) and fracture permeability (*K*after) at variable brine injection rates is shown in Figure 3. The Frr values decreased with the increase in brine injection flow rates, likely indicating that the chase water created a path

through or around the packed gel since no gel washout was observed with the increase in brine injection rates (explanation can be found in our CEJ paper).

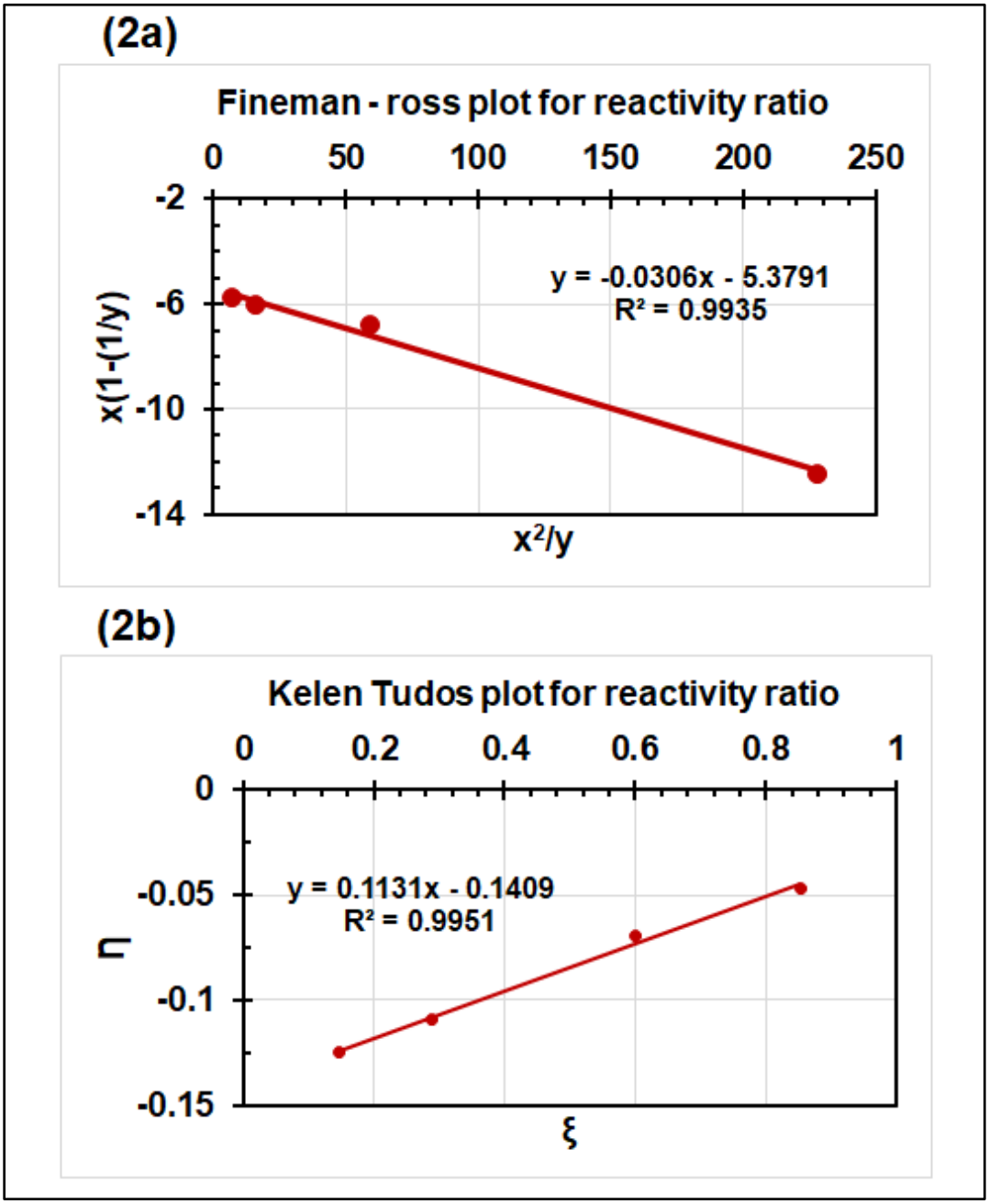

Figure 2. Reactivity ratios for monomers dimethylacrylamide [monomer 1] and p-(sodium styrenesulfonate) [monomer 2] using Fineman-Ross method (figure 2a) and Kelen-Tudos method (figure 2b).

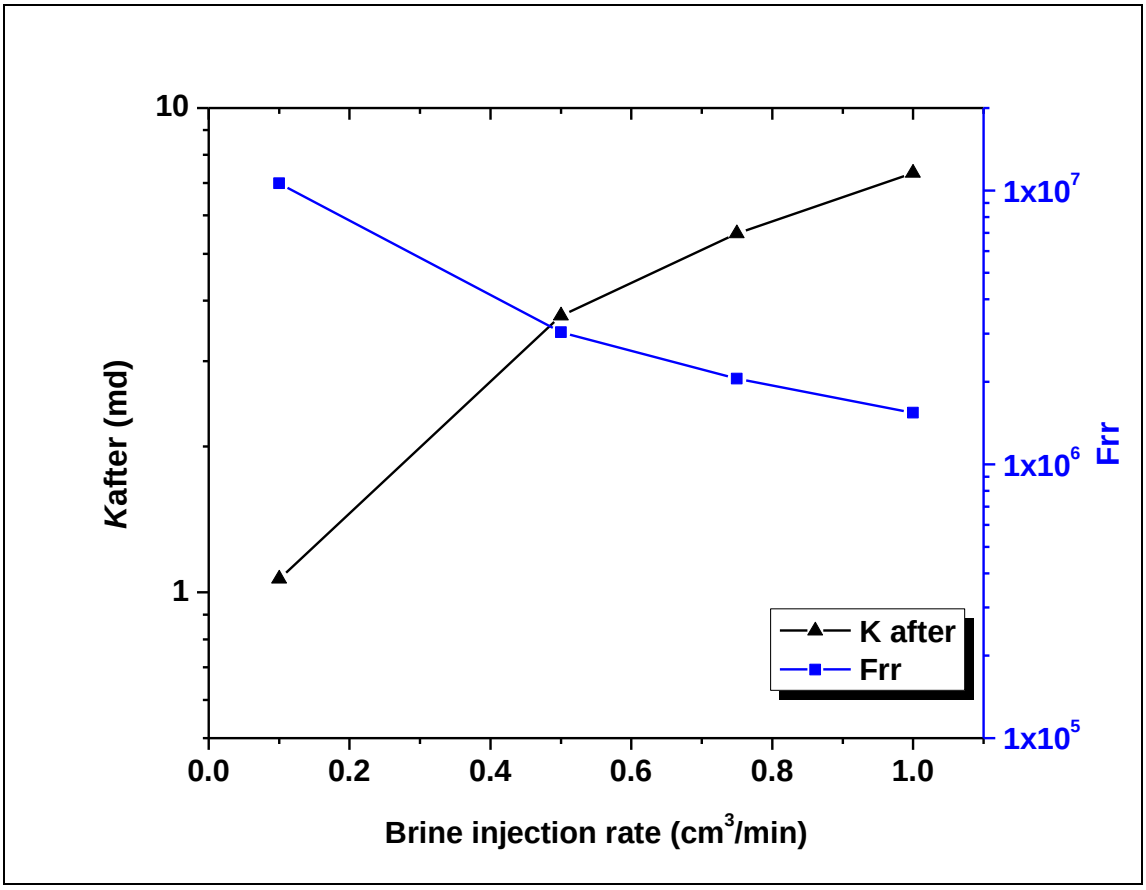

Figure 3. Residual resistance factor (Frr) and fracture permeability (*K*after) at variable brine injection rates

2. MATERIALS, METHODS, SAMPLE PREPARATION

2.1. MATERIALS

Polyacrylamide, Polyacrylic acid, Polyvinylpyrrolidone, Polydimethylacrylamide, Poly (sodium styrenesulfonate) commercial samples through Sigma-Aldrich, deuterium dioxide, Sodium styrenesulfonate (NaSS), N, N'-dimethylacrylamide (DMA), VA-044 initiator.

2.2. SAMPLE PREPARATION FOR THERMAL AND HYDROLYTIC STABILITY

Polymer aqueous solutions were prepared in different pH medium as acidic, neutral and basic in deionized water. Acidic solution of pH=2 was prepared using 0.1 M HCl and basic solution of pH=12 was prepared using 0.1 M NaOH along with neutral pH=7 solution. Polymer aqueous solutions prepared in these solutions, at a concentration, just enough to get measurable value on Brookfield viscometer. Glass pressure tubes were used for testing, where sample was transferred through canula transfer and sealed under argon atmosphere. These glass tubes were then kept in oven maintained at 130 °C and periodic measurements viscosity measurements were performed.

2.3. MONOMER REACTIVITY RATIO DETERMINATION

The polymerization of NaSS and DMA were conducted at different monomer feed ratio using VA-044 initiator in D_2O. The polymerization reaction was conducted under argon inert atmosphere at 40 °C. After specific time, ^{1}H NMR spectrum was collected on 400 MHz NMR system, where monomer conversions were determined by monitoring the change in the intensity of peaks associated with vinylic protons of the monomers.

2.4. RESIDUAL RESISTANCE FACTOR (Frr) CALCULATION FOR COREFLOODING EXPERIMENTS

The Frr is defined as the ratio of the mobility of water before the gel placement to the mobility of water after the gel placement [1].

$$F_{rr} = \frac{\lambda_b}{\lambda_a} = \frac{K_b/\mu_w}{K_a/\mu_w} = \left(\frac{\Delta P_a}{\Delta P_b}\right) q \qquad (1)$$

where K_b represents the initial permeability of the fractured core including both the matrix and the fracture parts, and Ka is the permeability of the fractured core to brine after the HT-PPG placement. μ_w is the viscosity of the injected brine.

By applying Darcy's law

$$q = \frac{KA\Delta P}{\mu L} \quad (2)$$

where q is the volumetric injection flow rate (cc/sec), A is the cross-sectional area of the fractured core (cm^2), ΔP is the pressure drop along the fractured core (atm), μ is the viscosity of the brine and L is the length of the fractured core. The Frr can be expressed in terms of pressure gradient along the fractured core once the steady state condition is achieved as a function of the injection flow rate. The data file for pressure gradient values obtained during a core-flood experiment is attached. These pressure gradient values were used for further calculations.

The initial permeability of the fractured core K_b = 11313 Darcy. The pressure drop across the fractured core during the first water flooding was calculated using the following equation of the flow through the parallel plate model

$$\Delta P_b = \frac{12\mu Lq}{9.86\ X\ 10^7\ {w_f}^3\ w_h} \quad (3)$$

where, w_f is the fracture width and w_h is the fracture height for core used in core-flooding experiment.

ACKNOWLEDGEMENTS

The authors would like to acknowledge funding from our JIP Consortium members ConocoPhillips, Occidental Petroleum, Daqing Xinwantong Technology Developing Company, Ltd. and Petrochina that supported this work.

REFERENCES

[1] R.R. Jennings, J.H. Rogers, T.J. West, Factors Influencing Mobility Control By Polymer Solutions, Journal of Petroleum Technology 23(03) (1971) 391-401. https://doi.org/10.2118/2867-pa.

IV. SUPER-ADSORBENT HYDROGELS FOR REMOVAL OF METHYLENE BLUE FROM AQUEOUS SOLUTION: DYE ADSORPTION ISOTHERMS, KINETICS, AND THERMODYNAMIC PROPERTIES

Buddhabhushan Salunkhe[a], Thomas Schuman[a,*]

[a] *Chemistry, Missouri University of Science and Technology, Rolla, MO 65409, USA.*

*Corresponding Author: Thomas Schuman, 335 Schrenk Hall, Department of Chemistry, Missouri University of Science and Technology, Rolla, MO 65409, USA.
Tel. - +1 573 341 6236, Email - tschuman@mst.edu

ABSTRACT

Removal of dyes through adsorption from wastewater has gained substantial interest in recent years, especially in development of hydrogel based adsorbents, owing to their easy use and economical nature. The aim of the present study was to design a super-adsorbent hydrogel based on sodium styrenesulfonate (NaSS) monomer for removal of dyes like methylene blue (MB). NaSS displays both an aromatic ring and strongly ionic group in its monomer structure that can enhance adsorption capacity. Poly(sodium styrenesulfonate-co-dimethylacrylamide) hydrogels were prepared by solution free radical polymerization using gelatin methacryloyl (GelMA) as crosslinker, creating a highly porous, three-dimensionally crosslinked polymer network contributing to higher swelling ratios of up to 27,500%. These super-adsorbent hydrogels exhibited high adsorption capacity of 1270 mg/g for MB adsorption with above 98% removal efficiency. This is the first report for such a high adsorption capacity for dye absorbance for NaSS-based hydrogels. Additionally, the adsorption kinetics using a pseudo-first-order and the

Freundlich adsorption isotherm models for multilayer, heterogeneous adsorption processes has been reported. The adsorbents reusability was confirmed through 4 repeated cycles of desorption-adsorption. The results discussed herein illustrates that NaSS based chemistries can be used as an efficient option for removal of organic dyes from contaminated wastewater.

GRAPHICAL ABSTRACT

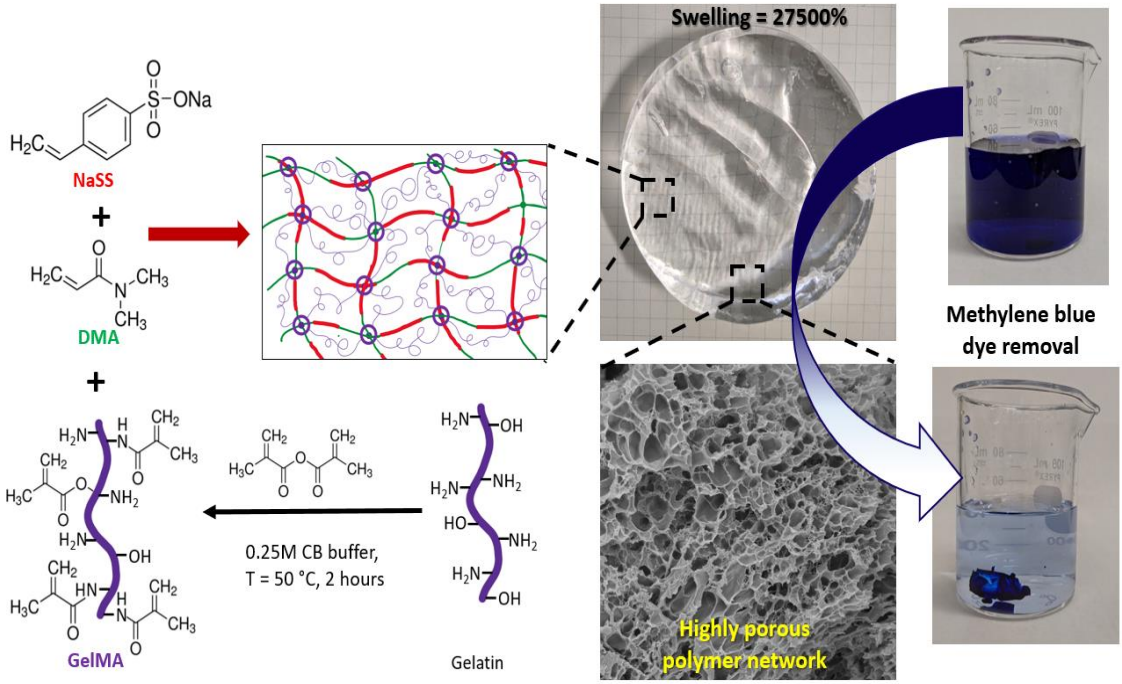

Keywords: super-adsorbent hydrogels, methylene blue, adsorption, kinetic, Isotherm

1. INTRODUCTION

Organic dyes are chemical compounds which are widely used in industries such as textile [1,2], paper, leather tanning [3], plastics [4], coatings [5,6], pharmaceutical [7], cosmetics [8], printing, ground water tracing, and many other chemical industries [9-13]. These industries consume large amounts of water at different stages and the wastewater generated is discharged as polluted effluents, which contain toxic substances such as heavy metals ions, dyes and other organic pollutants. The effluents cause serious environmental pollution and pose threats to human health as the pollutants are non-biodegradable, highly toxic, and often carcinogenic and/or mutagenic in nature [14]. Due to toxic effects of dyes, their removal from wastewater has become an important aspect in the field of water remediation. Among a variety of organic dyes, methylene blue (MB) is the most commonly used dye in textile and paper industries [15]. MB is toxic in nature with a carcinogenic and mutagenic character and is readily dissolved in the water. MB is harmful to humans at lower dosage of 1 to 7.5 ppm [16]and can cause increased heart rate, jaundice, vomiting, shock, eye burns and mental confusion.

A variety of methods are employed for removal of these dyes that include chemical oxidation [17], photochemistry [18], biological treatments, adsorption [12,19,20], ion exchange [21], and physical treatments [12]. Among these treatments, adsorption is among the most promising technique for dye removal from wastewater and has attracted interests of researchers and industry owing to its advantages like simple design, low cost, insensitivity to pollutants, easy regeneration, and effectiveness [22]. Hydrogels are most widely studied material as an adsorbent for organic dye removal from

wastewater owing to their excellent water absorption, high porosity, easy handling, and facile preparation resulting in a flexible network of polymer chains that helps penetration of solutes into the network [23]. The polymer backbone in these hydrogels can be designed with specific hydrophilic functional groups, e.g., carboxylic acids, amines, or sulfonic acids, which could be employed as complexing agents for dyes possessing opposite charge [15,24-26]. Hydrogels have physically well-defined, three-dimensional structures and can swell to several times of their original volume in aqueous solutions, creating a very large surface contact area for adsorption of these organic dyes [19,27].

In last decade, engineered hydrogels have emerged as an effective adsorbent for removal of a wide range of dyes from wastewater [20,28]. Some recent examples that utilize engineering materials such as graphene [29], carbon nanotubes [30,31], activated charcoal [32], and other surface-treated materials [33] in hydrogels for improvements in strength but at the expense of economic and/or environmental cost. Recently, a significant amount of attention in biopolymer derived materials in adsorbent hydrogels has provided improved sustainability and excellent performance with a low carbon footprint [34]. Among different polymer backbone chemistries, polyacrylic acid chemistries are widely used in adsorption studies of cationic dyes [35]. Due to the presence of oxygen atoms, acrylics can complex cationic dyes. But a weak acidity of the carboxylic groups leaves these acrylic-based materials sensitive to solution pH which affect dye adsorption capacity as a function of pH [25]. Novel adsorbents of the future should provide high adsorption capacity, low cost and effectiveness over wide pH range.

Herein, we report a super-adsorbent hydrogel based on sodium styrene sulfonate monomer (NaSS). After producing a poly(NaSS) containing backbone with a strongly

anionic polyelectrolyte results that provides negatively charged sulfonate groups along its backbone chain. These charges can be used for removal of cationic dyes like MB. An interesting feature of poly(NaSS) is that its pKa is approximately 1 [36] and hence the sulfonate groups contribution towards swelling behavior is largely pH independent and increases the interaction strength with cationic dye moieties [37]. A low ionic pKa is a unique characteristic property making them ideal candidates to use in dye removal from wastewater streams under either acidic or alkaline conditions.

To improve the structural integrity and toughness of hydrogels for reusability, the polymer network was strengthened by copolymerizing NaSS and N, N'-dimethylacrylamide (DMA) monomers through crosslinking with a modified biopolymer, gelatin methacryloyl (GelMA) as crosslinker. DMA can induce additional self-crosslinking in the crosslinked polymer matrix, thereby increasing the porosity and available pore surface area for adsorption [38]. According to our knowledge there are limited reports where NaSS was used as a monomer for hydrogel synthesis to be used as a dye-abatement adsorbent for methylene blue [39]. To date, most of the hydrogel adsorbents reported showing higher than 1000 mg/g adsorption capacities are based on advanced and expensive engineering materials such as graphene, carbon nanotubes [15,29,40] that compromise cost-effectiveness of an adsorption technique. The super-adsorbent hydrogels described herein demonstrated higher water absorption capacities with practical swelling ratios of over 27500% that allows internal absorption sites to be fully exposed to MB, resulting in a high sorption capacity that reaches 1270 mg/g under neutral pH conditions.

A maximum adsorption of more than 1000 mg/g of MB by a NaSS-based super-adsorbent hydrogel is reported for the first time. A multilayer and heterogeneous adsorption of MB behavior by the super-adsorbent hydrogels that is supported by pseudo-first-order and Freundlich adsorption isotherm models is postulated. In addition, these super-adsorbent hydrogels demonstrate excellent regeneration capability, making them a promising and economically viable candidate for effective removal of organic dyes from wastewater.

2. MATERIALS AND METHODS

2.1. MATERIALS

Gelatin (type B, 100 bloom, from bovine skin), methacrylic anhydride, sodium carbonate, sodium bicarbonate, 2,2'-Azobis[2-(2-imidazolin-2-yl) propane] dihydrochloride (VA-044), sodium styrene sulfonate (NaSS), methylene blue (MB), sodium hydroxide (NaOH), hydrochloric acid (HCl), deuterium oxide (D_2O) were obtained from Sigma Aldrich and used as received. N, N'-dimethylacrylamide (DMA) monomers was passed through a basic alumina column prior to use. Ultra-high purity argon gas (99.999%) was obtained from Airgas.

2.2. PREPARATION OF GELATIN METHACRYLOYL (GelMA)

GelMA was prepared using gelatin type B by following a procedure previously discussed by M Zhu et al. [41]. In brief, gelatin (20g) was dissolved in 250 mL of carbonate-bicarbonate (CB) buffer (0.25M) by continuous stirring at 50 °C maintained by

water bath. The pH of the gelatin solution was adjusted to 9.4 using sodium hydroxide. Under vigorous stirring, methacrylic anhydride (0.1 mL per gram of gelatin) was slowly added and reaction continued for 2 hours at 50 °C. The final pH of the reaction was adjusted to 7.4 to stop the reaction. The reaction mixture was filtered and then dialyzed against ultrapure water at 50 °C using a 12-14 kDa cutoff dialysis tubes, lyophilized, and stored at -20 °C until further use.

2.3. PREPARATION OF SUPER-ADSORBENT HYDROGELS

The super-adsorbent hydrogel was prepared using a free radical polymerization technique in aqueous solution using a closed kettle reactor assembly as per our previously reported procedure [42]. A typical polymerization process is as follows: a GelMA solution (1 % w/v) was prepared in 75 mL deionized water to which NaSS (13.5 g, 60 mol-% of total monomer) and DMA (4.34 g, 40 mol-% of total monomer) were added under argon gas and stirred until clear solution was obtained. Polymerization was initiated by adding VA-044 initiator (0.07 g, 0.2 mol-%) and reaction was continued for 24 hours at 30 °C. The resulting hydrogel was cut in small cubes, dried at 60 °C in oven and pulverized before characterization and evaluation.

2.4. PHYSIOCHEMICAL CHARACTERIZATION

Proton Proton nuclear magnetic resonance spectroscopy (^{1}H NMR) spectroscopy (Bruker 400 MHz Avance III HD Liquid state NMR) was used to quantify methacrylation of gelatin in D_2O. Fourier transform infrared spectroscopy (FT-IR) was used to examine the chemical structure of methacrylated gelatin and hydrogel samples.

FT-IR spectra were recorded between 4000 and 400 cm^{-1} with setting of 16 signal-averaged scans at a resolution of 2 cm^{-1} using Nicolet iS50 FT-IR spectrometer (Thermo Fischer Scientific). The morphology and porous crosslinked polymer structure of the freeze-dried swollen hydrogel was studied using a high-resolution scanning electron microscope (Helios 600 Nanolab) at operating voltage of 5 kV. The samples were gold sputter-coated for charge dissipation. An elastic modulus of ~4 kPa for the as-synthesized gel of about 1 part gel per 4 parts water was measured using a Haake MARS III rheometer with a parallel plate geometry (PP35L Ti L) at 1 s^{-1}.

2.5. SWELLING MEASUREMENTS

The equilibrium swelling ratio of hydrogel was determined by immersing a weighed dried hydrogel sample in deionized water for 24 hours. During this period water was changed every 8 hours. The excess surface water on swollen gel was removed using filter paper and weight of swollen gel was taken. The equilibrium swelling ratio (ESR) was calculated using the equation (1), where W_i is the initial mass of dried gel and W_f is the constant mass of swollen hydrogel at equilibrium. The temperature dependent equilibrium swelling ratio was investigated by conducting swelling experiments at temperatures of 295, 305 and 315 K.

$$\text{Equilibrium Swelling Ratio (ESR)} = W_f / W_i \times 100\% \quad (1)$$

2.6. DYE ADSORPTION STUDIES

MB adsorption experiments applied water swollen super-adsorbent NaSS-DMA hydrogel as an adsorbent. MB stock solution of 100 ppm was prepared and further used

to prepare MB solutions of different desired concentrations. A linear calibration curve of MB was constructed from absorbance measurements of 0.5, 1, 2, 3, 5, 8 and 10 ppm MB solutions. The absorbance was measured at the MB lambda maximum wavelength of 664 nm using absorbance spectra acquired in an Agilent Cary 60 UV-visible spectrometer over the wavelength range of 400 – 800 nm.

The concentration of MB before and after adsorption were measured from absorption values further converted to concentration using linear calibration curve. The removal ratio (*R%*) and the adsorption capacity (q_e) for MB were calculated using the equation (2) and (3), where C_0 (mg/L), C_t (mg/L) and C_e (mg/L) are MB concentrations at initial time, time *t*, and equilibrium concentration respectively, *V* (L) is the volume of MB dye solution used and *m* (g) is the weight of dried adsorbent. All the experiments were carried out in triplicate and results represented here are the average of the three readings.

$$R\% = (C_0 - C_e) / C_0 \times 100\% \quad (2)$$

$$q_e = (C_0 - C_t) \times V / m \quad (3)$$

The effect of adsorbent dosage toward MB adsorption was investigated to set the adsorbent dose for rest of the adsorption experiments. Different adsorbent doses were added to 50 mL of MB solution of concentration 10 mg/L at 295 K and at a solution pH of 7.0. Incubator shaker under a constant speed of 100 rpm was used to maintain quality control of measurements. The final MB concentration was determined after 24 hours of contact time.

For the effect of pH of MB solution on adsorption and removal of MB, 1 g of swollen hydrogel adsorbent was added into 50 mL of MB solution of concentration 50 mg/L at 295K temperature. Initial pH of this solution was adjusted using 0.1M HCl and

0.1M NaOH in the range of 1 to 13. The final MB concentration was determined after 24 hours of contact time.

For adsorption kinetics experiments, 1 g of swollen hydrogel adsorbent was added into 50 mL of MB solution of concentration 50 mg/L at 295 K temperature. A pH of 7.0 was found to provide optimum MB adsorption in early experiments of effect of solution pH. Concentration of MB in the solution was determined after designated time intervals. For adsorption isotherm and thermodynamic experiments, 1 g of swollen hydrogel adsorbent was added into MB solutions of different initial MB concentration with a solution pH of 7.0 and experiments were conducted at different temperatures (295 K, 305 K and 315 K). The final MB concentration was determined at 24 hours of contact time.

2.7. REUSABILITY

To investigate the reusability of the adsorbent, 1 g of swollen hydrogel adsorbent was added into 50 mL of MB solution of concentration 25 mg/L at 295K temperature and pH of 7.0 to achieve saturated adsorption. Excess 0.1M HCl was used to desorb MB that had adsorbed on hydrogel adsorbent [43]. The gel was regenerated in excess 0.1M NaOH to regenerate anionic binding sites and finally washed with excess deionized water prior to use in the next adsorption cycle. An adsorption and desorption cycle was repeated four additional times using 50 mL of MB solution of concentration 25 mg/L at 295K temperature and pH of 7.0.

3. RESULTS AND DISCUSSION

3.1. SYNTHESIS OF SUPER-ADSORBENT HYDROGEL

In the present work, a super-adsorbent hydrogel was prepared via free radical polymerization of NaSS and DMA monomers employing GelMA as an organic crosslinker. A general synthesis scheme for the super-adsorbent hydrogel preparation is shown in Scheme 1. In the first step, GelMA was synthesized from gelatin, which is composed of diverse amino acids with hydroxyl and amino functionalities that can be modified into methacryloyl functionality by reacting with methacrylic anhydride in CB buffer [41]. In the second step, a single pot free radical polymerization was performed using aqueous soluble, VA-044 free radical initiator through a graft copolymerization technique.

Figure 1a shows spectroscopic characterization of gelatin, GelMA and crosslinked superadsorbent hydrogel. The peaks at 3289 cm^{-1} (NH stretching), 2938 cm^{-1} (CH stretching), 1538 cm^{-1} (amide II), and an amide III bond present at 1238 cm^{-1}. These functional groups are from gelatin moiety of the GelMA product [44,45]. The peak around 1640 cm^{-1} in the spectrum of GelMA corresponds to the C=C stretching from the methacrylate functionalization, although amide I carbonyl, C=O, stretching peak observed in the same region, making it difficult to distinguish. This observation is consistent with the previously reported literature [46]. The peaks near 1046 cm^{-1} are assigned as aliphatic ether C-O-C stretching due to the addition of the methacrylic moiety to gelatin, which confirms the functionalization [45]. A slight shift was observed of the broad band at 3300 cm^{-1}, which is characteristic of the N-H bond stretching vibration for

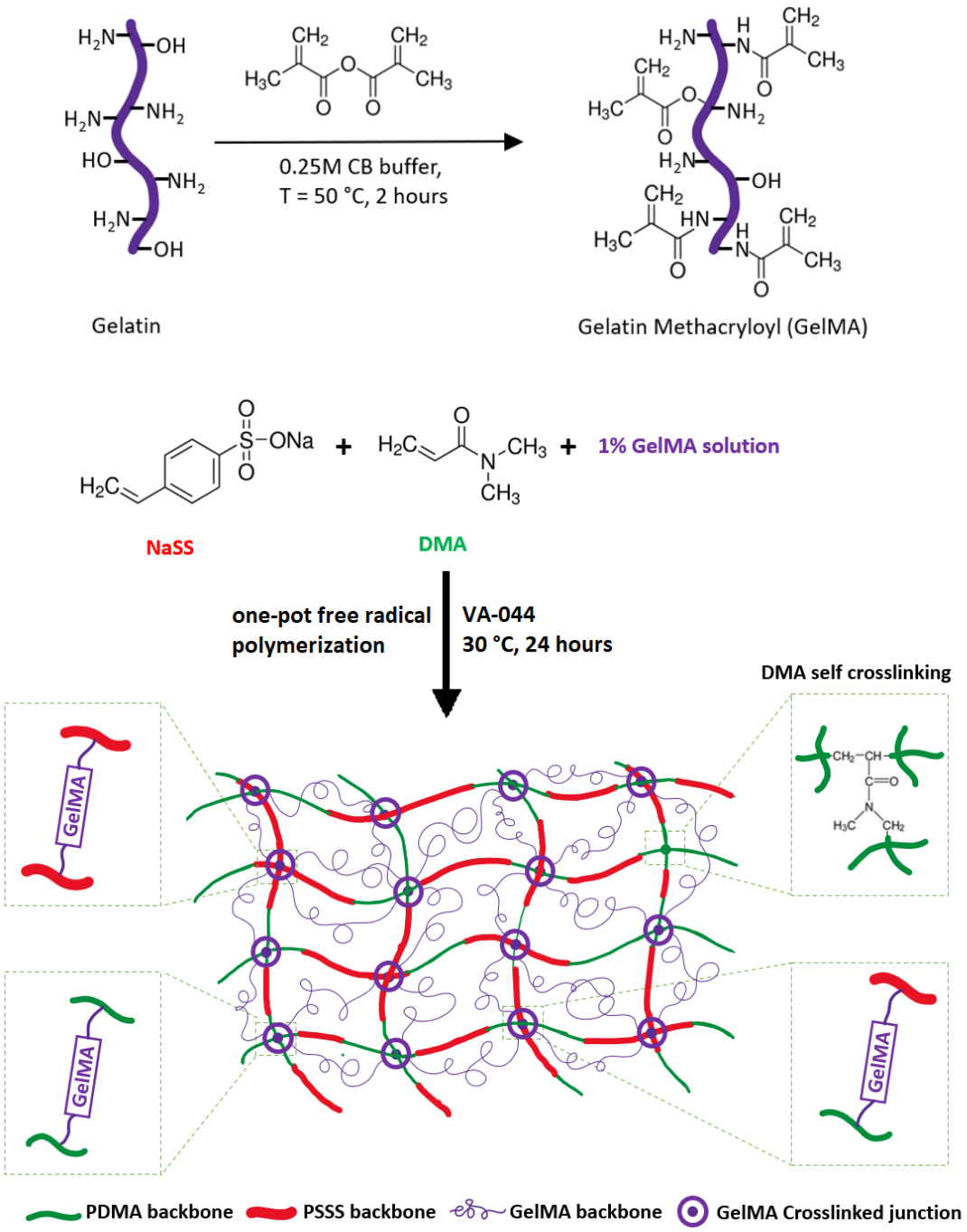

Scheme 1. Systematic synthesis of super-adsorbent hydrogels. Step 1: synthesis of gelatin methacryloyl (GelMA); Step 2: Free radical polymerization to obtain super-adsorbent hydrogel.

N, N-substituted amides with addition of carboxylic hydroxyl [44]. The functionalization on gelatin was confirmed further by ^{1}H NMR spectroscopy as seen in Figure 1b.

In comparison between ^{1}H NMR spectrum of gelatin and GelMA, new proton peaks attributed to methacryloyl groups are detected between 5.1 to 5.7 ppm for vinyl protons (CH_2=C(CH_3)CONH-) of methacrylamide groups (Figure 1c) and at 1.8 ppm for methyl protons (CH_2=C(CH_3)CO-) of methacryloyl groups. As a result of

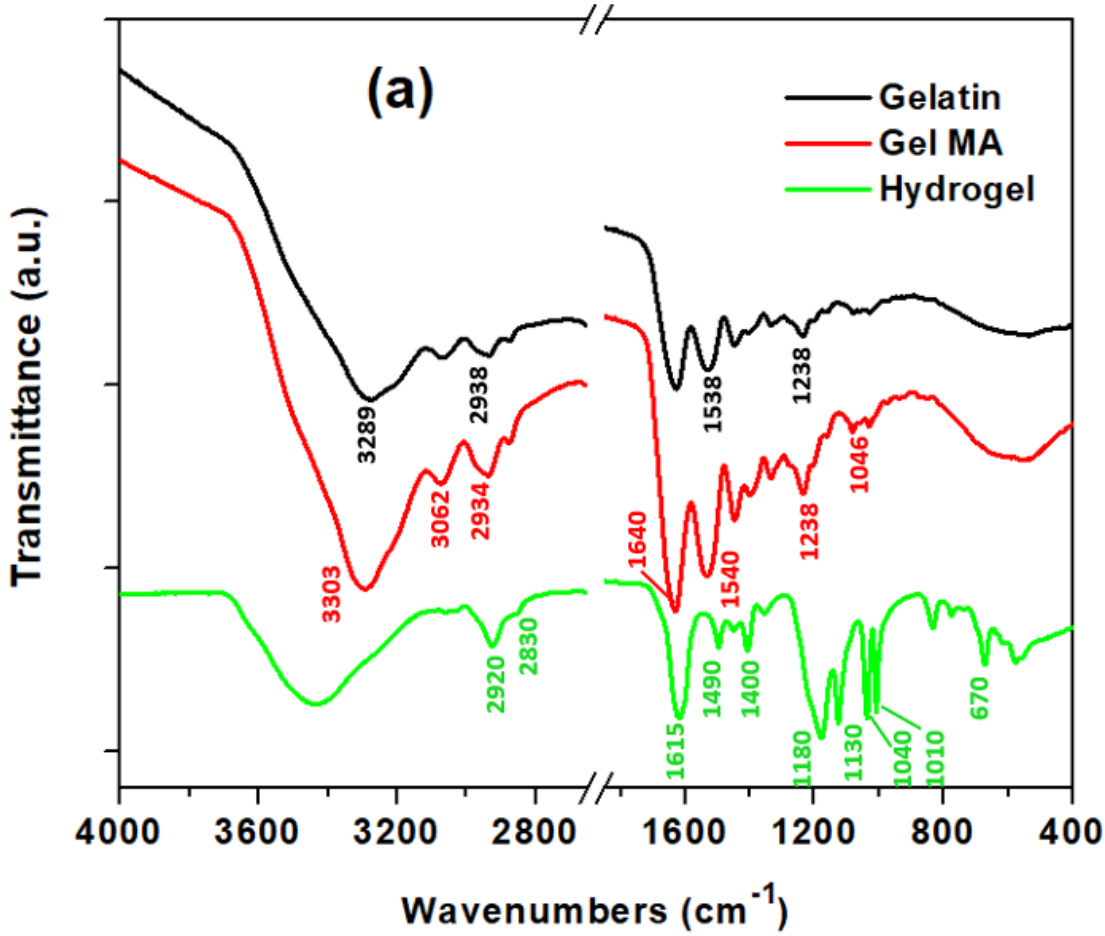

Figure 1. Spectroscopic characterization of gelatin, methacrylated gelatin (GelMA) and super-adsorbent hydrogel: (a) FT-IR, (b) ^{1}H NMR full spectra and (c) zoomed ^{1}H NMR spectra from 5.0 to 7.5 ppm.

functionalization, free lysine signal ($NH_2CH_2CH_2CH_2CH_2$-) of as such gelatin at 2.9 ppm was decreased significantly. Calculations based on NMR integration values indicate about 30% functionalization of free amino and hydroxyl groups. These results confirmed the successful functionalization of gelatin to GelMA and agreed well with previously reported studies [41,44,47].

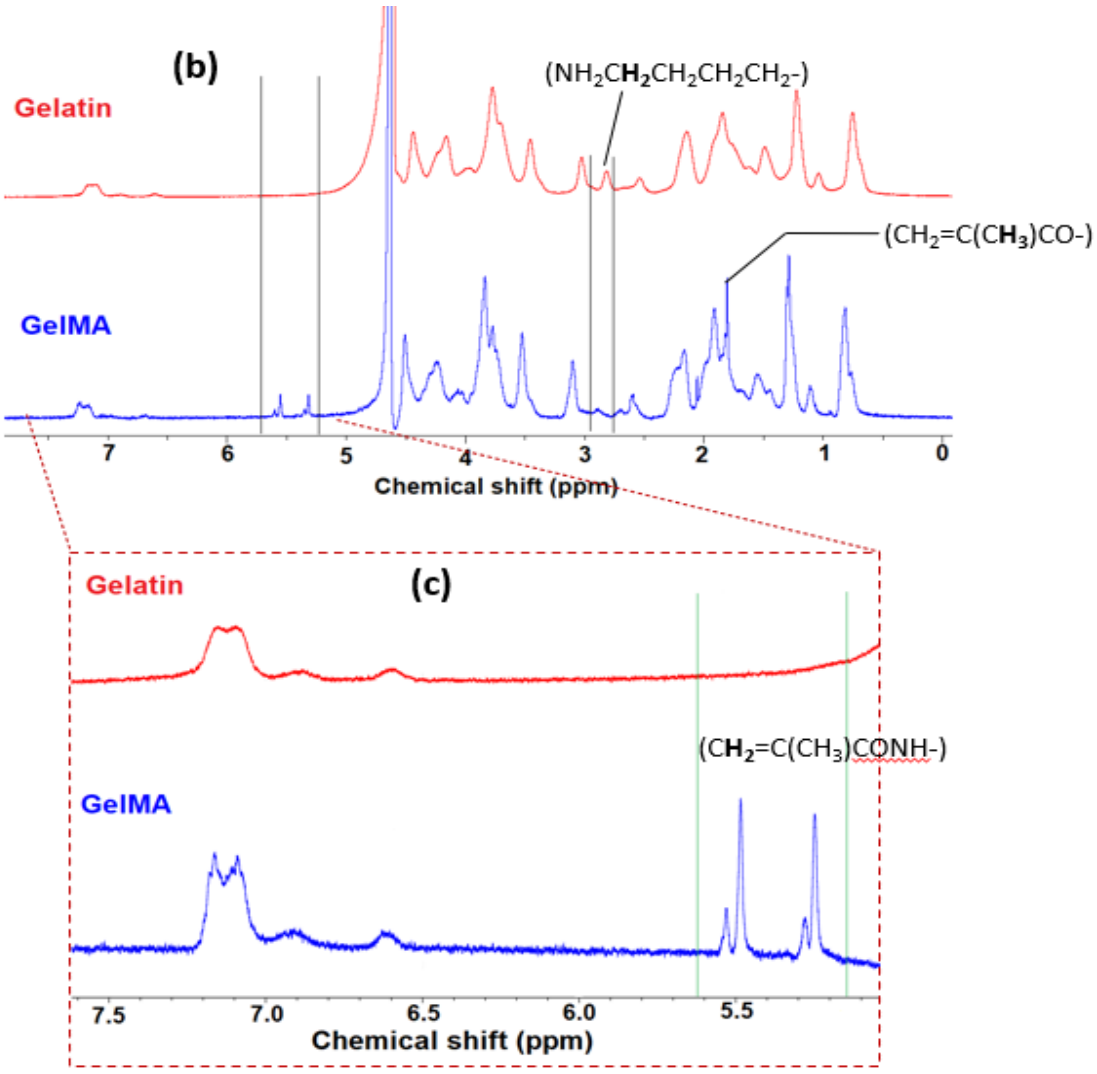

Figure 1. Spectroscopic characterization of gelatin, methacrylated gelatin (GelMA) and super-adsorbent hydrogel: (a) FT-IR, (b) ^{1}H NMR full spectra and (c) zoomed ^{1}H NMR spectra from 5.0 to 7.5 ppm. (Cont.)

The presence of NaSS-DMA copolymer in the synthesized hydrogel was confirmed with observed peaks corresponding to poly (NaSS) and poly (DMA) segments. The peak at 670 cm^{-1} for aromatic C-H out of plane bending vibration, 1010 and 1130 cm^{-1} for in-plane bending and in-plane skeleton vibrations of benzene ring, respectively corresponds to poly (NaSS) segment [48]. Additional absorptions at 1040 and 1180 cm^{-1} correspond to symmetric and asymmetric vibration absorption of SO_3^- groups, respectively [48]. Absorption at 1615 cm^{-1} confirmed carbonyl stretching absorption by amide functionality present in the copolymer corresponding to the poly (DMA) segment [42,49]. The characteristic C-H bond from poly (DMA) units at around 2920 cm^{-1} was observed for vibration due to CH_3 groups along with the band around 1500 - 1570 cm^{-1} corresponds to C-N bending. The OH stretching vibration in frequency range of 3000 – 3700 cm^{-1} corresponds to moisture absorption by hydrogel [48].

3.2. SWELLING OF SUPER-ADSORBENT HYDROGELS

The water absorption capacity of a super-adsorbent hydrogel has an important effect on adsorption behavior for the removal of MB from aqueous solutions. A high swelling capacity can increase the available surface area for MB adsorption to aid improved adsorption capacity and removal efficiency [50]. Ionic polymers tend to show higher swelling capacities at the expense of weaker hydrogel integrity [51-53] causing them to fell apart during their use and contribute to significant material loss. To avoid this, these super-adsorbent hydrogels were synthesized as a copolymer of NaSS and DMA, which forms a tough, strong, crosslinked polymer network with GelMA.

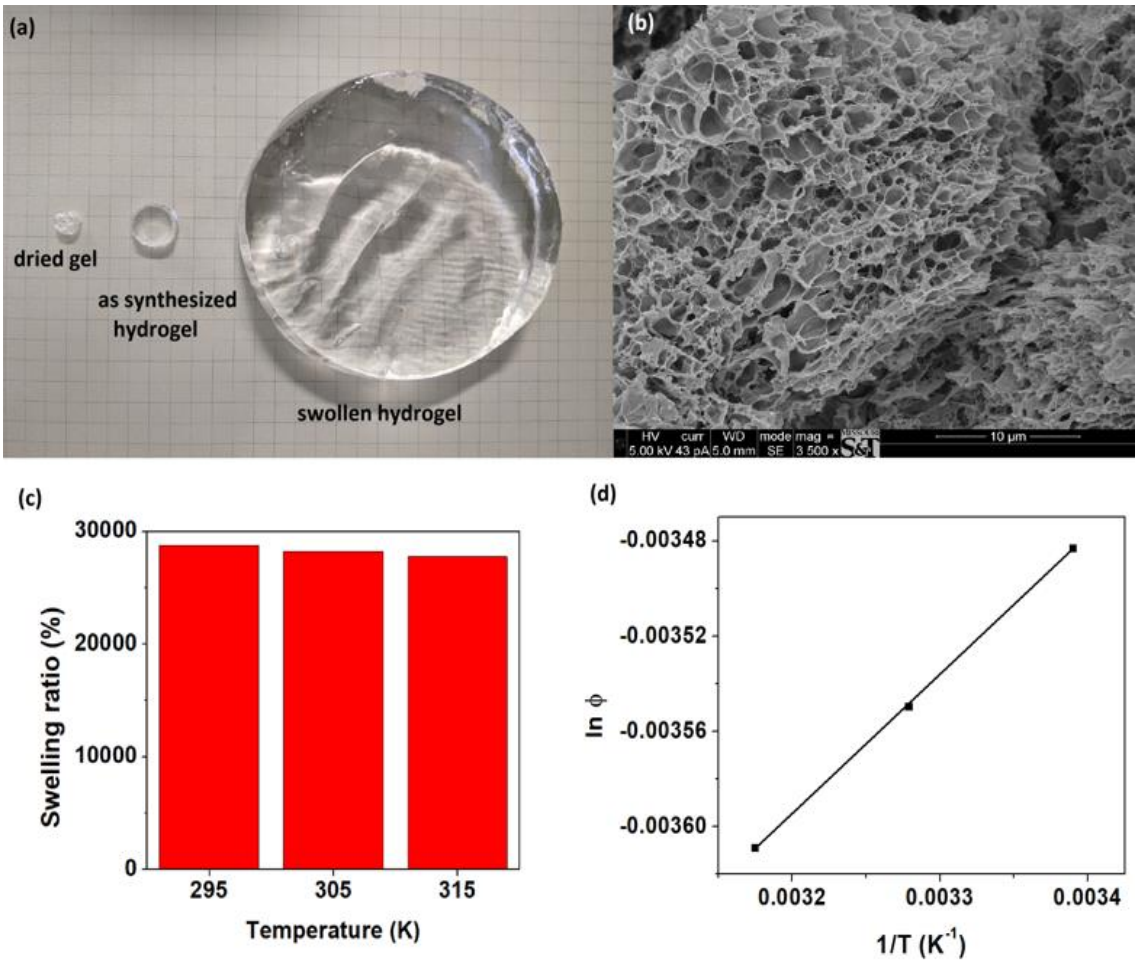

Figure 2. Swelling studies for super-adsorbent hydrogel. (a) pictorial representation of extents of swelling at 295 K in deionized water, (b) morphology and pore structure of the freeze-dried swollen super-adsorbent hydrogel, (c) equilibrium swelling ratio at different temperatures (295 K, 305 K and 315 K) and (d) van't Hoff analysis plot of ln ϕ versus 1/T.

The higher swelling ratios were observed that can reach up to 27500% and above, which is higher than previously reported hydrogels synthesized using biopolymer based crosslinkers [54-56]. Figure 2a shows a pictorial representation of dry and swollen hydrogel that maintained structural integrity after complete swelling. As shown in Figure 2b, the SEM image of the freeze-dried swollen super-adsorbent hydrogel demonstrates a highly porous structure with average pore size of 0.91 $\pm$ 0.27 microns along with

interconnected channels within pores. This internal porous structure is conducive to higher adsorption capacities. The extent of swelling ratio of super-adsorbent hydrogels at different temperatures is shown in Figure 2c. The swelling ratio of up to 28760%, 28220% and 27760% was observed at 295K, 305K and 315 K respectively.

The thermodynamics of super-adsorbent hydrogel equilibrium swelling (EQSR) as a function of temperature using van't Hoff analysis was investigated. The change in enthalpy (ΔH) for super-adsorbent hydrogel can be calculated by the integrated van't Hoff equation:

$$\ln \phi = -(\Delta H/2.303\ RT) + \text{constant} \quad (4)$$

where R = 8.314 J/(mol.K), T is the temperature (K) and $\phi = 1 - (1/EQSR)$ [55]. A linear plot of ln ϕ versus 1/T as shown in Figure 2d, gives a linear fit with a slope of 0.5854 which is equal to - (ΔH/2.303*R) from which the change in enthalpy (ΔH) of swelling process was calculated as -11.2087 kJ/mol. The negative change in enthalpy value suggests a fairly strong non-covalent bound-hydration and relaxation of polymer are occurring during the process of swelling and that a swollen state of the aqueous hydrogel is favored [58].

3.3. MB DYE ADSORPTION STUDIES

3.3.1. Effect of Adsorbent Dosage and pH. The dosage of adsorbent is an important parameter to adsorption behavior of hydrogel in removal of dyes from their aqueous solutions. MB adsorption capacity, q_e decreased with increasing adsorbent dose as seen in Figure 3, whereas the percent removal ratio remained nearly constant. A decrease in adsorption capacity can be attributed to the availability of adsorptive sites as a

function of osmotic pressure. At higher dosages of adsorbent, adsorption will reach equilibrium quickly because of osmotic pressure and irrespective of unused active sites in comparison with lower dosages of adsorbent, which results in an efficient use of adsorption sites. The other extreme is at lower dosages of adsorbent, when used in higher concentration MB solutions, the adsorbent readily collapses resulting in poor adsorption removal capacity. Therefore, after comprehensive experimentation, a median dose of 1g was selected for the remainder of adsorption experiments.

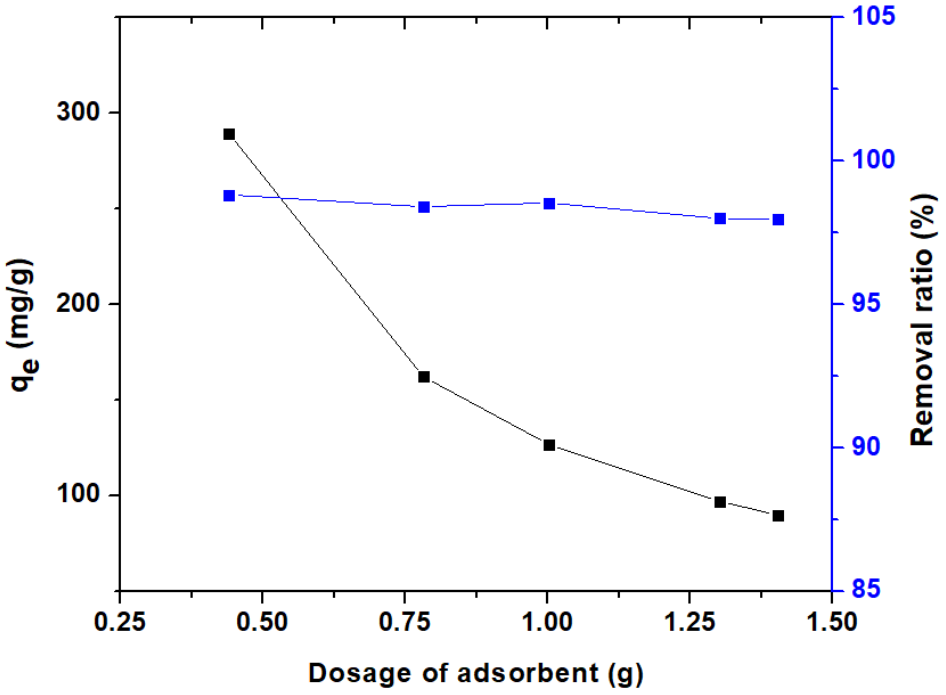

Figure 3. Effect of super-adsorbent gel dosage on adsorption capacity of MB and % removal ratio at 295K, in MB solution with pH=7.0, C_0 = 10 mg/L, after 24 hours of contact

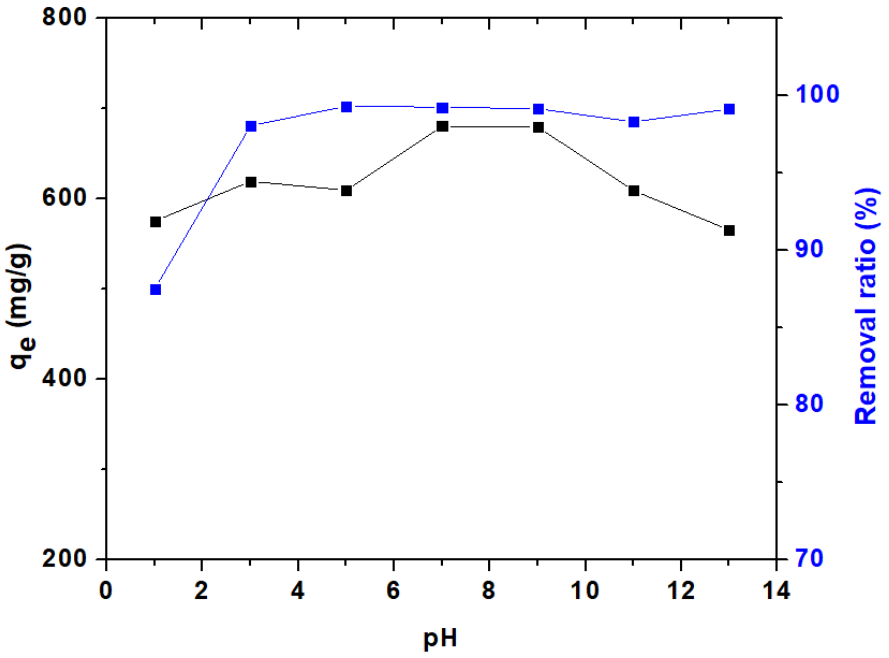

Figure 4. Effect of pH of MB dye solution on adsorption capacity q_e of MB and removal ratio at 295K; MB solution with C_0 = 50 mg/L, dosage of hydrogel = 1g; after 24 hours of contact

Effect of pH of MB dye solution on adsorption capacity was investigated in MB solution of concentration 50 mg/L at 295 K as seen in Figure 4. The pH of dye solution did not show a significant effect on MB adsorption by super-adsorbent hydrogel, where > 650 mg/g adsorption capacity was measured at pH =7 with 99% removal ratio. A greater than 98% of MB removal ratio from aqueous dye solution on super-adsorbent hydrogel was measured at all pHs except at pH = 1, which showed a 87% removal ratio. The lower removal ratio can be attributed to the pH approaching the pKa of the sulfonate group (pKa ~ 1.0) [54,59] that is responsible for the adsorption of MB via an ionic interaction between the adsorbent and cationic dye molecules. In strongly acidic solution, a competition for adsorption of dye moieties versus H^+ ions exist in addition to the H-

bonding and charge-charge repulsion interactions between sulfonate groups from polymer and nitrogen units of MB with water. The competition causes a reduced adsorption capacity of adsorbent towards dye uptake in the strongly acidic solution.

It was also observed that adsorption capacity increased slightly from pH 1 until pH 9 and then decreased upon a further increase in pH from 9 to 13. The observation indicates that the adsorption efficiency is also dependent on other physical adsorbant interactions besides electrostatic and hydrogen bonding. Under strongly acidic conditions of pH 1 and below, a decreased charge-charge attraction and thus a greater reliance on hydrogen bonding between the hydrogel adsorbent and MB is expected. On the other hand, in strongly alkaline conditions of pH > 10, a charge screening effect by excess Na^+ ions can also elicit a breakdown of hydrogen bonding interactions and cause the observed decrease in adsorption capacity. Overall, super-adsorbent hydrogel copolymers based on NaSS exhibit better adsorption of MB over a wide pH range of 2 to 12 compared to previously reported super-adsorbent hydrogels which showed significant change in adsorption capacity as a function of pH [25].

3.3.2. Adsorption Kinetics. Adsorption kinetics is another important parameter as it provides important information about adsorption rate and adsorption mechanism. In general, the accepted mechanism for adsorption of dye involves several steps, including penetration of dye molecules from solution into the adsorbent surface, diffusion of dye from the outer surface to internal adsorption sites, the interaction between dye molecules and the reactive sites present on polymer backbone through chemical bonding, electrostatic interactions, ion-exchange, hydrogen bonds, hydrophobic attractions, and so on [54,58-60]. The hydrogels discussed herein are based on NaSS, possessing aromatic

side groups within the polymer backbone that can establish short range π - π interactions with aromatic groups present in MB. The NaSS structure thus presents not only sulfonate charge attraction but also π - π interactions that can result in stronger binding and increased adsorption capacity, as demonstrated in previous studies [16,61,62]. The effect of contact time on MB removal is shown in Figure 5, a typical adsorption capacity pattern increasing rapidly initially followed by an equilibrium as the adsorption sites are saturated. The adsorption equilibrium was achieved within 5 hours contact time at 295K in MB solution with C_0 = 50 mg/L, pH= 7.

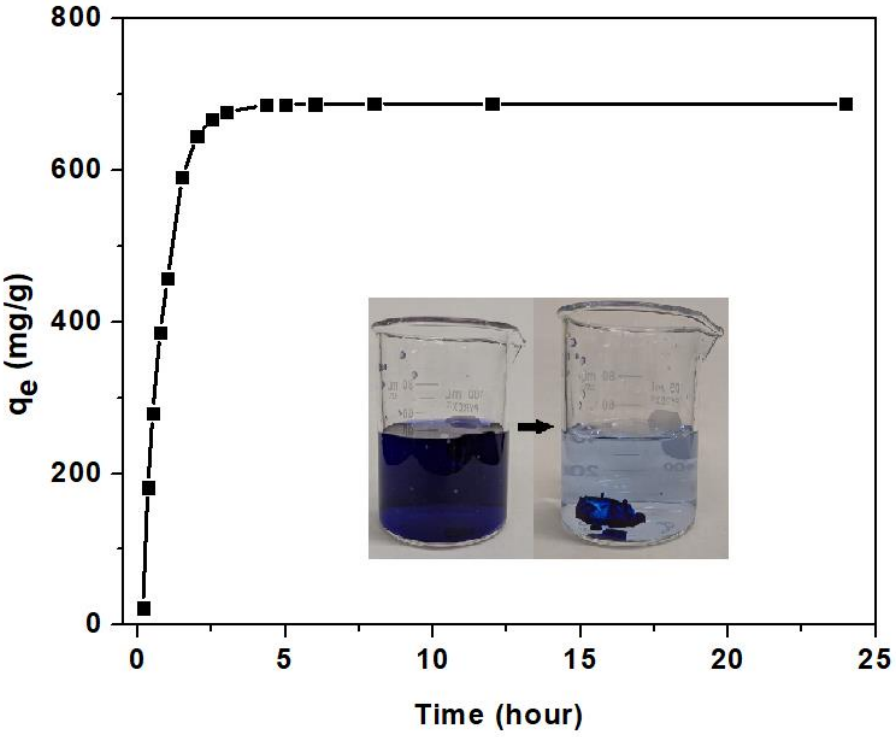

Figure 5. Adsorption of MB on super-adsorbent hydrogel as a function of time using MB solution at 295K, with C_0 = 50 mg/L, pH= 7, dosage of super-adsorbent hydrogel = 1g. Representation shows MB dye removal from solution.

To evaluate adsorption kinetics mechanisms and potential rate controlling steps, the experimental data were fitted to pseudo-first order (Equation 5), pseudo-second order (Equation 6), Boyd liquid-film diffusion model (Equation 7), and Elovich models (Equation 8) [65].

$$log\ (q_e - q_t) = log\ (q_e) - k_1 * t/2.303 \quad (5)$$

$$t/q_t = t/q_e + 1/(k_2 * q_e^2) \quad (6)$$

$$-ln\ (1-F) = k_{fd} t \quad (7)$$

$$q_t = \ln(\alpha\beta)/\beta + \ln t/\beta \quad (8)$$

where q_e (mg/g) and q_t (mg/g) are the adsorption capacity at equilibrium time and time t (min), respectively. k_1 (/min), pseudo first order rate constant, k_2 (g (mg /min)), pseudo second order rate constant, k_{fd} (/min) adsorption constant corresponding to Boyd liquid-film diffusion model, α (mg /g /min), initial adsorption rate constant and β (g/mg), desorption constant related to the adsorbent surface covering and the adsorption chemical energy. F is a fractional attainment of equilibrium ($F = q_t/q_e$) at time t for liquid-film diffusion. Based on the correlation coefficient (R^2), a best fit and most probable adsorption kinetics model for the adsorption was selected.

Each model was fitted with data obtained until time of equilibrium adsorption capacity attained (5 hours) to avoid methodological bias of using q_t data at the equilibrium [66]. Plots are shown in Figure 6 and constants obtained from the plots summarized in Table 1. A pseudo-first-order model is based on the hypothesis that the rate of solute adsorption with time is proportional to the saturated concentration and number of unoccupied sites whereas a pseudo-second-order model assumes that the adsorption rate is controlled by chemical adsorption through sharing or exchange of

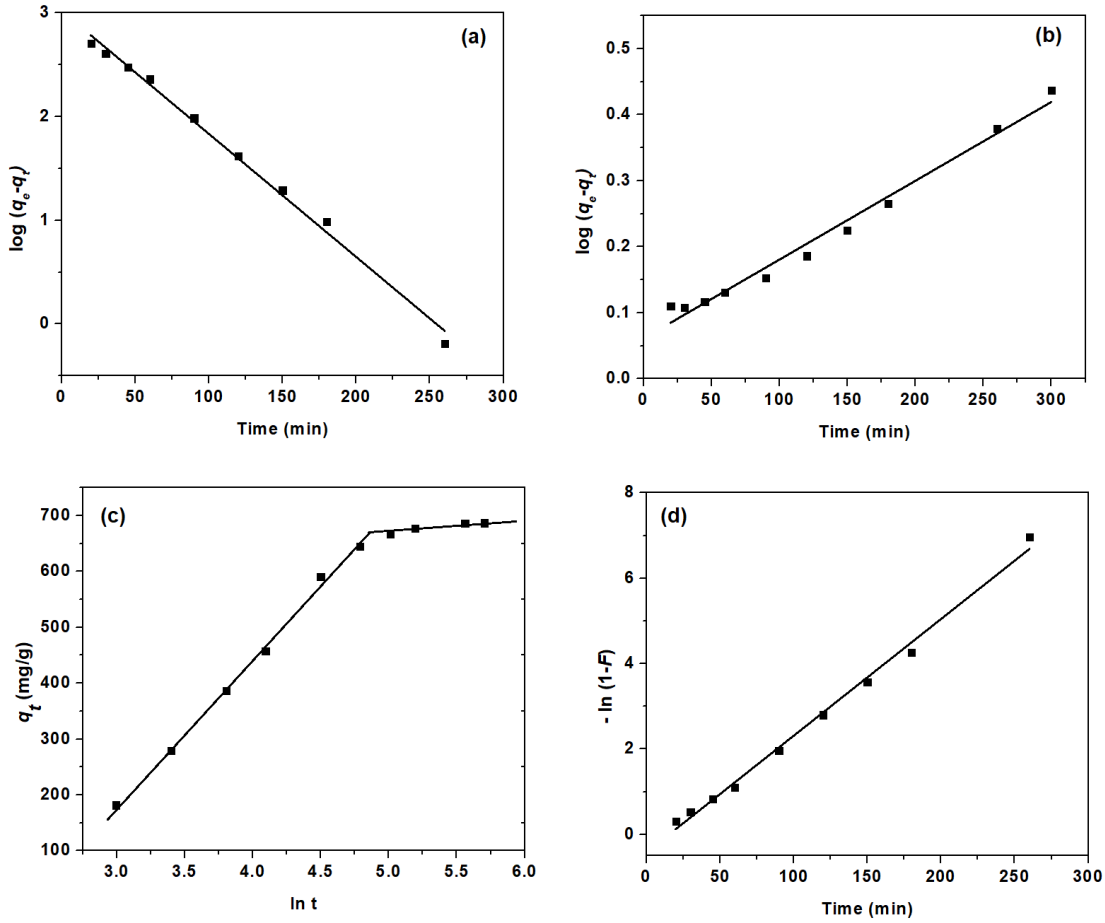

Figure 6. Kinetic curves for (a) pseudo-first-order, (b) pseudo-second-order, (c) Elovich model and (d) Liquid film diffusion model on super-adsorbent hydrogel using MB solution at 295K, with C_0 = 50 mg/L, pH= 7, dosage of super-adsorbent hydrogel = 1g

electrons between the adsorbent and adsorbate. The Elovich model, on the other hand, predicts multilayer adsorption where the rate of adsorption of solute decreases exponentially with the increase in the amount of adsorbed solute [67,68]. All three models are reaction-based models while the Boyd model is diffusion-based, which assumes that the boundary layer surrounding the adsorbent has the greatest effect on diffusion of solute and film diffusion is a rate limiting step during the initial phase of adsorption, followed by intraparticle diffusion [67,69,70].

Table 1. Kinetic parameters for MB adsorption on super-adsorbent hydrogels

Pseudo-first-order model			
C_0 (mg/L)	q_e (mg/g)	k_1 (/min)	R^2
50	1048.14	0.0273	0.9933
Pseudo-second-order model			
C_0 (mg/L)	q_e (mg/g)	k_2 x 10-5(/min)	R^2
50	833.33	2.3598	0.9813
Elovich model			
C_0 (mg/L)	α (mg /g /min)	β (g/mg)	R^2
50	31.0951	0.005	0.9323
Liquid film diffusion model			
C_0 (mg/L)	k_{fd} (/min)		R^2
50	0.02733		0.9933

Based on correlation coefficient, a pseudo-first-order model was found to best represent the experimental data for adsorption of MB, thus the rate-controlling step is ascribed to a number of unoccupied sites on super-adsorbent hydrogel. Moreover, according to an Elovich model, which shows two distinct linear regions, the adsorption process is found to be a multilayer and heterogeneous adsorption process. Where a liquid-film diffusion model was considered, a correlation coefficient R^2 of 0.9933 was observed that supports applicability of the model. The plot of – (ln (1-F)) versus time, however, did not pass through origin, implying that a liquid-film diffusion process was not the only

rate-limiting step. The first linear portion of the plot – (ln (1-F)) versus time would be ascribed to surface diffusion, i.e., diffusion of MB from the bulk solution into the surface of super-adsorbent hydrogel, while the second linear portion would represent the gradual adsorption stage. In general, the whole process of adsorption of MB dye onto the super-adsorbent hydrogel involves multiple mechanisms, where π - π interactions, ion-exchange, hydrogen bonding, hydrophobic interactions, and liquid external diffusion are considered the main factors responsible for the observed adsorption capacities.

The effect of π - π interactions, aromatic hydrophobic interactions can be verified through proton NMR experiments (Figure S1, supplementary file). Proton NMR demonstrated the broadening of signals for the MB protons associated with aromatic rings in the presence of aromatic polymer poly (NaSS) whereas no changes in proton signal broadening observed in presence of poly (DMA) polymer. This is consistent with the previous reports focusing on aromatic π stackings interaction among aromatic dyes and aromatic polymers, by delocalization of aromatic π clouds leading to enhanced intermolecular electrostatic interactions [63,64,71].

3.3.3. Adsorption Isotherm Study. Figure 7 presents adsorption capacities of the super-adsorbent hydrogels as a function of temperature for MB adsorption at various initial concentrations of the MB solutions maintained at pH of 7.0. The lower initial concentration does not affect adsorption capacity significantly irrespective of temperature because of unsaturation of the adsorption sites. On the other hand, at higher initial MB concentration a temperature dependent adsorption phenomenon was observed where the active sites become saturated with dye molecules. With increase in temperature, a slight decrease in swelling ratio was observed, which will reduce bulk volume, pore volumes,

and surface area available for adsorption [25,55,70]. As a result, adsorption capacity at 315 K was lower than at 295 K at highest initial MB concentrations. The q_e values thus depend on initial concentration of MB solution and other factors that determine the overall efficiency of the adsorption process.

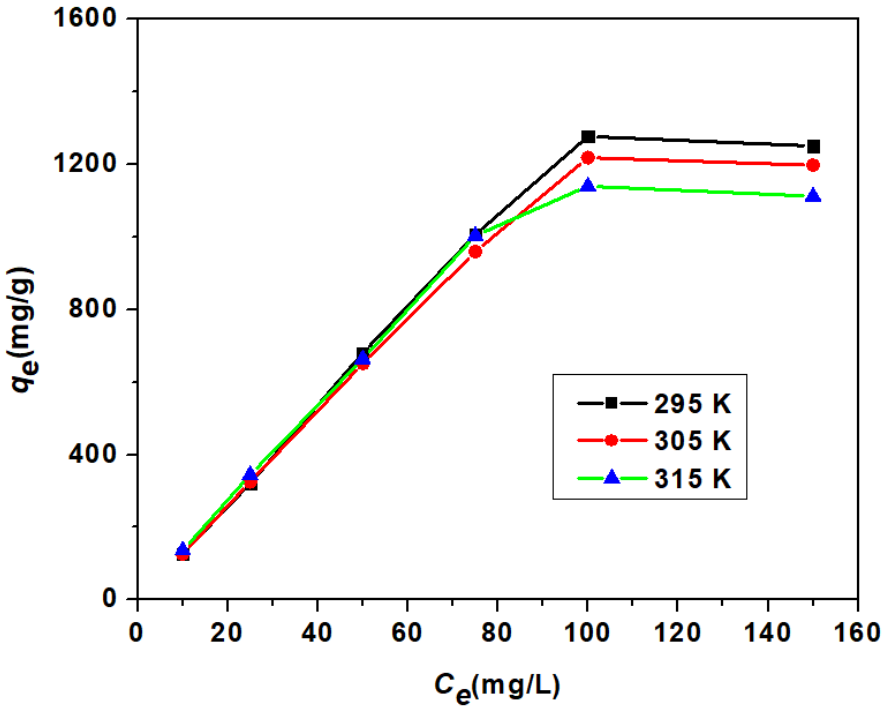

Figure 7. Effect of initial concentration of MB on adsorption capacity by super-adsorbent hydrogel as a function of concentration and temperature, pH= 7, dosage of super-adsorbent hydrogel = 1g

The adsorption capacity of the super-adsorbent hydrogels for MB adsorption was compared with other polymer systems reported in literature as shown in **Table 2**. This is the first report of a NaSS monomer based copolymer hydrogel adsorbent system, without expensive nanofiller, showing a greater than 1000 mg/g of adsorption capacities towards MB with value of 1270 mg/g.

Table 2. Comparison of maximum adsorption capacities for MB dye using adsorbent with variable chemical signature

Adsorbent chemical signature	**Adsorption capacity (mg/g)**	**Reference**
Poly (AA-co-VPA) hydrogel cross-linked with N-maleyl chitosan	66.89	[54]
Chitosan-crosslinked κ-carrageenan bionanocomposites	130.4	[55]
Tannic Acid–Poly (vinyl alcohol)/Sodium Alginate	147.06	[73]
PVA/carboxymethyl cellulose hydrogel	165.73	[74]
κ-Carrageenan/poly (glycidyl methacrylate) hydrogel	166.62	[56]
Amine functionalized sodium alginate hydrogel	400	[75]
Poly (acrylic acid) (PAA), cassava starch (CS) and poly (vinyl alcohol)	417	[76]
Poly (gellan gum-co-acrylamide-co-acrylic acid) hydrogel	423.46 ± 13.60	[77]
Gg-cl-P(AAm-co-MAA) hydrogel polymer	694.44	[78]
Cellulose/MMT	782.9	[33]
Xanthan gum-cl-poly (acrylic acid) based-reduced GO hydrogel	793.65	[40]
Sulfonate chitosan microspheres	820.1	[39]

Table 2. Comparison of maximum adsorption capacities for MB dye using adsorbent with variable chemical signature (Cont.)

Poly (sodium styrenesulfonate-co-dimethylacrylamide) crosslinked with gelatin methacryloyl	1270	**This work**
Poly (sodium styrene sulfonate) functionalized graphene (PSS-rGO)	1300	[29]

For a better comprehension of the thermodynamics of MB adsorption on these super-adsorbent hydrogels, different adsorption isotherm equations of Langmuir, Freundlich and Temkin were examined at different temperatures (295 K, 305 K and 315 K) as a function of concentration. Adsorption isotherm study helps to describe the interaction of a dye molecule with adsorbent by providing a relationship between the concentration of dye in solution and an amount of dye adsorbed onto the hydrogel at equilibrium. The Langmuir isotherm is often applicable to a homogeneous adsorption surface with all the adsorption sites having equal adsorbate affinity, thus adsorbent-adsorbate intermolecular forces decrease quickly over time. The Freundlich isotherm is an empirical relationship for adsorption over heterogenous surfaces where adsorption occurs on a heterogeneous surface via multilayer adsorption with non-uniform heat of adsorption. On the other hand, the Temkin isotherm is based on the assumption that adsorption heat of all molecules decreases linearly as a function of increased coverage of the adsorbent surface where uniform distribution of binding energies can be expected.

The equations used for Langmuir (Equation 9), Freundlich (Equation 10) and Temkin (Equation 11) isotherms [77] are as follows:

$$C_e/ q_e = C_e/ q_m + 1/(K_L q_m) \quad (9)$$

$$\ln q_e = \ln K_F + \ln C_e/ n \quad (10)$$

$$q_e = B_T \ln K_T + B_T \ln C_e \quad (11)$$

where C_e (mg/L) is the equilibrium concentration of MB solution used; q_e (mg/g) is the adsorption capacity at equilibrium; q_m (mg/g) maximum adsorption capacity; K_L and K_F (L/mg) are the Langmuir and Freundlich adsorption equilibrium constants respectively; K_T (L/mg) is maximum binding energy constant; n is a heterogeneity factor indicating how favorable the adsorption process is; $B_T = RT/\beta$ and β (J/mol) is the Temkin constant related to the heat of adsorption, R is the universal gas constant (8.314 J/mol/); and T is absolute temperature (K).

Linear plots for each isotherm model are shown in Figure 8. The adsorption constants obtained from the plots associated with Langmuir, Freundlich and Temkin isotherm models are provided in Table 3. It is readily observed that the Freundlich model was best suited for MB adsorption to the hydrogel with R^2 values > 0.99, which supports multilayer and heterogeneous adsorption process that was also supported by the Elovich kinetic modeling of Figure 6. The favorability and surface affinity for the adsorbate was investigated using n values which confirmed a transition of normal adsorption (n > 1) to cooperative adsorption (n < 1) as a function of decreasing temperature [79].

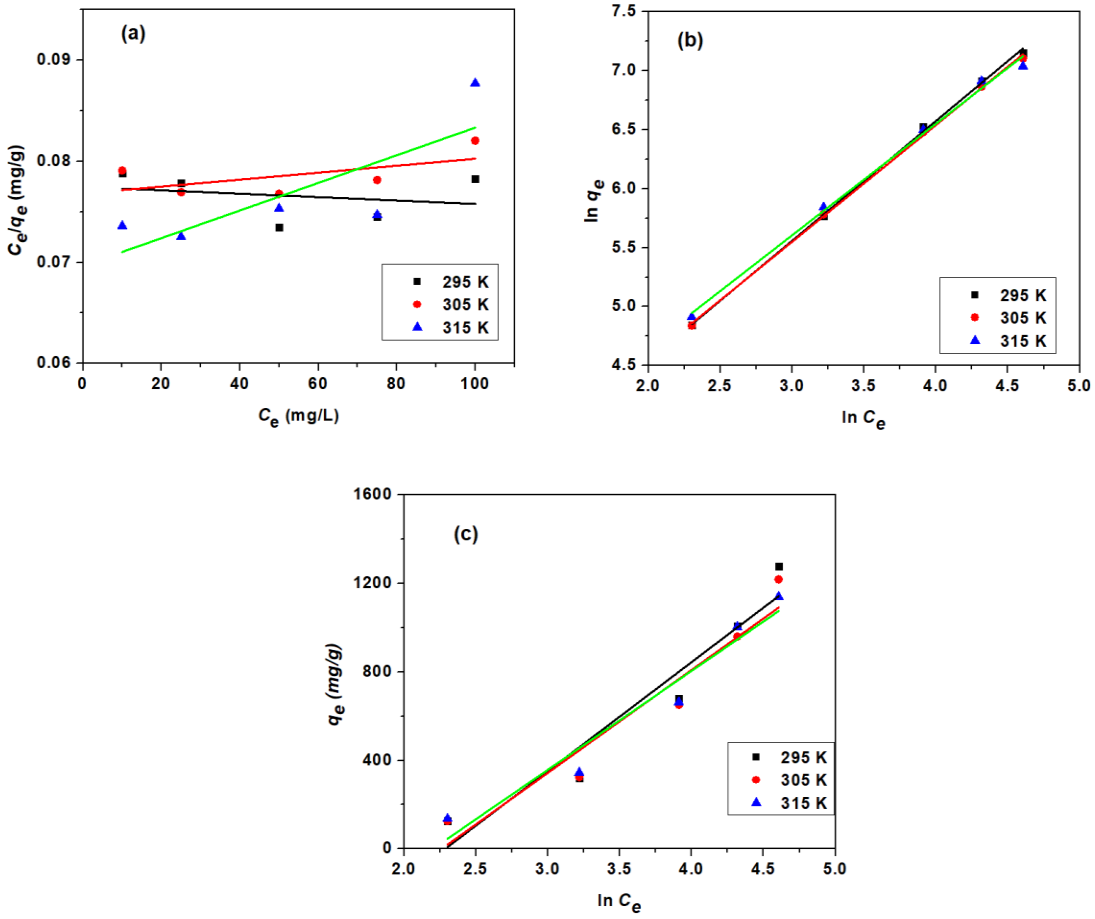

Figure 8. Fitting curves of (a) the Langmuir isotherm model, (b) Freundlich isotherm model and (c) Temkin isotherm model for MB adsorption on super-adsorbent hydrogel at different temperatures using MB solutions at pH= 7 with dosage of super-adsorbent hydrogel = 1g.

Table 3. Adsorption Isotherm Parameters for MB Adsorption on NaSS-DMA Hydrogels

Model	Parameter	Unit	295 K	305 K	315 K
Langmuir Isotherm	q_m	mg/g	3861	3344.48	2439.02
	K_L	L/mg	0.00392	0.00454	0.00702
	R^2		0.5617	0.6528	0.7572

Table 3. Adsorption Isotherm Parameters for MB Adsorption on NaSS-DMA Hydrogels (Cont.)

Freundlich Isotherm	n		0.9843	1.0095	1.0572
	K_F	L/mg	12.317	13.1713	15.9272
	R^2		0.9988	0.9989	0.994
Temkin Isotherm	β	J/mol	4.9755	5.2674	5.4859
	K_T	L/mg	0.1016	0.1041	0.1107
	R^2		0.902	0.9063	0.9295

3.3.4. Thermodynamics of the Adsorption Process. In an adsorption process, standard enthalpy change, ΔH^0 (kJ/mol), standard entropy change, ΔS^0 (J/mol/K) and Gibbs free energy, ΔG^0 (kJ/mol), can be calculated for the adsorption isotherm to characterize the behavior of reaction and provide insight towards the favorability of adsorption process. The following Equations 11 and 12 can be used to calculate these thermodynamic parameters:

$$\Delta G^0 = -RT \ln K_F \quad (11)$$

$$\ln K_F = -(\Delta H^0)/ RT + \Delta S^0/R \quad (12)$$

where R is the universal gas constant, 8.314 J/mol/K, T is absolute temperature (K), K_F is the Freundlich isotherm constant, which can be expressed as standard enthalpy and entropy changes of adsorption as functions of temperature. A plot of ln K_F versus 1/T can be used to determine the values of ΔH^0 and ΔS^0 from the slope and intercept [79].

Thermodynamic parameters were calculated for 295 K, 305 K and 315 K system temperatures where initial MB concentration was varied, as shown in Table 4. Negative

values of Gibbs free energy interpret that the adsorption process was spontaneous at all the temperatures. Furthermore, a positive value of entropy change confirms spontaneity and a high level of (aqueous) disorder occurs in the adsorption process. A positive value of enthalpy change suggests that the adsorption process is endothermic in nature and driven by a strong entropy [80].

Table 4. Thermodynamic Parameters for Adsorption of MB onto NaSS-DMA Hydrogels

Thermodynamic Parameters				
ΔG^0 (kJ/mol)			ΔH^0 (kJ/mol)	ΔS^0 (J/mol/K)
295 K	305 K	315 K		
-37.2	-38.6	-40.4	0.14	2.3

The thermodynamic parameters are attributed to the aromatic ring structures present in NaSS hydrogel polymer backbone and MB dye, which cause improved aggregation of aromatic groups and displacement of water of hydration from dye and polymer as a result of a hydrophobic planar stacking geometry. Release of surface-solvating water molecules would provide the favorable entropic and observed enthalpic contributions to the free energy. In addition to aqueous solvent contributions, site-specific interactions, such as short-range electrostatic interactions, hydrogen bond formation, π-π interaction other than aromatic, or cation-π interactions may also contribute to the free energy [16].

3.4. RECYCLABILITY/ REUSABILITY OF NaSS-DMA SUPER-ADSORBENT HYDROGELS

A capability to regenerate and reuse an adsorbent is a crucially important issue for an economic industrial application of adsorbent. The reusability of the NaSS-DMA copolymer hydrogel adsorbent was investigated over four repeat (five total) cycles of the adsorption - desorption -washing process, as shown in Figure 9. In the 4th repeat cycle, the adsorption capacity was 286 mg/g with a > 90% removal efficiency, which supports the reusability of super-adsorbent hydrogels. A decrease in adsorption capacity in reuse is attributed to a partial, irreversible occupation of hydrogel active sites by MB dye molecules and a minimal mass loss of the hydrogel during the adsorption, desorption, and washing cyclic processing.

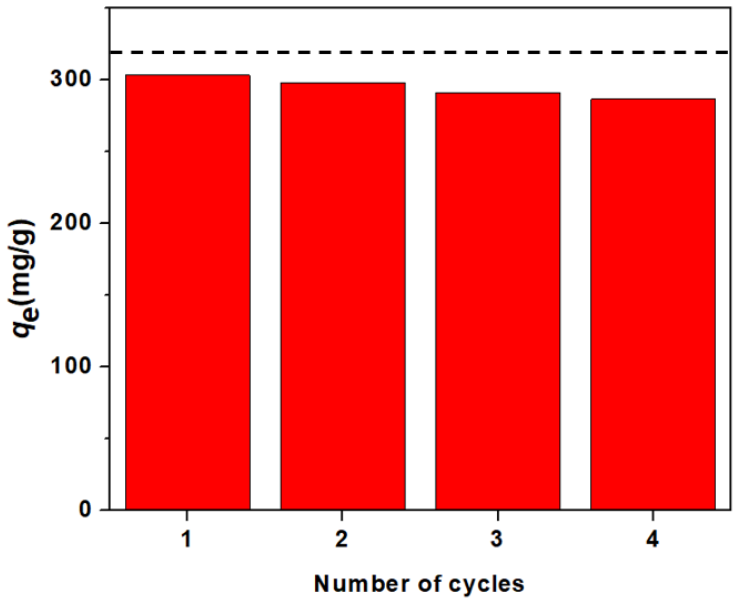

Figure 9. Reusability results for NaSS-DMA copolymer hydrogel for MB adsorption capacity at 295 K in MB solution at pH=7.0, C_0 = 25 mg/L, and adsorbent dosage = 1g. A dashed line represents original adsorption capacity before repeating adsorption - desorption cycles.

4. CONCLUSIONS

A super-adsorbent copolymer hydrogel based on NaSS and DMA monomers was synthesized using a single-step, bulk free radical polymerization using a lab synthesized GelMA organic crosslinker. Incorporation of GelMA created a well-crosslinked, tough polymer network that maintained hydrogel integrity even at very high equilibrium swelling ratios of up to 27500%, which is an important aspect for reusability of hydrogels as adsorbent. Aromatic rings present in the polymer backbone structure enhances aromatic π - π interactions with MB dye that result in an improved adsorption capacity. The adsorption of MB to NaSS-DMA hydrogel is a complex process involving several mechanisms, where heterogenous and multilayer adsorption occurs as described by Elovich kinetics and Freundlich isotherm with a high adsorption capacity for MB dye, reaching upwards of 1270 mg/g. After 4 repeated cycles of desorption-adsorption, the hydrogel maintained structural integrity along with good adsorption performance with more than >90% removal efficiency that supports its use as a high-performance, recyclable adsorbent in industrial remediation applications. As a first report, NaSS copolymer-based hydrogels of high adsorption capacities towards cationic contaminants is a new approach toward high performance, super-adsorbent hydrogel adsorbent wastewater treatments.

ACKNOWLEDGEMENTS

The authors would like to express their acknowledgement to the Instrumentation Lab of Chemistry department at Missouri University of Science and Technology, Rolla, Missouri, USA.

SUPPORTING INFORMATION

NMR analysis to confirm π - π interactions, aromatic hydrophobic interactions:

Commercial samples of poly (NaSS), $\bar{M}$~70,000 Da obtained from Sigma-Aldrich and poly (DMA), $\bar{M}$~100,000 Da, obtained from Scientific Polymer Products, Inc. (Ontario, NY) were used for proton NMR analysis. Aromatic protons of MB are

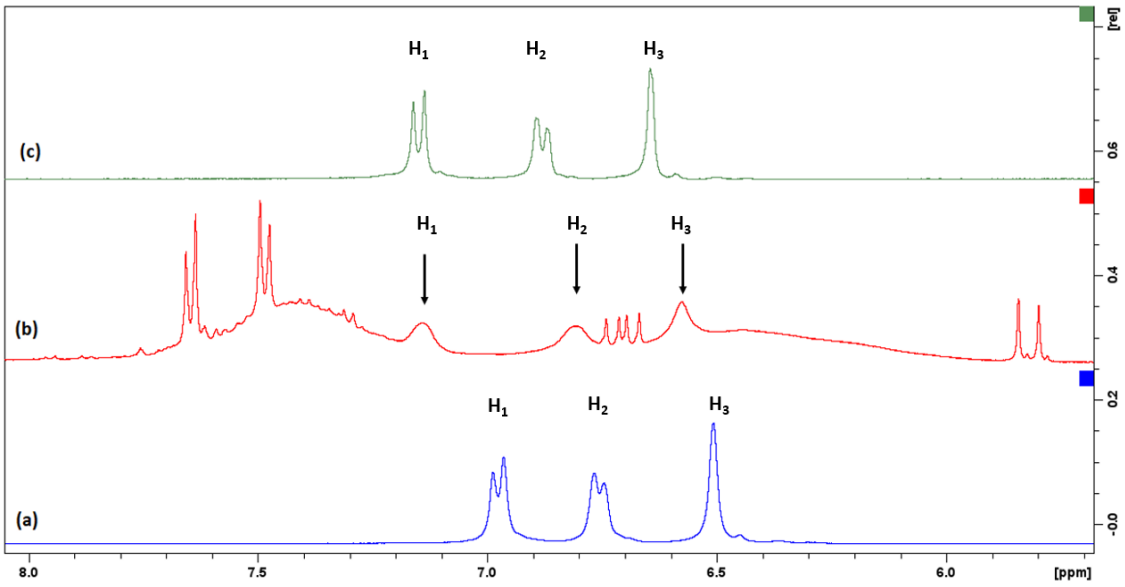

Figure S1. ^{1}H NMR spectra comparison for (a) 10^{-3} M MB solution in D_2O, (b) 10^{-3} M MB solution in 10^{-2} M poly (NaSS) and (c) 10^{-3} M MB solution in 10^{-2} M poly (DMA)

labelled as H_1, H_2 and H_3 which showed broadening of signals in the presence of aromatic polymer like poly (NaSS) whereas no peak broadening of signals observed in poly (DMA) solutions. This effect confirms the π - π interactions, aromatic hydrophobic interactions as a result of delocalization of electron clouds.

REFERENCES

1. Sokolowska-Gajda, J.; Freeman, H.S.; Reife, A. Synthetic dyes based on environmental considerations. Part 2: Iron complexes formazan dyes. *Dyes Pigments* **1996**, *30*, 1-20, doi:https://doi.org/10.1016/0143-7208(95)00048-8.

2. Methneni, N.; Morales-González, J.A.; Jaziri, A.; Mansour, H.B.; Fernandez-Serrano, M. Persistent organic and inorganic pollutants in the effluents from the textile dyeing industries: Ecotoxicology appraisal via a battery of biotests. *Environ. Res.* **2021**, *196*, 110956, doi:https://doi.org/10.1016/j.envres.2021.110956.

3. Kabdaşli, I.; Tünay, O.; Orhon, D. Wastewater control and management in a leather tanning district. *Wat. Sci. Technol.* **1999**, *40*, 261-267, doi:https://doi.org/10.1016/S0273-1223(99)00393-5.

4. Farhan Hanafi, M.; Sapawe, N. A review on the water problem associate with organic pollutants derived from phenol, methyl orange, and remazol brilliant blue dyes. *Mater. Today-Proc.* **2021**, doi:https://doi.org/10.1016/j.matpr.2021.01.258.

5. Bohgard, M.; Ekholm, A.K. A method for the characterization of the aerosols emitted from handling of dye pigments in the paint manufacturing industry. *J. Aerosol Sci.* **1990**, *21*, S733-S736, doi:https://doi.org/10.1016/0021-8502(90)90344-W.

6. Kaur, B.; Bhattacharya, S.N. 7 - Automotive dyes and pigments. In *Handbook of Textile and Industrial Dyeing*, Clark, M., Ed.; Woodhead Publishing: 2011; Volume 2, pp. 231-251.

7. Wainwright, M. 6 - Dyes for the medical industry. In *Handbook of Textile and Industrial Dyeing*, Clark, M., Ed.; Woodhead Publishing: 2011; Volume 2, pp. 204-230.

8. Hefford, R.J.W. 5 - Colourants and dyes for the cosmetics industry. In *Handbook of Textile and Industrial Dyeing*, Clark, M., Ed.; Woodhead Publishing: 2011; Volume 2, pp. 175-203.

9. Rafatullah, M.; Sulaiman, O.; Hashim, R.; Ahmad, A. Adsorption of methylene blue on low-cost adsorbents: A review. *J. Hazard. Mater.* **2010**, *177*, 70-80, doi:https://doi.org/10.1016/j.jhazmat.2009.12.047.

10. Sinha, V.; Chakma, S. Advances in the preparation of hydrogel for wastewater treatment: A concise review. *J Environ. Chem. Eng.* **2019**, *7*, 103295, doi:https://doi.org/10.1016/j.jece.2019.103295.

11. Varjani, S.; Rakholiya, P.; Shindhal, T.; Shah, A.V.; Ngo, H.H. Trends in dye industry effluent treatment and recovery of value added products. *J. Water Process. Eng.* **2021**, *39*, 101734, doi:https://doi.org/10.1016/j.jwpe.2020.101734.

12. Yagub, M.T.; Sen, T.K.; Afroze, S.; Ang, H.M. Dye and its removal from aqueous solution by adsorption: A review. *Adv. Colloid Interface Sci.* **2014**, *209*, 172-184, doi:https://doi.org/10.1016/j.cis.2014.04.002.

13. Gupta, V.K.; Pathania, D.; Agarwal, S.; Singh, P. Adsorptional photocatalytic degradation of methylene blue onto pectin–CuS nanocomposite under solar light. *J. Hazard. Mater.* **2012**, *243*, 179-186, doi:https://doi.org/10.1016/j.jhazmat.2012.10.018.

14. Banat, I.M.; Nigam, P.; Singh, D.; Marchant, R. Microbial decolorization of textile-dyecontaining effluents: A review. *Bioresour. Technol.* **1996**, *58*, 217-227, doi:https://doi.org/10.1016/S0960-8524(96)00113-7.

15. Makhado, E.; Pandey, S.; Nomngongo, P.N.; Ramontja, J. Preparation and characterization of xanthan gum-cl-poly(acrylic acid)/o-MWCNTs hydrogel nanocomposite as highly effective re-usable adsorbent for removal of methylene blue from aqueous solutions. *J. Colloid Interface Sci.* **2018**, *513*, 700-714, doi:https://doi.org/10.1016/j.jcis.2017.11.060.

16. Moreno-Villoslada, I.; González, R.; Hess, S.; Rivas, B.L.; Shibue, T.; Nishide, H. Complex Formation between Rhodamine B and Poly(sodium 4-styrenesulfonate) Studied by 1H-NMR. *J. Phys. Chem. B.* **2006**, *110*, 21576-21581, doi:10.1021/jp0640169.

17. Guimarães, J.R.; Guedes Maniero, M.; Nogueira de Araújo, R. A comparative study on the degradation of RB-19 dye in an aqueous medium by advanced oxidation processes. *J. Environ. Manage.* **2012**, *110*, 33-39, doi:https://doi.org/10.1016/j.jenvman.2012.05.020.

18. Zhang, M.; Gong, J.; Zeng, G.; Zhang, P.; Song, B.; Cao, W.; Liu, H.; Huan, S. Enhanced degradation performance of organic dyes removal by bismuth vanadate-reduced graphene oxide composites under visible light radiation. *Colloids Surf. A Physicochem. Eng. Asp*. **2018**, *559*, 169-183, doi:https://doi.org/10.1016/j.colsurfa.2018.09.049.

19. Shalla, A.H.; Bhat, M.A.; Yaseen, Z. Hydrogels for removal of recalcitrant organic dyes: A conceptual overview. *J. Environ. Chem. Eng.* **2018**, *6*, 5938-5949, doi:https://doi.org/10.1016/j.jece.2018.08.063.

20. Pereira, A.G.B.; Rodrigues, F.H.A.; Paulino, A.T.; Martins, A.F.; Fajardo, A.R. Recent advances on composite hydrogels designed for the remediation of dye-contaminated water and wastewater: A review. *J. Clean. Prod.* **2021**, *284*, 124703, doi:https://doi.org/10.1016/j.jclepro.2020.124703.

21. Labanda, J.; Sabaté, J.; Llorens, J. Modeling of the dynamic adsorption of an anionic dye through ion-exchange membrane adsorber. *J. Membr. Sci.* **2009**, *340*, 234-240, doi:https://doi.org/10.1016/j.memsci.2009.05.036.

22. Mu, B.; Wang, A. Adsorption of dyes onto palygorskite and its composites: A review. *J. of Environ. Chem. Eng.* **2016**, *4*, 1274-1294, doi:https://doi.org/10.1016/j.jece.2016.01.036.

23. Muya, F.N.; Sunday, C.E.; Baker, P.; Iwuoha, E. Environmental remediation of heavy metal ions from aqueous solution through hydrogel adsorption: a critical review. *Water Sci. Technol.* **2015**, *73*, 983-992, doi:10.2166/wst.2015.567.

24. Zhao, S.; Zhou, F.; Li, L.; Cao, M.; Zuo, D.; Liu, H. Removal of anionic dyes from aqueous solutions by adsorption of chitosan-based semi-IPN hydrogel composites. *Compos. B. Eng.* **2012**, *43*, 1570-1578, doi:https://doi.org/10.1016/j.compositesb.2012.01.015.

25. Hu, X.-S.; Liang, R.; Sun, G. Super-adsorbent hydrogel for removal of methylene blue dye from aqueous solution. *J Mater. Chem. A.* **2018**, *6*, 17612-17624, doi:10.1039/C8TA04722G.

26. Le, H.Q.; Sekiguchi, Y.; Ardiyanta, D.; Shimoyama, Y. CO2-Activated Adsorption: A New Approach to Dye Removal by Chitosan Hydrogel. *ACS Omega* **2018**, *3*, 14103-14110, doi:10.1021/acsomega.8b01825.

27. Kim, S.; Park, C.; Kim, T.-H.; Lee, J.; Kim, S.-W. COD reduction and decolorization of textile effluent using a combined process. *J. Biosci. Bioeng.* **2003**, *95*, 102-105, doi:https://doi.org/10.1016/S1389-1723(03)80156-1.

28. Gad, Y.H.; Aly, R.O.; Abdel-Aal, S.E. Synthesis and characterization of Na-alginate/acrylamide hydrogel and its application in dye removal. *J. Appl. Polym. Sci.* **2011**, *120*, 1899-1906, doi:https://doi.org/10.1002/app.33269.

29. Hong, M.; Wang, Y.; Wang, R.; Sun, Y.; Yang, R.; Qu, L.; Li, Z. Poly(sodium styrene sulfonate) functionalized graphene as a highly efficient adsorbent for cationic dye removal with a green regeneration strategy. *J. Phys. Chem. Solids.* **2021**, *152*, 109973, doi:https://doi.org/10.1016/j.jpcs.2021.109973.

30. Mallakpour, S.; Rashidimoghadam, S. Poly(vinyl alcohol)/Vitamin C-multi walled carbon nanotubes composites and their applications for removal of methylene blue: Advanced comparison between linear and nonlinear forms of adsorption isotherms and kinetics models. *Polymer* **2019**, *160*, 115-125, doi:https://doi.org/10.1016/j.polymer.2018.11.035.

31. Mallakpour, S.; Behranvand, V.; Mallakpour, F. Adsorptive performance of alginate/carbon nanotube-carbon dot-magnesium fluorohydroxyapatite hydrogel for methylene blue-contaminated water. *J. Environ. Chem. Eng.* **2021**, *9*, 105170, doi:https://doi.org/10.1016/j.jece.2021.105170.

32. Bhattacharyya, A.; Ghorai, S.; Rana, D.; Roy, I.; Sarkar, G.; Saha, N.R.; Orasugh, J.T.; De, S.; Sadhukhan, S.; Chattopadhyay, D. Design of an efficient and selective adsorbent of cationic dye through activated carbon - graphene oxide nanocomposite: Study on mechanism and synergy. *Mater. Chem. Phys.* **2021**, *260*, 124090, doi:https://doi.org/10.1016/j.matchemphys.2020.124090.

33. Peng, N.; Hu, D.; Zeng, J.; Li, Y.; Liang, L.; Chang, C. Superabsorbent Cellulose–Clay Nanocomposite Hydrogels for Highly Efficient Removal of Dye in Water. *ACS Sustain. Chem. Eng.* **2016**, *4*, 7217-7224, doi:10.1021/acssuschemeng.6b02178.

34. Zubair, M.; Ullah, A. Chapter 14 - Biopolymers in environmental applications: industrial wastewater treatment. In *Biopolymers and their Industrial Applications*, Thomas, S., Gopi, S., Amalraj, A., Eds.; Elsevier: 2021; pp. 331-349.

35. Mohammadzadeh Pakdel, P.; Peighambardoust, S.J. A review on acrylic based hydrogels and their applications in wastewater treatment. *J. Environ. Manage.* **2018**, *217*, 123-143, doi:https://doi.org/10.1016/j.jenvman.2018.03.076.

36. Li, L.; Ferng, L.; Wei, Y.; Yang, C.; Ji, H.-F. Effects of acidity on the size of polyaniline-poly(sodium 4-styrenesulfonate) composite particles and the stability of corresponding colloids in water. *J. Colloid Interface Sci.* **2012**, *381*, 11-16, doi:https://doi.org/10.1016/j.jcis.2012.05.004.

37. Kabiri, K.; Zohuriaan-Mehr, M.J.; Mirzadeh, H.; Kheirabadi, M. Solvent-, ion- and pH-specific swelling of poly(2-acrylamido-2-methylpropane sulfonic acid) superabsorbing gels. *J. Polym. Res.* **2010**, *17*, 203-212, doi:10.1007/s10965-009-9306-7.

38. Cipriano, B.H.; Banik, S.J.; Sharma, R.; Rumore, D.; Hwang, W.; Briber, R.M.; Raghavan, S.R. Superabsorbent Hydrogels That Are Robust and Highly Stretchable. *Macromolecules* **2014**, *47*, 4445-4452, doi:10.1021/ma500882n.

39. Shi, H.; Dong, C.; Yang, Y.; Han, Y.; Wang, F.; Wang, C.; Men, J. Preparation of sulfonate chitosan microspheres and study on its adsorption properties for methylene blue. *Int. J. Biol. Macromol.* **2020**, *163*, 2334-2345, doi:https://doi.org/10.1016/j.ijbiomac.2020.09.078.

40. Makhado, E.; Pandey, S.; Ramontja, J. Microwave assisted synthesis of xanthan gum-cl-poly (acrylic acid) based-reduced graphene oxide hydrogel composite for adsorption of methylene blue and methyl violet from aqueous solution. *Int. J. Biol. Macromol.* **2018**, *119*, 255-269, doi:https://doi.org/10.1016/j.ijbiomac.2018.07.104.

41. Zhu, M.; Wang, Y.; Ferracci, G.; Zheng, J.; Cho, N.-J.; Lee, B.H. Gelatin methacryloyl and its hydrogels with an exceptional degree of controllability and batch-to-batch consistency. *Sci. Rep.* **2019**, *9*, 6863, doi:10.1038/s41598-019-42186-x.

42. Salunkhe, B.; Schuman, T.; Al Brahim, A.; Bai, B. Ultra-high temperature resistant preformed particle gels for enhanced oil recovery. *Chem. Eng. J.* **2021**, *426*, 130712, doi:https://doi.org/10.1016/j.cej.2021.130712.

43. Bekiari, V.; Sotiropoulou, M.; Bokias, G.; Lianos, P. Use of poly(N,N-dimethylacrylamide-co-sodium acrylate) hydrogel to extract cationic dyes and metals from water. *Colloids Surf. A. Physicochem. Eng. Asp.* **2008**, *312*, 214-218, doi:https://doi.org/10.1016/j.colsurfa.2007.06.053.

44. Ruiz, C.; Vera, M.; Rivas, B.L.; Sánchez, S.; Urbano, B.F. Magnetic methacrylated gelatin-g-polyelectrolyte for methylene blue sorption. *RSC Adv.* **2020**, *10*, 43799-43810, doi:10.1039/D0RA08188D.

45. Shirahama, H.; Lee, B.H.; Tan, L.P.; Cho, N.-J. Precise Tuning of Facile One-Pot Gelatin Methacryloyl (GelMA) Synthesis. *Sci. Rep.* **2016**, *6*, 31036, doi:10.1038/srep31036.

46. Yang, J.C.; Jablonsky, M.J.; Mays, J.W. NMR and FT-IR studies of sulfonated styrene-based homopolymers and copolymers. *Polymer* **2002**, *43*, 5125-5132, doi:https://doi.org/10.1016/S0032-3861(02)00390-7.

47. Alpaslan, D.; Dudu, T.E.; Şahiner, N.; Aktas, N. Synthesis and preparation of responsive poly(Dimethyl acrylamide/gelatin and pomegranate extract) as a novel food packaging material. *Mater. Sci. Eng. C.* **2020**, *108*, 110339, doi:https://doi.org/10.1016/j.msec.2019.110339.

48. Zdravković, A.; Nikolić, L.; Ilić-Stojanović, S.; Nikolić, V.; Najman, S.; Mitić, Ž.; Ćirić, A.; Petrović, S. The removal of heavy metal ions from aqueous solutions by hydrogels based on N-isopropylacrylamide and acrylic acid. *Polym. Bull.* **2018**, *75*, 4797-4821, doi:10.1007/s00289-018-2295-0.

49. Rubinstein, M.; Colby, R.H.; Dobrynin, A.V.; Joanny, J.-F. Elastic Modulus and Equilibrium Swelling of Polyelectrolyte Gels. *Macromolecules* **1996**, *29*, 398-406, doi:10.1021/ma9511917.

50. Koda, T.; Dohi, S.; Tachi, H.; Suzuki, Y.; Kojima, C.; Matsumoto, A. One-Shot Preparation of Polyacrylamide/Poly(sodium styrenesulfonate) Double-Network Hydrogels for Rapid Optical Tissue Clearing. *ACS Omega* **2019**, *4*, 21083-21090, doi:10.1021/acsomega.9b02493.

51. Brannon-Peppas, L.; Peppas, N.A. Equilibrium swelling behavior of pH-sensitive hydrogels. *Chem. Eng. Sci.* **1991**, *46*, 715-722, doi:https://doi.org/10.1016/0009-2509(91)80177-Z.

52. Nakhjiri, M.T.; Marandi, G.B.; Kurdtabar, M. Poly(AA-co-VPA) hydrogel cross-linked with N-maleyl chitosan as dye adsorbent: Isotherms, kinetics and thermodynamic investigation. *Int. J. Biol. Macromol.* **2018**, *117*, 152-166, doi:https://doi.org/10.1016/j.ijbiomac.2018.05.140.

53. Mahdavinia, G.R.; Mosallanezhad, A. Facile and green rout to prepare magnetic and chitosan-crosslinked κ-carrageenan bionanocomposites for removal of methylene blue. *J. Water Process. Eng.* **2016**, *10*, 143-155, doi:https://doi.org/10.1016/j.jwpe.2016.02.010.

54. Lapwanit, S.; Sooksimuang, T.; Trakulsujaritchok, T. Adsorptive removal of cationic methylene blue dye by kappa-carrageenan/poly(glycidyl methacrylate) hydrogel beads: Preparation and characterization. *J. Environ. Chem. Eng.* **2018**, *6*, 6221-6230, doi:https://doi.org/10.1016/j.jece.2018.09.050.

55. Xiang, T.; Lu, T.; Zhao, W.-F.; Zhao, C.-S. Ionic-Strength Responsive Zwitterionic Copolymer Hydrogels with Tunable Swelling and Adsorption Behaviors. *Langmuir* **2019**, *35*, 1146-1155, doi:10.1021/acs.langmuir.8b01719.

56. Safronov, A.P.; Smirnova, Y.A.; Pollack, G.H.; Blyakhman, F.A. Enthalpy of Swelling of Potassium Polyacrylate and Polymethacrylate Hydrogels. Evaluation of Excluded-Volume Interaction. *Macromol. Chem. Phys.* **2004**, *205*, 1431-1438, doi:https://doi.org/10.1002/macp.200400067.

57. Lewis, S.R.; Datta, S.; Gui, M.; Coker, E.L.; Huggins, F.E.; Daunert, S.; Bachas, L.; Bhattacharyya, D. Reactive nanostructured membranes for water purification. *Proc. Natl. Acad. Sci. U.S.A.* **2011**, *108*, 8577-8582, doi:10.1073/pnas.1101144108.

58. Dąbrowski, A. Adsorption — from theory to practice. *Adv. Colloid Interface Sci.* **2001**, *93*, 135-224, doi:https://doi.org/10.1016/S0001-8686(00)00082-8.

59. Noroozi, B.; Sorial, G.A. Applicable models for multi-component adsorption of dyes: A review. *J. Environ. Sci.* **2013**, *25*, 419-429, doi:https://doi.org/10.1016/S1001-0742(12)60194-6.

60. Melo, B.C.; Paulino, F.A.A.; Cardoso, V.A.; Pereira, A.G.B.; Fajardo, A.R.; Rodrigues, F.H.A. Cellulose nanowhiskers improve the methylene blue adsorption capacity of chitosan-g-poly(acrylic acid) hydrogel. *Carbohydr. Polym.* **2018**, *181*, 358-367, doi:https://doi.org/10.1016/j.carbpol.2017.10.079.

61. Moreno-Villoslada, I.; Torres, C.; González, F.; Shibue, T.; Nishide, H. Binding of Methylene Blue to Polyelectrolytes Containing Sulfonate Groups. *Macromol. Chem. Phys.* **2009**, *210*, 1167-1175, doi:https://doi.org/10.1002/macp.200900042.

62. Moreno-Villoslada, I.; Jofré, M.; Miranda, V.; Chandía, P.; González, R.; Hess, S.; Rivas, B.L.; Elvira, C.; San Román, J.; Shibue, T.; et al. π-Stacking of rhodamine B onto water-soluble polymers containing aromatic groups. *Polymer* **2006**, *47*, 6496-6500, doi:https://doi.org/10.1016/j.polymer.2006.07.059.

63. Lopičić, Z.R.; Stojanović, M.D.; Marković, S.B.; Milojković, J.V.; Mihajlović, M.L.; Kaluđerović Radoičić, T.S.; Kijevčanin, M.L.J. Effects of different mechanical treatments on structural changes of lignocellulosic waste biomass and subsequent Cu(II) removal kinetics. *Arab. J. Chem.* **2019**, *12*, 4091-4103, doi:https://doi.org/10.1016/j.arabjc.2016.04.005.

64. Simonin, J.-P. On the comparison of pseudo-first order and pseudo-second order rate laws in the modeling of adsorption kinetics. *Chem. Eng. J.* **2016**, *300*, 254-263, doi:https://doi.org/10.1016/j.cej.2016.04.079.

65. George William Kajjumba, S.E., Atakan Öngen, H. Kurtulus Özcan and Serdar Aydın. Modelling of Adsorption Kinetic Processes—Errors, Theory and Application. *Modelling of Adsorption Kinetic Processes—Errors, Theory and Application,* In *Advanced Sorption Process Applications,* Serpil Edebali, *IntechOpen* **2019**, doi:10.5772/intechopen.80495.

66. León, G.; Saura, F.; Hidalgo, A.M.; Miguel, B. Activated Olive Stones as a Low-Cost and Environmentally Friendly Adsorbent for Removing Cephalosporin C from Aqueous Solutions. *Int. J. Environ. Res. Public Health.* **2021**, *18*, 4489.

67. Singh, S.K.; Townsend, T.G.; Mazyck, D.; Boyer, T.H. Equilibrium and intra-particle diffusion of stabilized landfill leachate onto micro- and meso-porous activated carbon. *Water Res.* **2012**, *46*, 491-499, doi:https://doi.org/10.1016/j.watres.2011.11.007.

68. Boyd, G.E.; Adamson, A.W.; Myers, L.S. The Exchange Adsorption of Ions from Aqueous Solutions by Organic Zeolites. II. Kinetics1. *J. Am. Chem. Soc.* **1947**, *69*, 2836-2848, doi:10.1021/ja01203a066.

69. Parenti, F.; Tassinari, F.; Libertini, E.; Lanzi, M.; Mucci, A. Π-Stacking Signature in NMR Solution Spectra of Thiophene-Based Conjugated Polymers. *ACS Omega* **2017**, *2*, 5775-5784, doi:10.1021/acsomega.7b00943.

70. Yu, H.; Grainger, D.W. Thermo-sensitive swelling behavior in crosslinked N-isopropylacrylamide networks: Cationic, anionic, and ampholytic hydrogels. *J. Appl. Polym. Sci.* **1993**, *49*, 1553-1563, doi:https://doi.org/10.1002/app.1993.070490906.

71. Hu, T.; Liu, Q.; Gao, T.; Dong, K.; Wei, G.; Yao, J. Facile Preparation of Tannic Acid–Poly(vinyl alcohol)/Sodium Alginate Hydrogel Beads for Methylene Blue Removal from Simulated Solution. *ACS Omega* **2018**, *3*, 7523-7531, doi:10.1021/acsomega.8b00577.

72. Dai, H.; Huang, Y.; Huang, H. Eco-friendly polyvinyl alcohol/carboxymethyl cellulose hydrogels reinforced with graphene oxide and bentonite for enhanced adsorption of methylene blue. *Carbohydr. Polym.* **2018**, *185*, 1-11, doi:https://doi.org/10.1016/j.carbpol.2017.12.073.

73. Godiya, C.B.; Xiao, Y.; Lu, X. Amine functionalized sodium alginate hydrogel for efficient and rapid removal of methyl blue in water. *Int. J. Biol. Macromol.* **2020**, *144*, 671-681, doi:https://doi.org/10.1016/j.ijbiomac.2019.12.139.

74. Arayaphan, J.; Maijan, P.; Boonsuk, P.; Chantarak, S. Synthesis of photodegradable cassava starch-based double network hydrogel with high mechanical stability for effective removal of methylene blue. *Int. J. Biol. Macromol.* **2021**, *168*, 875-886, doi:https://doi.org/10.1016/j.ijbiomac.2020.11.166.

75. Zheng, M.; Cai, K.; Chen, M.; Zhu, Y.; Zhang, L.; Zheng, B. pH-responsive poly(gellan gum-co-acrylamide-co-acrylic acid) hydrogel: Synthesis, and its application for organic dye removal. *Int. J. Biol. Macromol.* **2020**, *153*, 573-582, doi:https://doi.org/10.1016/j.ijbiomac.2020.03.024.

76. Mittal, H.; Maity, A.; Ray, S.S. Effective removal of cationic dyes from aqueous solution using gum ghatti-based biodegradable hydrogel. *Int. J. Biol. Macromol.* **2015**, *79*, 8-20, doi:https://doi.org/10.1016/j.ijbiomac.2015.04.045.

77. Al-Ghouti, M.A.; Al-Absi, R.S. Mechanistic understanding of the adsorption and thermodynamic aspects of cationic methylene blue dye onto cellulosic olive stones biomass from wastewater. *Sci. Rep.* **2020**, *10*, 15928, doi:10.1038/s41598-020-72996-3.

78. Khajeh, M.; Dastafkan, K.; Bohlooli, M.; Ghaffari-Moghaddam, M. CHAPTER 10 Sample Preparation and Extraction Techniques Using Nanomaterials. In *Advanced Environmental Analysis: Applications of Nanomaterials, Volume 1*; The Royal Society of Chemistry: 2017; Volume 1, pp. 221-283**.**

SECTION

2. CONCLUSIONS

Robust, thermally and hydrolytically stable hydrogels were developed based on new copolymer compositions with N, N'- dimethylacrylamide and sodium styrenesulfonate monomers. A systematic approach to design these robust compositions was discussed through polymer screening through their hydrothermal stability under brine, acidic, neutral, and basic pH conditions.

In first part, we discussed development of the novel design of hydrogel compositions that can withstand temperatures up to 150 °C for more than 24 months in high salinity brines. The effect of salinity, pH, temperature, and multivalent ions on swelling and rheological behavior on these novel hydrogel compositions was demonstrated. These hydrogel compositions also showed phase stability under conditions of high pressure, supercritical carbon dioxide and concentrated acids or bases. We successfully demonstrated the applicability of these compositions in reducing the effective permeability of open fractures through a core flood test. This novel technology fills a technology gap between the existing polyacrylamide-based preformed particle gels (PPGs) technology and an ideal candidate for on-going problems associated with conformance control of reservoirs with harsh temperature and salinity conditions.

In the second part, we discussed the application of these hydrogel compositions as superadsorbent materials for removal of organic dyes from industrial wastewater. Another novel hydrogel composition discussed showed superabsorbance properties with

very high swelling ratios of up to 27,500% that successfully contributes towards an excellent methylene blue dye adsorption capacity of 1270 mg/g with more than 98% dye removal efficiency. As a first report, sodium styrenesulfonate copolymer-based hydrogels of high adsorption capacities towards cationic contaminants is a new approach toward high performance, super-adsorbent hydrogel adsorbent with economic feasibility in wasterwater treatments.

This new approach and hydrogel compositions, their excellent characteristics show significant potential for use in many other high-performance, advanced applications.

BIBLIOGRAPHY

1. Vishnyakov, V., et al., *7 - Oil recovery stages and methods*, in *Primer on Enhanced Oil Recovery*, V. Vishnyakov, et al., Editors. 2020, Gulf Professional Publishing. p. 53-63.

2. Green, D.W. and G.P. Willhite, *Enhanced Oil Recovery*. 1998: Henry L. Doherty Memorial Fund of AIME, Society of Petroleum Engineers.

3. *Chapter 16 - Enhanced oil recovery*, in *Petroleum Engineer's Guide to Oil Field Chemicals and Fluids (Second Edition)*, J. Fink, Editor. 2015, Gulf Professional Publishing: Boston. p. 477-565.

4. Council, N.R., *Induced Seismicity Potential in Energy Technologies*. 2013, Washington, DC: The National Academies Press. 262.

5. Bai, B., M. Wei, and Y. Liu, *Field and Lab Experience With a Successful Preformed Particle Gel Conformance Control Technology*, in *SPE Production and Operations Symposium*. 2013, Society of Petroleum Engineers: Oklahoma City, Oklahoma, USA. p. 17.

6. Benko, K.L. and J.E. Drewes, *Produced Water in the Western United States: Geographical Distribution, Occurrence, and Composition.* Environmental Engineering Science, 2008. **25**(2): p. 239-246.

7. Clark, C.E. and J.A. Veil, *Produced water volumes and management practices in the United States*. 2009, ; Argonne National Lab. (ANL), Argonne, IL (United States). p. Medium: ED.

8. Bai, B., et al., *Preformed Particle Gel for Conformance Control: Factors Affecting Its Properties and Applications.* SPE Reservoir Evaluation & Engineering, 2004. **10**.

9. Babadagli, T., *Development of mature oil fields — A review.* Journal of Petroleum Science and Engineering, 2007. **57**(3): p. 221-246.

10. Seright, R.S., R.H. Lane, and R.D. Sydansk, *A Strategy for Attacking Excess Water Production.* SPE Production & Facilities, 2003. **18**(03): p. 158-169.

11. Seright, R. and B. Brattekas, *Water shutoff and conformance improvement: an introduction.* Petroleum Science, 2021. **18**(2): p. 450-478.

12. Bailey, et al., *The Challenge of Water Control.* Oilfield Review, 2000. **12**.

13. Kazemi, S. *Review of Polymer Gels for Conformance Control in Oil Reservoirs*. 2019.

14. Bai, B., et al., *Preformed Particle Gel for Conformance Control: Transport Mechanism Through Porous Media.* SPE Reservoir Evaluation & Engineering, 2007. **10**(02): p. 176-184.

15. Needham, R.B., C.B. Threlkeld, and J.W. Gall. *Control Of Water Mobility Using Polymers and Multivalent Cations*. in *SPE Improved Oil Recovery Symposium*. 1974.

16. Moradi-Araghi, A., D.H. Beardmore, and G.A. Stahl, *The Application of Gels in Enhanced Oil Recovery: Theory, Polymers and Crosslinker Systems*, in *Water-Soluble Polymers for Petroleum Recovery*, G.A. Stahl and D.N. Schulz, Editors. 1988, Springer US: Boston, MA. p. 299-312.

17. Amir, Z., I.M. Said, and B.M. Jan, *In situ organically cross-linked polymer gel for high-temperature reservoir conformance control: A review.* Polymers for Advanced Technologies, 2019. **30**(1): p. 13-39.

18. Sydansk, R.D., *A New Conformance-Improvement-Treatment Chromium(III) Gel Technology,* in *SPE Enhanced Oil Recovery Symposium*. 1988.

19. Chauveteau, G., et al., *Controlling In-Situ Gelation of Polyacrylamides by Zirconium for Water Shutoff,* in *SPE International Symposium on Oilfield Chemistry*. 1999.

20. Zhu, D., et al., *Effect of Different Phenolic Compounds on Performance of Organically Cross-Linked Terpolymer Gel Systems at Extremely High Temperatures.* Energy & Fuels, 2017. **31**(8): p. 8120-8130.

21. Liu, Y., et al., *New insights into the hydroquinone (HQ)-hexamethylenetetramine (HMTA) gel system for water shut-off treatment in high temperature reservoirs.* Journal of Industrial and Engineering Chemistry, 2016.

22. Yi, Q., et al., *Dynamic thickening investigation of the gelation process of PAM/PEI system at high temperature and high pressure.* Journal of Dispersion Science and Technology, 2017. **38**(11): p. 1640-1646.

23. Bai, Y., et al., *Gelation Study on a Hydrophobically Associating Polymer/Polyethylenimine Gel System for Water Shut-off Treatment.* Energy & Fuels, 2015. **29**(2): p. 447-458.

24. ElKarsani, K.S.M., et al., *Performance of PAM/PEI gel system for water shut-off in high temperature reservoirs: Laboratory study.* Journal of Applied Polymer Science, 2015. **132**(17).

25. Chauveteau, G., et al., *Controlling Gelation Time and Microgel Size for Water Shutoff,* in *SPE/DOE Improved Oil Recovery Symposium*. 2000, Society of Petroleum Engineers: Tulsa, Oklahoma. p. 8.

26. Bryant, S.L., M. Bartosek, and T.P. Lockhart, *Laboratory evaluation of phenol—formaldehyde/polymer gelants for high-temperature applications.* Journal of Petroleum Science and Engineering, 1997. **17**(3): p. 197-209.

27. Jia, H., et al., *Experimental Investigation of the Novel Phenol−Formaldehyde Cross-Linking HPAM Gel System: Based on the Secondary Cross-Linking Method of Organic Cross-Linkers and Its Gelation Performance Study after Flowing through Porous Media.* Energy & Fuels, 2011. **25**(2): p. 727-736.

28. Jia, H., et al., *New Insights into the Gelation Behavior of Polyethyleneimine Cross-Linking Partially Hydrolyzed Polyacrylamide Gels.* Industrial & Engineering Chemistry Research, 2012. **51**(38): p. 12155-12166.

29. Al-Muntasheri, G.A., H.A. Nasr-El-Din, and I.A. Hussein, *A rheological investigation of a high temperature organic gel used for water shut-off treatments.* Journal of Petroleum Science and Engineering, 2007. **59**(1): p. 73-83.

30. Al-Muntasheri, G.A., H.A. Nasr-El-Din, and P.L.J. Zitha, *Gelation Kinetics and Performance Evaluation of an Organically Crosslinked Gel at High Temperature and Pressure.* SPE Journal, 2008. **13**(03): p. 337-345.

31. Saghafi, H.R., et al., *Improvement in thermo-chemical stability of nanocomposite preformed particle gels for conformance control in harsh oil reservoir conditions.* The Canadian Journal of Chemical Engineering, 2016. **94**(10): p. 1880-1890.

32. Yu, B., et al., *Comprehensive evaluation of a high-temperature resistant re-crosslinkable preformed particle gel for water management.* Fuel, 2022. **309**: p. 122086.

33. Alhuraishawy, A.K., et al., *Experimental study of combining low salinity water flooding and preformed particle gel to enhance oil recovery for fractured carbonate reservoirs.* Fuel, 2018. **214**: p. 342-350.

34. Goudarzi, A., et al., *A laboratory and simulation study of preformed particle gels for water conformance control.* Fuel, 2015. **140**: p. 502-513.

35. Pu, J., et al., *Development of Thermotransformable Controlled Hydrogel for Enhancing Oil Recovery.* Energy & Fuels, 2017. **31**(12): p. 13600-13609.

36. Long, Y., et al., *Investigation and Characterization of a Robust Nanocomposite Preformed Particle Gel for Enhanced Oil Recovery.* Energy & Fuels, 2019. **33**(6): p. 5055-5066.

37. Pu, J., et al., *A Recrosslinkable Preformed Particle Gel for Conformance Control in Heterogeneous Reservoirs Containing Linear-Flow Features.* SPE Journal, 2019. **24**(04): p. 1714-1725.

38. Bai, B. and H. Zhang, *Preformed-Particle-Gel Transport Through Open Fractures and Its Effect on Water Flow.* SPE Journal, 2011. **16**(02): p. 388-400.

39. Imqam, A., et al., *Preformed-Particle-Gel Extrusion Through Open Conduits During Conformance-Control Treatments.* SPE Journal, 2015. **20**(05): p. 1083-1093.

40. Imqam, A., Z. Wang, and B. Bai, *The plugging performance of preformed particle gel to water flow through large opening void space conduits.* Journal of Petroleum Science and Engineering, 2017. **156**: p. 51-61.

41. Wang, L., et al., *Mechanically robust re-crosslinkable polymeric hydrogels for water management of void space conduits containing reservoirs.* Chemical Engineering Journal, 2017. **317**: p. 952-960.

42. Imqam, A., Z. Wang, and B. Bai, *Preformed-Particle-Gel Transport Through Heterogeneous Void-Space Conduits.* SPE Journal, 2017. **22**(05): p. 1437-1447.

43. P Wang, J.L., Y Liu, H Zhu, C Xiong, Q Liu, R Jiang, Y Li, Y Zhang, *Flexible polymer, particles prepared therefrom and process for preparing the same*, in *US786795B2*. 2011.

44. Cui, X.-h., et al., *A Novel PPG Enhanced Surfactant-Polymer System for EOR*, in *SPE Enhanced Oil Recovery Conference*. 2011.

45. Beaman, D.J., et al., *Qualification and Deployment of a Unique Polymer Conformance Control System*, in *International Petroleum Technology Conference*. 2009.

46. Xiong, B., et al., *Polyacrylamide degradation and its implications in environmental systems.* npj Clean Water, 2018. **1**(1): p. 17.

47. Kwok, A.Y., G.G. Qiao, and D.H. Solomon, *Synthetic hydrogels. 1. Effects of solvent on poly(acrylamide) networks.* Polymer, 2003. **44**(20): p. 6195-6203.

48. van Vliet, T., et al., *Relation between syneresis and rheological properties of particle gels.* Colloid and Polymer Science, 1991. **269**(6): p. 620-627.

49. Tongwa, P., R. Nygaard, and B. Bai, *Evaluation of a nanocomposite hydrogel for water shut-off in enhanced oil recovery applications: Design, synthesis, and characterization.* Journal of Applied Polymer Science, 2013. **128**(1): p. 787-794.

50. Cassidy, P.E., *Polymers for extreme service conditions.* Journal of Chemical Education, 1981. **58**(11): p. 951.

51. Chatterji, J. and J.K. Borchardt, *Applications of Water-Soluble Polymers in the Oil Field.* Journal of Petroleum Technology, 1981. **33**(11): p. 2042-2056.

52. Shupe, R.D., *Chemical Stability of Polyacrylamide Polymers.* Journal of Petroleum Technology, 1981. **33**(08): p. 1513-1529.

53. Zhang, K., G.H. Lim, and H.J. Choi, *Mechanical degradation of water-soluble acrylamide copolymer under a turbulent flow: Effect of molecular weight and temperature.* Journal of Industrial and Engineering Chemistry, 2016. **33**: p. 156-161.

54. Karami, H.R., M. Rahimi, and S. Ovaysi, *Degradation of drag reducing polymers in aqueous solutions.* Korean Journal of Chemical Engineering, 2018. **35**(1): p. 34-43.

55. Lu, M., X. Wu, and X. Wei, *Chemical degradation of polyacrylamide by advanced oxidation processes.* Environmental Technology, 2012. **33**(9): p. 1021-1028.

56. Gröllmann, U. and W. Schnabel, *Free radical-induced oxidative degradation of polyacrylamide in aqueous solution.* Polymer Degradation and Stability, 1982. **4**(3): p. 203-212.

57. Kheradmand, H., J. François, and V. Plazanet, *Hydrolysis of polyacrylamide and acrylic acid-acrylamide copolymers at neutral pH and high temperature.* Polymer, 1988. **29**(5): p. 860-870.

58. Ma, Q., et al., *Theoretical studies of hydrolysis and stability of polyacrylamide polymers.* Polymer Degradation and Stability, 2015. **121**: p. 69-77.

59. Ramsden, D.K. and K. McKay, *Degradation of polyacrylamide in aqueous solution induced by chemically generated hydroxyl radicals: Part I—Fenton's reagent.* Polymer Degradation and Stability, 1986. **14**(3): p. 217-229.

60. Guthrie, J.P., *Hydration of carboxamides. Evaluation of the free energy change for addition of water to acetamide and formamide derivatives.* Journal of the American Chemical Society, 1974. **96**(11): p. 3608-3615.

61. Moens, J. and G. Smets, *Alkaline and acid hydrolysis of polyvinylamides.* Journal of Polymer Science, 1957. **23**(104): p. 931-948.

62. Gelfi, C., et al., *Investigation of the properties of novel acrylamido monomers by capillary zone electrophoresis.* Journal of Chromatography A, 1992. **608**(1): p. 333-341.

63. Chiari, M., et al., *Towards new formulations for polyacrylamide matrices: N-acryloylaminoethoxyethanol, a novel monomer combining high hydrophilicity with extreme hydrolytic stability.* Electrophoresis, 1994. **15**(2): p. 177-86.

64. Chiari, M., et al., *Preparative isoelectric focusing in multicompartment electrolyzers: novel, hydrolytically stable and hydrophilic isoelectric membranes.* Electrophoresis, 1994. **15**(7): p. 953-9.

65. Deslongchamps, P., R. Barlet, and R.J. Taillefer, *Hydrolysis and carbonyl-oxygen exchange in tertiary amides. Estimation of the free energy changes for breakdown and conformational changes of tetrahedral intermediates.* Canadian Journal of Chemistry, 1980. **58**(20): p. 2167-2172.

66. Yang, W., et al., *Self-Assembling Structure in Solution of a Semirigid Polyelectrolyte.* Macromolecules, 2008. **41**(5): p. 1791-1799.

67. Wang, Y., et al., *Double helical conformation and extreme rigidity in a rodlike polyelectrolyte.* Nature Communications, 2019. **10**(1): p. 801.

68. Takahashi, R., et al., *Double network hydrogels based on semi-rigid polyelectrolyte physical networks.* Journal of Materials Chemistry B, 2019. **7**(41): p. 6347-6354.

69. Tsuda, Y., et al., *Thermoresponsive Microtextured Culture Surfaces Facilitate Fabrication of Capillary Networks.* Advanced Materials, 2007. **19**(21): p. 3633-3636.

70. De, P., et al., *Temperature-Regulated Activity of Responsive Polymer−Protein Conjugates Prepared by Grafting-from via RAFT Polymerization.* Journal of the American Chemical Society, 2008. **130**(34): p. 11288-11289.

71. Fuchise, K., *General Introduction*, in *Design and Precise Synthesis of Thermoresponsive Polyacrylamides*, K. Fuchise, Editor. 2014, Springer Japan: Tokyo. p. 1-25.

72. Beckingham, B.S., G.E. Sanoja, and N.A. Lynd, *Simple and Accurate Determination of Reactivity Ratios Using a Nonterminal Model of Chain Copolymerization.* Macromolecules, 2015. **48**(19): p. 6922-6930.

73. Rafatullah, M., et al., *Adsorption of methylene blue on low-cost adsorbents: A review.* Journal of Hazardous Materials, 2010. **177**(1): p. 70-80.

74. Sinha, V. and S. Chakma, *Advances in the preparation of hydrogel for wastewater treatment: A concise review.* Journal of Environmental Chemical Engineering, 2019. **7**(5): p. 103295.

75. Varjani, S., et al., *Trends in dye industry effluent treatment and recovery of value added products.* Journal of Water Process Engineering, 2021. **39**: p. 101734.

76. Yagub, M.T., et al., *Dye and its removal from aqueous solution by adsorption: A review.* Advances in Colloid and Interface Science, 2014. **209**: p. 172-184.

77. Gupta, V.K., et al., *Adsorptional photocatalytic degradation of methylene blue onto pectin–CuS nanocomposite under solar light.* Journal of Hazardous Materials, 2012. **243**: p. 179-186.

78. Banat, I.M., et al., *Microbial decolorization of textile-dyecontaining effluents: A review.* Bioresource Technology, 1996. **58**(3): p. 217-227.

79. Mu, B. and A. Wang, *Adsorption of dyes onto palygorskite and its composites: A review.* Journal of Environmental Chemical Engineering, 2016. **4**(1): p. 1274-1294.

80. Muya, F.N., et al., *Environmental remediation of heavy metal ions from aqueous solution through hydrogel adsorption: a critical review.* Water Science and Technology, 2015. **73**(5): p. 983-992.

81. Zhao, S., et al., *Removal of anionic dyes from aqueous solutions by adsorption of chitosan-based semi-IPN hydrogel composites.* Composites Part B: Engineering, 2012. **43**(3): p. 1570-1578.

82. Hu, X.-S., R. Liang, and G. Sun, *Super-adsorbent hydrogel for removal of methylene blue dye from aqueous solution.* Journal of Materials Chemistry A, 2018. **6**(36): p. 17612-17624.

83. Makhado, E., et al., *Preparation and characterization of xanthan gum-cl-poly(acrylic acid)/o-MWCNTs hydrogel nanocomposite as highly effective re-usable adsorbent for removal of methylene blue from aqueous solutions.* Journal of Colloid and Interface Science, 2018. **513**: p. 700-714.

84. Le, H.Q., et al., *CO2-Activated Adsorption: A New Approach to Dye Removal by Chitosan Hydrogel.* ACS Omega, 2018. **3**(10): p. 14103-14110.

85. Kim, S., et al., *COD reduction and decolorization of textile effluent using a combined process.* Journal of Bioscience and Bioengineering, 2003. **95**(1): p. 102-105.

86. Shalla, A.H., M.A. Bhat, and Z. Yaseen, *Hydrogels for removal of recalcitrant organic dyes: A conceptual overview.* Journal of Environmental Chemical Engineering, 2018. **6**(5): p. 5938-5949.

87. Mohammadzadeh Pakdel, P. and S.J. Peighambardoust, *A review on acrylic based hydrogels and their applications in wastewater treatment.* Journal of Environmental Management, 2018. **217**: p. 123-143.

88. Simonin, J.-P., *On the comparison of pseudo-first order and pseudo-second order rate laws in the modeling of adsorption kinetics.* Chemical Engineering Journal, 2016. **300**: p. 254-263.

89. Lopičić, Z.R., et al., *Effects of different mechanical treatments on structural changes of lignocellulosic waste biomass and subsequent Cu(II) removal kinetics.* Arabian Journal of Chemistry, 2019. **12**(8): p. 4091-4103.

90. Srinivasan, A. and T. Viraraghavan, *Decolorization of dye wastewaters by biosorbents: A review.* Journal of Environmental Management, 2010. **91**(10): p. 1915-1929.

91. Ayawei, N., A.N. Ebelegi, and D. Wankasi, *Modelling and Interpretation of Adsorption Isotherms.* Journal of Chemistry, 2017. **2017**: p. 3039817.

92. Ringot, D., et al., *In vitro biosorption of ochratoxin A on the yeast industry by-products: Comparison of isotherm models.* Bioresource Technology, 2007. **98**(9): p. 1812-1821.

93. Culver, H.R., J.R. Clegg, and N.A. Peppas, *Analyte-Responsive Hydrogels: Intelligent Materials for Biosensing and Drug Delivery.* Accounts of Chemical Research, 2017. **50**(2): p. 170-178.

94. Tavakoli, J. and Y. Tang, *Hydrogel Based Sensors for Biomedical Applications: An Updated Review.* Polymers, 2017. **9**(8): p. 364.

95. Liu, L., et al., *Mechanically strong and thermosensitive hydrogels reinforced with cellulose nanofibrils.* Polymer Chemistry, 2016. **7**(46): p. 7142-7151.

96. Qu, F., et al., *Electrochemical Biosensing Platform Using Hydrogel Prepared from Ferrocene Modified Amino Acid as Highly Efficient Immobilization Matrix.* Analytical Chemistry, 2014. **86**(2): p. 973-976.

97. Homma, T., et al., *Amperometric glucose sensing with polyaniline/poly(acrylic acid) composite film bearing covalently-immobilized glucose oxidase: A novel method combining enzymatic glucose oxidation and cathodic O2 reduction.* Journal of Electroanalytical Chemistry, 2014. **712**: p. 119-123.

98. Li, L., et al., *A Nanostructured Conductive Hydrogels-Based Biosensor Platform for Human Metabolite Detection.* Nano Letters, 2015. **15**(2): p. 1146-1151.

VITA

Buddhabhushan Pundlik Salunkhe was born and raised in Ulhasnagar, Maharashtra, India. He graduated from the Institute of Chemical Technology (ICT, formerly U.D.C.T.), Mumbai, India and received his Bachelor of Technology degree in Surface Coatings Technology in 2011. He then joined one of the leading coating industries, Asian Paints Ltd. Mumbai, India as a Research Associate and worked for over five years to develop coating formulations and applications skillsets. He joined Missouri S&T in Fall 2016 in the Department of Chemistry under the guidance of Prof. Thomas Schuman. His research focused on synthesis of new monomers, crosslinkers, polymers and developing novel hydrogel compositions for high-performance applications. He published four research papers as a first author and one co-authored paper in cross-functional collaboration along with a co-inventor of a US patent filed in 2020. He presented his research in many numerous meetings. He was in cohort of 2019 Graduate Leadership Development Program offered by University of Missouri system. He received his PhD in Chemistry from Missouri University of Science & Technology, Rolla, Missouri, USA in December 2021.